



DALHOUSIE UNIVERSITY

Retrieved from DalSpace, the institutional repository of
Dalhousie University

<https://dalspace.library.dal.ca/handle/10222/79946>

Version: Post-print

Publisher's version: Smithen, D. A., Monro, S., Pinto, M., Roque III, J. A., Diaz-Rodriguez, R. M., Yin, H., ... & Yin, H. (2020). Bis [Pyrrolyl Ru (II)] Triads: a New Class of Photosensitizers for Metal-Organic Photodynamic Therapy.
doi.org/10.26434/chemrxiv.12824216.v1

Bis[Pyrrolyl Ru(II)] Triads: a New Class of Photosensitizers for Metal-Organic Photodynamic Therapy

Deborah A. Smithen, Susan Monro, Mitch Pinto, John A. Roque III, Roberto M. Diaz-Rodriguez, Huimin Yin, Colin G. Cameron, Alison Thompson, [Sherri A. McFarland](#)

Submitted date: 18/08/2020 • Posted date: 25/08/2020

Licence: CC BY-NC-ND 4.0

Citation information: Smithen, Deborah A.; Monro, Susan; Pinto, Mitch; Roque III, John A.; Diaz-Rodriguez, Roberto M.; Yin, Huimin; et al. (2020): Bis[Pyrrolyl Ru(II)] Triads: a New Class of Photosensitizers for Metal-Organic Photodynamic Therapy. ChemRxiv. Preprint. <https://doi.org/10.26434/chemrxiv.12824216.v1>

A new family of ten dinuclear Ru(II) complexes based on the bis[pyrrolyl Ru(II)] triad scaffold, where two Ru(bpy)₂ centers are separated by a variety of organic linkers, was prepared to evaluate the influence of the organic chromophore on the spectroscopic and in vitro photodynamic therapy (PDT) properties of the compounds. The bis[pyrrolyl Ru(II)] triads absorbed strongly throughout the visible region, with several members having molar extinction coefficients (ϵ) $\geq 10^4$ at 600–620 nm and longer. Phosphorescence quantum yields were generally less than 0.1% and in some cases undetectable. The singlet oxygen quantum yields ranged from 5% to 77% and generally correlated with their photocytotoxicities toward human leukemia (HL-60) cells regardless of the wavelength of light used. Dark cytotoxicities varied ten-fold, with EC₅₀ values in the range of 10–100 μ M and phototherapeutic indices (PIs) as large as 5,400 and 260 with broadband visible (28 J cm⁻², 7.8 mW cm⁻²) and 625-nm red (100 J cm⁻², 42 mW cm⁻²) light, respectively. The bis[pyrrolyl Ru(II)] triad with a pyrenyl linker (5h) was especially potent, with an EC₅₀ value of 1 nM and PI >27,000 with visible light and subnanomolar activity with 625-nm light (100 J cm⁻², 28 mW cm⁻²). The lead compound 5h was also tested in a tumor spheroid assay using the HL60 cell line and exhibited greater photocytotoxicity in this more resistant model (EC₅₀=60 nM and PI>1,200 with 625-nm light) despite a lower dark cytotoxicity. The in vitro PDT effects of 5h extended to bacteria, where submicromolar EC₅₀ values and PIs >300 against *S. mutans* and *S. aureus* were obtained with visible light. This activity was attenuated with 625-nm red light, but PIs were still near 50. The ligand-localized ³ $\pi\pi^*$ state contributed by the pyrenyl linker of 5h likely plays a key role in its phototoxic effects toward cancer cells and bacteria.

File list (2)

MS_Ru-pyrrolide-triads_200724.pdf (1.16 MiB)

[view on ChemRxiv](#) • [download file](#)

Bis[Pyrrolyl Ru(II)] Triads: a New Class of Photosensitizers for Metal-Organic Photodynamic Therapy

Deborah A. Smithen,^a Susan Monro,^b Mitch Pinto^b, John Roque III,^{c,d} Roberto M. Diaz-Rodriguez,^a Huimin Yin,^b Colin G. Cameron,^{c,d} Alison Thompson,^{a,*} and Sherri A. McFarland^{d*}

^aDepartment of Chemistry, Dalhousie University, P.O. Box 15000, Halifax, NS, Canada, B3H 4R2

^bDepartment of Chemistry, Acadia University, Wolfville, NS, Canada, B4P 2R6

^cDepartment of Chemistry and Biochemistry, The University of North Carolina at Greensboro, PO Box 26170, Greensboro, NC 27402-6170 USA

^dDepartment of Chemistry and Biochemistry, The University of Texas at Arlington, 700 Planetarium Pl, Arlington, TX 76019-0065 USA

*Corresponding authors: A.T. <alison.thompson@dal.ca>, ORCID 0000-0003-4231-3446; S.A.M.

<sherri.mcfarland@uta.edu>, ORCID 0000-0002-8028-5055

ABSTRACT

A new family of ten dinuclear Ru(II) complexes based on the bis[pyrrolyl Ru(II)] triad scaffold, where two Ru(bpy)₂ centers are separated by a variety of organic linkers, was prepared to evaluate the influence of the organic chromophore on the spectroscopic and in vitro photodynamic therapy (PDT) properties of the compounds. The bis[pyrrolyl Ru(II)] triads absorbed strongly throughout the visible region, with several members having molar extinction coefficients (ϵ) $\geq 10^4$ at 600–620 nm and longer. Phosphorescence quantum yields (Φ_p) were generally less than 0.1% and in some cases undetectable. The singlet oxygen quantum yields (Φ_Δ) ranged from 5% to 77% and generally correlated with their photocytotoxicities toward human leukemia (HL-60) cells regardless of the wavelength of light used. Dark cytotoxicities varied ten-fold, with EC₅₀ values in the range of 10–100 μ M and phototherapeutic indices (PIs) as large as 5,400 and 260 with broadband visible (28 J cm⁻², 7.8 mW cm⁻²) and 625-nm red (100 J cm⁻², 42 mW cm⁻²) light, respectively. The bis[pyrrolyl Ru(II)] triad with a pyrenyl linker (**5h**) was especially potent, with an EC₅₀ value of 1 nM and PI >27,000 with visible light and subnanomolar activity with 625-nm light (100 J cm⁻², 28 mW cm⁻²). The lead compound **5h** was also tested in a tumor spheroid assay using the HL60 cell line and exhibited greater photocytotoxicity in this more resistant model (EC₅₀=60 nM and PI>1,200 with 625-nm light) despite a lower dark cytotoxicity. The in vitro PDT effects of **5h** extended to bacteria, where submicromolar EC₅₀ values and PIs >300 against *S. mutans* and *S. aureus* were obtained with visible light. This activity was attenuated with 625-nm red light, but PIs were still near 50. The ligand-localized ³ $\pi\pi^*$ state contributed by the pyrenyl linker of **5h** likely plays a key role in its phototoxic effects toward cancer cells and bacteria.

1. INTRODUCTION

Light-responsive prodrugs are the basis for selectively targeting unwanted cells and tissue in photodynamic therapy (PDT). Activation of an otherwise nontoxic photosensitizer (PS) produces cytotoxic singlet oxygen (¹O₂) and other reactive oxygen species (ROS) in regions where the PS, light, and oxygen overlap spatiotemporally,^{1–3} thus confining toxicity to diseased tissue while sparing healthy tissue. The antitumor effects of PDT result from destruction of primary tumors and tumor vasculature, but can also include a systemic immunological response.^{4–12} Photofrin, a mixture of oligomeric tetrapyrroles, remains arguably the most utilized PS for PDT.^{12–15} However, a variety of second- and third-generation derivatives, including metallated tetrapyrroles, that seek

44 to improve upon the properties of earlier PSs have gained attention and (in some cases) approval
45 in certain countries.^{16,17}

46 Metal complexes that are not simply metallated tetrapyrroles are particularly intriguing as PSs
47 for PDT,^{18,19} and there are numerous reports highlighting their rich photophysical and
48 photochemical properties.²⁰ Their modular architectures can be exploited to produce a variety of
49 energetically accessible excited state configurations: metal-to-ligand charge transfer (MLCT),²¹
50 metal centered (MC),^{22–24} ligand centered (LC) or intraligand (IL),^{25–27} intraligand charge transfer
51 (ILCT),^{28–30} ligand-to-ligand charge transfer (LLCT),^{31–33} ligand-to-metal charge transfer
52 (LMCT),³⁴ and metal-to-metal charge transfer (MMCT) in the case of multimetallic systems.^{35–38}
53 Some of these excited states (and combinations thereof) may undergo the type I and II
54 photoprocesses that define PDT or they may exert phototoxic effects via alternate mechanisms that
55 do not involve oxygen. The oxygen-independent pathways, which includes stoichiometric
56 photodissociation of ligands,^{22,24,39–45} have been collectively grouped as photochemotherapy
57 (PCT) although no PCT agents have been approved for cancer therapy to date.^{16,46}

58 Through our search for PSs that produce phototoxic effects in hypoxia via catalytic
59 photosensitization pathways, we have found that the best features of both organic and inorganic
60 PSs can be combined to produce hybrid systems, and the resulting metal-organic dyads exhibit
61 unprecedented photocytotoxicities and phototherapeutic indices (PIs).^{26,47,48} Organic
62 chromophores, either contiguously fused or tethered to coordinating diimine ligands, serve as
63 excellent collection points for excitation energy from singlet excited states provided their localized
64 ³IL states are energetically accessible through equilibration or relaxation. Organic triplets offer a
65 unique means of slowing T→S intersystem crossing (ISC) in metal complexes, while the metal
66 facilitates efficient formation of these triplet excited states and the possibility of oxygen-
67 independent photoreactivity. Pure ³IL states that are lower in energy than the lowest lying ³MLCT
68 state(s) tend to possess exceptionally long lifetimes (>20 μs) and proved very effective for *in vitro*
69 PDT.^{26,47,49–52}

70 From our extensive work in this area, we have found that organic triplets having charge transfer
71 character (³ILCT) contributed by α-oligothienyl groups in certain systems are particularly
72 photoreactive and make excellent PDT agents.^{16,48,53–61} Our TLD1433 is one example, which is a
73 bis-heteroleptic Ru(II) complex based on the α-terthienyl-appended imidazo[4,5-
74 *f*][1,10]phenanthroline (IP-3T) ligand that generates ¹O₂ with almost unity efficiency.^{16,17,48,62–66}
75 TLD1433 is the first Ru(II) complex to enter a human clinical trial and is being evaluated in a
76 Phase 2 clinical trial for treating nonmuscle invasive bladder cancer with PDT (Clinicaltrials.gov
77 identifier: NCT03945162).^{16,17,66}

78 Our ongoing interest in exploring the photoreactivity of Ru(II) metal-organic systems, including
79 TLD1433, inspired the present study. Herein, we explore the bis[Ru(II)-pyrrolide] scaffold, a
80 metal-organic-metal triad, to push the envelope for achieving unprecedented *in vitro* PDT potency
81 with ³IL excited states. This construct simultaneously satisfies three criteria: (i) low energy singlet
82 and triplet MLCT states, (ii) utilization of two metal centers to funnel energy to an organic triplet,
83 and (iii) incorporation of an organic chromophore with a triplet excited state of suitable energy
84 and lifetime. Previously, we have shown that 2-formyl and 2-keto pyrroles can replace one of the
85 2,2'-bipyridyl (bpy) ligands in [Ru(bpy)₃]²⁺ to form stable complexes under ambient conditions
86 with MLCT states shifted as much as 1.52 eV relative to the parent complex.⁶⁷ In these model

87 mononuclear complexes, continuous absorption out to 600 nm was achieved without the need for
88 sterically-demanding diimines such as 2,2'-biquinoline (biq) that are known to lower the energies
89 of both MLCT and MC states, leading to red-shifted absorption, but also photodissociation. The
90 small, bidentate pyrrolide ligand forms strong N- σ (η^1) bonds to Ru(II), lowering the energy of
91 MLCT states without promoting ligand loss from dissociative 3 MC states. Conversion of this 2-
92 formyl pyrrole ligand into its symmetric bis(formylpyrrole) counterpart with a central organic
93 chromophore linker and coordination of the termini to Ru(II) diimine units was expected to result
94 in complexes with a larger percentage of accessible 3 IL triplets. Herein we report the synthesis and
95 characterization of a family of bis[Ru(II)-pyrrolide] triads that differ in the identity of the organic
96 chromophore used as the central linker. The influence of this unit on the photobiological activities
97 within this class of compounds is examined in detail, and the potent *in vitro* PDT effects discussed.

98 **2. EXPERIMENTAL PROCEDURES**

99 **2.1 Materials**

100 All chemicals and reagents were purchased from commercial sources and were used as received,
101 unless otherwise noted. Ethyl acetate, hexanes and dichloromethane were obtained crude and
102 purified via distillation, under air and at 1 atm pressure, before use. Reagent-grade tetrahydrofuran
103 (THF), ethylene glycol, isopropanol (IPA) and acetone were employed where stated. Anhydrous
104 dichloromethane and dimethylformamide (DMF) were purchased from EMD Chemicals and
105 Sigma Aldrich, respectively. All glassware was oven dried and purged with inert gas before use.
106 Gravity column chromatography was performed using 230–400 mesh Silicycle ultra-pure silica
107 gel or 150-mesh Brockman III activated neutral aluminum oxide. TLC was performed on silica
108 gel or aluminum oxide plates and visualized using UV light (254 and/or 365 nm) and/or developed
109 with vanillin stain.

110 Characterized fetal bovine serum (FBS) and Iscove's Modified Dulbecco's Medium (IMDM)
111 supplemented with 4 mM L-glutamine were purchased from Fisher Scientific. Human
112 promyelocytic leukemia cells (HL-60), *Streptococcus mutans*, and *Streptococcus aureus* were
113 purchased from American Type Culture Collection (ATCC) through Cedarlane (Burlington, ON).
114 Prior to use, FBS was aliquoted in 40-mL volumes, heat inactivated for 30 min at 55 °C, and stored
115 at –20 °C. Plasmid pUC19 DNA was purchased from New England BioLabs and transformed
116 using NovaBlue Singles Competent Cells (Novagen). Transformed pUC19 was purified using the
117 QIAprep Spin Miniprep Kit from Qiagen (yield \approx 62 μ g of plasmid DNA per 20-mL culture). Water
118 for biological experiments was deionized to a resistivity of 18 M Ω -cm using a Barnstead filtration
119 system.

120 **2.2 Instrumentation**

121 NMR spectra were recorded using a 500 MHz spectrometer. All 1 H and 13 C NMR chemical shifts
122 are expressed in parts per million (ppm) using the solvent signal [CDCl₃ (1 H 7.26 ppm; 13 C 77.16
123 ppm); DMSO-*d*₆ (1 H 2.50 ppm; 13 C 39.52 ppm); THF-*d*₈ (1 H 1.73, 3.58 ppm; 13 C 25.4, 67.6 ppm);
124 CD₂Cl₂ (1 H 5.32 ppm; 13 C 53.8 ppm)] as the internal reference. Splitting patterns are indicated as
125 follows: br, broad; s, singlet; d, doublet; t, triplet; at, apparent triplet; q, quartet; m, multiplet; sep,
126 septet. All coupling constants (*J*) are reported in Hertz (Hz). Ultraviolet-visible spectra were
127 recorded using a Varian-Cary Bio 100 spectrophotometer. Mass spectra were recorded using ion
128 trap (ESI or APCI) instruments. Microwave-promoted reactions were carried out using a Biotage
129 Initiator 8 Microwave with 0–400 W power at 2.45 GHz. Melting points are uncorrected.

130 2.3 Synthesis and Characterization

131 2.3.1 General procedures

132 **General procedure for the synthesis of bis(pyrrole)s (2) by Heck Reaction (GP1).** Palladium
133 (II) acetate (1 mol%) and 2,4-pentanedione (2 mol%) were added to a solution of aryl dibromide
134 (0.35 mmol, 1 equiv.) in anhydrous DMF (2.0 mL) at room temperature under argon, and stirred
135 for 10 minutes. 2-Vinyl-*N*-Boc pyrrole (**1a**) (0.88 mmol, 2.5 equiv.) was then added as an oil,
136 followed by potassium carbonate (0.7 mmol, 2 equiv.) as a solid in one portion, and the flask was
137 sealed with a glass stopper before heating to 130 °C (caution: always use a blast shield when
138 heating a sealed system), using a sand bath covered with aluminum foil, with stirring for 6 hours.
139 After cooling slightly, the reaction mixture was poured into ice-water (40 mL), neutralized with a
140 few drops of 1 M HCl and refrigerated (4 °C) overnight. The resulting precipitate was collected
141 using a Millipore filtration apparatus and then dried in a vacuum oven to give the crude product,
142 which was subsequently washed with 0–30% diethyl ether/hexanes on a Millipore filter to give the
143 desired bis(pyrrole) without the need for further purification, unless otherwise stated.

144 **General procedure for the synthesis of bis(pyrrole)s (2) by Suzuki Reaction (GP2).** A
145 solution of aryl dibromide (0.15 mmol, 1 equiv.) and 1-Boc-pyrrole-2-boronic acid (**1b**) (0.45
146 mmol, 3 equiv.) in anhydrous DMF (3 mL) was sparged with nitrogen gas for 10 minutes.
147 Tetrakis(triphenylphosphine)palladium(0) (0.015 mmol, 0.1 equiv.) and potassium carbonate
148 (0.60 mmol, 4 equiv.) were then added with stirring, and the solution was sparged with nitrogen
149 for a further 5 minutes before the flask was sealed and heated to 110 °C for 24 hours. The reaction
150 mixture was then cooled to room temperature and separated between dichloromethane (50 mL)
151 and water (50 mL). The aqueous phase was extracted with dichloromethane (2 × 50 mL) and the
152 combined organic extracts were washed with water (4 × 100 mL) and brine (100 mL), dried over
153 anhydrous sodium sulfate, and concentrated to give the crude product which was purified using
154 column chromatography on silica gel.

155 **General procedure for the synthesis of bis(formylpyrrole)s (3) using Vilsmeier-Haack**
156 **Reaction (GP3).** The desired bis(pyrrole) (**2**) (0.2 mmol, 1 equiv.) was dissolved in anhydrous
157 DMF (4 mL) with stirring under nitrogen, and the solution was cooled to 0 °C in an ice bath.
158 Phosphorous oxychloride (0.44 mmol, 2.2 equiv.), was then added drop-wise and the reaction
159 mixture was warmed to 60 °C with stirring for 1.5 hours. After cooling to room temperature, 5%
160 (w/v) aqueous potassium carbonate solution (~3 mL) was added slowly until the solution became
161 basic (~pH 8, pH paper). The reaction mixture was then heated to 80 °C with stirring for 2 hours,
162 before being poured into ice-water to precipitate the product which was collected using a Millipore
163 filtration apparatus. The product was then dried in a vacuum oven and finally washed with 50–
164 100% diethyl ether/hexanes.

165 **General procedure for the synthesis of bis(ruthenium(II)) hexafluorophosphate complex**
166 **salts (4) (GP4).** Triethylamine (0.24 mmol, 8 equiv.) was added to a suspension of dipyrrolic
167 ligand (**3**) (0.031 mmol, 1.03 equiv.) and *cis*-bis-(2,2'-bipyridine)dichlororuthenium(II) dihydrate
168 (0.06 mmol, 2 equiv.) in ethylene glycol (2.0 mL) in a Biotage microwave vial (2–5 mL capacity).
169 The vial was then sealed using a manual cap crimper and placed in the microwave reactor, where
170 it was heated at 125 °C for 80 minutes, at a maximum of 400 W power. After cooling, the reaction
171 mixture was poured into a solution of ammonium hexafluorophosphate (0.45 mmol, 15 equiv.) in
172 water (20 mL) and left to stand at room temperature overnight. The solution was then extracted
173 thoroughly with dichloromethane (4 × 20 mL). The combined organic extracts were washed with

174 brine (50 mL), dried over anhydrous sodium sulfate and concentrated to give the crude product,
175 which was purified using column chromatography on silica gel (0–8% IPA/dichloromethane)
176 and/or neutral alumina (0–8% methanol/dichloromethane).

177 **General procedure for the conversion of bis(ruthenium(II)) hexafluorophosphate complex**
178 **salts to chloride salts (5) (GP5).** Tetrabutylammonium chloride monohydrate (0.25 mmol, 20
179 equiv.) was added to a solution of the bis(ruthenium) hexafluorophosphate salt (**4**) (0.0125 mmol,
180 1.0 equiv.) in acetone (12 mL, 1 mM) with stirring at room temperature for 15 minutes. The desired
181 chloride salt was generally observed to form as a precipitate during this time (unless otherwise
182 stated), which was collected using Millipore filtration and washed with 30% acetone/hexanes
183 before drying in a vacuum oven.

184 2.3.2 Experimental data

185 **(E)-2-styryl-1H-pyrrole (2a).**⁶⁸ Compound **2a** was synthesized from 2-vinyl-*N*-Boc pyrrole (**1a**,
186 1.3 equiv.) and bromobenzene (**a**) using **GP1** and a reaction time of 3 h. After cooling to room
187 temperature, the reaction mixture was separated between diethyl ether (30 mL) and water (20 mL).
188 The aqueous phase was extracted with diethyl ether (4 × 20 mL) and the combined organic extracts
189 were washed with water (100 mL) and brine (100 mL), dried over anhydrous magnesium sulfate
190 and concentrated *in vacuo*. The crude product was purified using column chromatography on silica
191 gel eluting with 15% ethyl acetate/hexanes to give the title compound (34 mg, 64% yield) as a pale
192 yellow solid. M.p. 110–115 °C. ¹H NMR (CDCl₃, 500 MHz) δ: 7.43 (d, 2H, *J* = 7.5 Hz, ArH),
193 7.33 (at, 2H, *J* = 7.8 Hz, ArH), 7.21 (t, 1H, *J* = 7.3 Hz, ArH), 6.98 (d, 1H, *J* = 16.5 Hz, ArH), 6.83–
194 6.82 (m, 1H), 6.67 (d, 2H, *J* = 16.5 Hz, ArH), 6.35–6.36 (m, 1H), 6.25 (aq, 1H, *J* = 3.0 Hz) ppm.
195 ¹³C NMR (CDCl₃, 125 MHz) δ: 137.6, 130.9, 128.8, 127.1, 126.0, 123.5, 119.2, 119.1, 110.2,
196 109.3 ppm. LRMS: 170.1 (M+H)⁺; HRMS calculated for C₁₂H₁₂N: 170.0964; found 170.0964.

197 **1,4-Bis((E)-2-(1H-pyrrol-2-yl)vinyl)benzene (2b).** Compound **2b** was synthesized from 2-
198 vinyl-*N*-Boc pyrrole (**1a**) and 1,4-dibromobenzene (**b**) using **GP1** to give the title compound (95
199 mg, 86% yield) as a dark yellow solid. M.p./d.p. > 280 °C. ¹H NMR (THF-*d*₈, 500 MHz) δ: 10.27
200 (br s, 2H, NH), 7.34 (s, 4H, ArH), 6.97 (d, 2H, *J* = 16.5 Hz, C=CH), 6.72–6.71 (m, 2H, PyH), 6.68
201 (d, 2H, *J* = 16.5 Hz, C=CH), 6.20–6.19 (m, 2H, PyH), 6.06–6.05 (m, 2H, PyH) ppm. ¹³C NMR
202 (THF-*d*₈, 125 MHz) δ: 137.5, 132.0, 126.6, 122.8, 120.0, 119.9, 109.9, 109.8 ppm. LRMS: 259.1
203 (M–H)[–]; HRMS calculated for C₁₈H₁₅N₂: 259.1241; found 259.1238. ε_{386nm} = 48,000 (THF).

204 **4,4'-Bis((E)-2-(1H-pyrrol-2-yl)vinyl)-1,1'-biphenyl (2c)** Compound **2c** was synthesized from
205 2-vinyl-*N*-Boc pyrrole (**1a**) and 4,4'-dibromobiphenyl (**c**) using **GP1**. The crude product was
206 washed with 1:1 diethyl ether:hexanes to give the title compound (95 mg, 86% yield) as a light
207 brown solid. M.p./d.p. > 250 °C. ¹H NMR (DMSO-*d*₆, 500 MHz) δ: 11.20 (br s, 2H, NH), 7.67 (d,
208 4H, *J* = 8.3 Hz, ArH), 7.52 (d, 4H, *J* = 8.3 Hz, ArH), 7.09 (d, 2H, *J* = 16.5 Hz, C=CH), 6.88 (d,
209 2H, *J* = 16.5 Hz, C=CH), 6.84 (br s, 2H, pyH), 6.28 (br s, 2H, PyH), 6.08 (br s, 2H, PyH) ppm.
210 ¹³C NMR (DMSO-*d*₆, 125 MHz) δ: 137.5, 136.8, 130.4, 126.5, 126.0, 121.6, 119.9, 119.8, 109.3,
211 109.0 ppm. LRMS: 337.2 (M+H)⁺; HRMS calculated for C₂₄H₂₁N₂: 337.1699; found 337.1688.
212 ε_{380nm} = 74,000 (THF).

213 **2,6-Bis((E)-2-(1H-pyrrol-2-yl)vinyl)naphthalene (2d).** Compound **2d** was synthesized from 2-
214 vinyl-*N*-Boc pyrrole (**1a**) and 2,6-dibromonaphthalene (**d**) using **GP1** to give the title compound
215 (95 mg, 97% yield) as a light brown solid. M.p./d.p. > 250 °C. ¹H NMR (DMSO-*d*₆, 500 MHz) δ:

216 11.23 (br s, 2H, NH), 7.82 (d, 2H, $J = 8.5$ Hz, ArH), 7.76 (s, 2H, ArH), 7.69 (d, 2H, $J = 8.5$ Hz,
217 ArH), 7.17 (d, 2H, $J = 16.5$ Hz, C=CH), 6.99 (d, 2H, $J = 16.5$ Hz, C=CH), 6.86 (dd, 2H, $J = 2.5$,
218 4.0 Hz, PyH), 6.30 (br s, 2H, PyH), 6.09 (dd, 2H, $J = 2.5$, 5.5 Hz, PyH) ppm. ^{13}C NMR (DMSO-
219 d_6 , 125 MHz) δ : 135.0, 132.5, 130.5, 128.1, 124.5, 123.6, 122.2, 120.0, 119.9, 109.4, 109.0 ppm.
220 LRMS: 311.2 (M+H) $^+$; HRMS (APCI) calculated for $\text{C}_{24}\text{H}_{21}\text{N}_2$: 311.1543; found 311.1528. $\epsilon_{384\text{nm}}$
221 = 59,000 (THF).

222 **4,7-Bis((E)-2-(1H-pyrrol-2-yl)vinyl)benzo[*c*][1,2,5]thiadiazole (2e).** Compound **2e** was
223 synthesized from 2-vinyl-*N*-Boc pyrrole (**1a**) and 4,7-dibromobenzo[*c*]-1,2,5-thiadiazole (**e**) using
224 **GP1**. After cooling to room temperature, the reaction mixture was separated between 1:2
225 THF:diethyl ether (30 mL) and water (20 mL). The aqueous phase was extracted with 1:2
226 THF:diethyl ether (4 \times 20 mL) and the combined organic extracts were concentrated *in vacuo*. The
227 crude product was purified using column chromatography on silica eluting with 30% ethyl
228 acetate/hexanes to give the title compound (99 mg, 91% yield) as a red solid. M.p. 200–205 $^\circ\text{C}$.
229 ^1H NMR (CDCl_3 , 500 MHz) δ : 8.51 (br s, 2H, NH), 7.84 (d, 2H, $J = 16.5$ Hz, C=CH), 7.52 (s, 2H,
230 ArH), 7.17 (d, 2H, $J = 16.5$ Hz, C=CH), 6.88 (dd, 2H, $J = 2.5$, 4.0 Hz, PyH), 6.51 (br s, 2H, PyH),
231 6.30 (dd, 2H, $J = 2.5$, 6.0 Hz, PyH) ppm. ^{13}C NMR (CDCl_3 , 125 MHz) δ : 153.9, 131.5, 128.8,
232 125.9, 122.8, 120.1, 119.3, 110.6, 110.4 ppm. LRMS: 319.1 (M+H) $^+$; HRMS (APCI) calculated
233 for $\text{C}_{18}\text{H}_{15}\text{N}_4\text{S}$: 319.1012; found 319.1000. $\epsilon_{520\text{nm}} = 18,000$; $\epsilon_{360\text{nm}} = 27,000$; $\epsilon_{266\text{nm}} = 14,000$ (THF).

234 **9,10-Bis((E)-2-(1H-pyrrol-2-yl)vinyl)anthracene (2f).** Compound **2f** was synthesized from 2-
235 vinyl-*N*-Boc pyrrole (**1a**) and 9,10'-dibromoanthracene (**f**) using **GP1**. The crude product was
236 washed with 10% diethyl ether/hexanes to give the title compound (114 mg, 97% yield) as a light
237 brown solid. M.p. 215–220 $^\circ\text{C}$. ^1H NMR (THF- d_8 , 500 MHz) δ : 10.60 (br s, 2H, NH), 8.44–8.42
238 (m, 4H, ArH), 7.56 (d, 2H, $J = 16.5$ Hz, C=CH), 7.43–7.41 (m, 4H, ArH), 6.84 (br s, 2H, PyH),
239 6.76 (d, 2H, $J = 16.5$ Hz, C=CH), 6.33 (br s, 2H, PyH), 6.15 (br s, 2H, PyH) ppm. ^{13}C NMR (THF-
240 d_8 , 125 MHz) δ : 133.4, 131.8, 130.6, 129.4, 127.3, 125.6, 120.2, 118.8, 110.1, 109.9 ppm. LRMS:
241 361.2 (M+H) $^+$; HRMS (APCI) calculated for $\text{C}_{26}\text{H}_{21}\text{N}_2$: 361.1699; found 361.1688. $\epsilon_{424\text{nm}} =$
242 12,600; $\epsilon_{259\text{nm}} = 60,000$ (THF).

243 **2,7-Bis((E)-2-(1H-pyrrol-2-yl)vinyl)-9H-fluorene (2g).** Compound **2g** was synthesized from 2-
244 vinyl-*N*-Boc pyrrole (**1a**) and 2,7-dibromofluorene (**g**) using **GP1** to give the title compound (108
245 mg, quantitative) as a yellow/brown solid. M.p./d.p. > 250 $^\circ\text{C}$. ^1H NMR (THF- d_8 , 500 MHz) δ :
246 10.30 (br s, 2H, NH), 7.67 (d, 2H, $J = 8.0$ Hz, ArH), 7.61 (s, 2H, ArH), 7.39 (d, 2H, $J = 8.0$ Hz,
247 ArH), 7.05 (d, 2H, $J = 16.5$ Hz, C=CH), 6.78 (d, 2H, $J = 16.5$ Hz, C=CH), 6.73–6.72 (m, 2H,
248 PyH), 6.22 (br s, 2H, PyH), 6.07–6.06 (m, 2H, PyH), 3.87 (s, 2H, CH_2) ppm. ^{13}C NMR (THF- d_8 ,
249 125 MHz) δ : 144.8, 141.2, 137.8, 132.0, 125.7, 123.4, 122.5, 120.4, 120.0, 110.0, 109.8, 37.3 ppm
250 (one signal missing). LRMS: 349.2 (M+H) $^+$; HRMS (APCI) calculated for $\text{C}_{25}\text{H}_{21}\text{N}_2$: 349.1699;
251 found 349.1694. $\epsilon_{390\text{nm}} = 55,000$ (THF).

252 **1,6-Bis((E)-2-(1H-pyrrol-2-yl)vinyl)pyrene (2h).** Compound **2h** was synthesized from 2-vinyl-
253 *N*-Boc pyrrole (**1a**) and 1,6-dibromopyrene (**h**) using **GP1** to give the title compound (48 mg,
254 quantitative) as a dark yellow/brown solid. M.p./d.p. > 250 $^\circ\text{C}$. ^1H NMR (THF- d_8 , 500 MHz) δ :
255 10.56 (br s, 2H, NH), 8.48 (d, 2H, $J = 8.5$ Hz, ArH), 8.30 (d, 2H, $J = 8.5$ Hz, ArH), 8.10 (d, 2H, J
256 = 9.0 Hz, ArH), 8.05 (d, 2H, $J = 9.0$ Hz, ArH), 7.87 (d, 2H, $J = 16.0$ Hz, C=CH), 7.29 (d, 2H, J
257 = 16.0 Hz, C=CH), 6.83 (br s, 2H, PyH), 6.37 (br s, 2H, PyH), 6.14 (br s, 2H, PyH) ppm. ^{13}C NMR
258 (THF- d_8 , 125 MHz) δ : 133.7, 132.6, 131.0, 129.2, 127.9, 126.7, 125.7, 123.4, 123.2, 123.1, 120.4,

259 119.6, 110.8, 110.1 ppm (one signal missing). LRMS: 385.2 (M+H)⁺; HRMS calculated for
260 C₂₈H₂₁N₂: 385.1699; found 385.1686. $\epsilon_{433\text{nm}} = 37,000$; $\epsilon_{299\text{nm}} = 24,000$ (THF).

261 **4,7-Bis(4-((E)-2-(1H-pyrrol-2-yl)vinyl)phenyl)benzo[c][1,2,5]thiadiazole (2i)**. Compound **2i**
262 was synthesized from 2-vinyl-*N*-Boc pyrrole (**1a**) and 4,7-bis(4-
263 bromophenyl)benzo[c][1,2,5]thiadiazole (**i**)⁶⁹ using **GP1** to give the title compound (127 mg,
264 quantitative) as a dark yellow/brown solid. M.p./d.p. > 250 °C. ¹H NMR (THF-*d*₈, 500 MHz) δ :
265 10.37 (br s, 2H, NH), 8.07 (d, 4H, *J* = 8.5 Hz, ArH), 7.91 (s, 2H, ArH), 7.58 (d, 4H, *J* = 8.5 Hz,
266 ArH), 7.13 (d, 2H, *J* = 16.5 Hz, C=CH), 6.81 (d, 2H, *J* = 16.5 Hz, C=CH), 6.77 (br s, 2H, PyH),
267 6.28 (br s, 2H, PyH), 6.09 (br s, 2H, PyH) ppm. ¹³C NMR (THF-*d*₈, 125 MHz) δ : 155.1, 139.3,
268 136.3, 133.3, 131.9, 130.3, 128.4, 126.4, 122.4, 121.2, 120.3, 110.5, 110.0 ppm. LRMS: 471.2
269 (M+H)⁺; HRMS calculated for C₃₀H₂₃N₄S: 471.1638; found 471.1624. $\epsilon_{447\text{nm}} = 31,000$; $\epsilon_{354\text{nm}} =$
270 52,000 (THF).

271 **4,7-Bis(1-methyl-1H,1'H-[2,2'-bipyrrol]-5-yl)benzo[c][1,2,5]thiadiazole (2j)**. Compound **2j**
272 was synthesized from *N*-Boc-pyrrole-2-boronic acid (**1b**) and 4,7-bis(5-bromo-1-methyl-1H-
273 pyrrol-2-yl)benzo[c][1,2,5]thiadiazole (**j**)⁷⁰ using **GP2**. After cooling to room temperature the
274 reaction mixture was separated between 2:1 diethyl ether:THF (100 mL) and water (100 mL). The
275 aqueous phase was extracted with 2:1 diethyl ether:THF (2 × 100 mL) and the combined organic
276 extracts were washed with water (200 mL) and brine (200 mL), dried over anhydrous magnesium
277 sulfate, and concentrated *in vacuo*. The crude product was washed with 0–20% diethyl
278 ether/hexanes and then further purified using column chromatography on silica eluting with 50%
279 diethyl ether/hexanes to give the title compound (140 mg, 85% yield) as a dark red/purple solid.
280 M.p. 184–187 °C. ¹H NMR (THF-*d*₈, 500 MHz) δ : 10.26 (br s, 2H, NH), 7.64 (s, 2H, ArH), 6.78
281 (br s, 2H, PyH), 6.54 (d, 2H, *J* = 3.5 Hz, PyH), 6.29 (d, 2H, *J* = 3.5 Hz, PyH), 6.26 (br s, 2H, PyH),
282 6.16 (d, 2H, *J* = 2.5 Hz, PyH), 3.68 (s, 6H, 2 × NCH₃) ppm. ¹³C NMR (THF-*d*₈, 125 MHz) δ :
283 155.2, 132.3, 132.1, 128.9, 126.1, 125.4, 118.8, 112.6, 109.3, 108.2, 107.7, 35.1 ppm. LRMS:
284 425.2 (M+H)⁺; HRMS calculated for C₂₄H₂₁N₆S: 425.1543; found 425.1556. $\epsilon_{519\text{nm}} = 11,300$;
285 $\epsilon_{311\text{nm}} = 29,000$ (THF).

286 ***N,N'*-Bis(2-ethylhexyl)-6,6'-Bis(1H-pyrrol-2-yl)isoindigo (2k)**. Compound **2k** was
287 synthesized from *N*-Boc-pyrrole-2-boronic acid (**1b**) and *N,N'*-bis(2-ethylhexyl)-6,6'-
288 dibromoisindigo (**k**)⁷¹ using **GP2** with stirring at 115 °C for 18 h, then 125 °C for an additional
289 5 h. The crude product was purified using column chromatography on silica eluting with 30–60%
290 diethyl ether in hexanes to give the title compound (203 mg, 53% yield) as a dark blue/black solid.
291 M.p. 232–234 °C. ¹H NMR (THF-*d*₈, 500 MHz) δ : 10.63 (br s, 2H, NH), 9.30 (d, 2H, *J* = 8.5 Hz,
292 ArH), 7.16 (dd, 2H, *J* = 8.5, 1.5 Hz, ArH), 7.04 (d, 2H, *J* = 1.5 Hz, ArH), 6.85 (br s, 2H, PyH),
293 6.63 (br s, 2H, PyH), 6.18 (dd, 2H, *J* = 5.5, 2.5 Hz, PyH), 3.79–3.71 (m, 4H, 2 × NCH₂), 2.00–
294 1.95 (m, 2H, 2 × CH), 1.48–1.29 (m, 16 H, 8 × CH₂), 0.97 (t, 6H, *J* = 7.5 Hz, 2 × CH₃), 0.91 (t,
295 6H, *J* = 7.0 Hz, 2 × CH₃) ppm. ¹³C NMR (THF-*d*₈, 125 MHz) δ : 169.5, 146.6, 137.3, 132.9, 131.4,
296 131.2, 121.2, 120.4, 116.7, 110.6, 108.5, 103.5, 44.4, 38.6, 31.5, 29.5, 24.8, 24.0, 14.4, 11.0 ppm.
297 LRMS: 617.4 (M+H)⁺; HRMS calculated for C₄₀H₄₉N₄O₂: 617.3850; found 617.3849. $\epsilon_{578\text{nm}} =$
298 32,800; $\epsilon_{470\text{nm}} = 19,200$; $\epsilon_{310\text{nm}} = 31,700$ (THF).

299 **(E)-5-Styryl-1H-pyrrole-2-carbaldehyde (3a)**.⁷² 2-Styryl pyrrole (**2a**, 53 mg, 0.31 mmol) was
300 dissolved in anhydrous DMF (1.0 mL) with stirring under nitrogen, and the solution was cooled to
301 0 °C in an ice bath. Phosphorous oxychloride (30 μ L, 0.33 mmol), was then added dropwise with

302 continued stirring at 0 °C for 2 hours. 10% (w/v) aqueous potassium carbonate solution (2 mL)
303 was then added, and the reaction mixture was separated between dichloromethane and water. The
304 aqueous phase was extracted with dichloromethane (3 × 10 mL) and the combined organic extracts
305 were washed with water (2 × 40 mL) and brine (30 mL), dried over anhydrous sodium sulfate and
306 concentrated *in vacuo*. The crude product was purified using column chromatography on silica
307 eluting with 20–30% ethyl acetate in hexanes to give the title compound (26 mg, 42% yield) as a
308 light yellow solid. M.p. 141–144 °C. ¹H NMR (CDCl₃, 500 MHz) δ: 9.65 (brs, 1H, NH), 9.49 (s,
309 1H, CHO), 7.49 (d, 2H, *J* = 7.5 Hz, ArH), 7.38 (t, 2H, *J* = 7.5 Hz, ArH), 7.30 (t, 1H, *J* = 7.5 Hz,
310 ArH), 7.07 (d, 1H, *J* = 16.5 Hz, CH=C), 6.99–6.97 (m, 1H, PyH), 6.97 (d, 1H, *J* = 16.5 Hz, CH=C),
311 6.49 (dd, 1H, *J* = 3.5, 2.5 Hz, PyH) ppm. ¹³C NMR (CDCl₃, 125 MHz) δ: 178.7, 139.1, 136.4,
312 133.0, 131.0, 129.0, 128.5, 126.7, 123.0, 117.4, 110.9 ppm. LRMS: 220.1 (M+Na)⁺; HRMS
313 calculated for C₁₃H₁₁NONa: 220.0733; found 220.0734.

314 **5,5'-((1*E*,1'*E*)-1,4-Phenylenebis(ethene-2,1-diyl))bis(1H-pyrrole-2-carbaldehyde) (3b).**
315 Compound **3b** was synthesized from **2b** (130 mg, 0.50 mmol) using **GP3** to give the title
316 compound (135 mg, 85% yield) as a dark yellow solid. M.p./d.p. > 250 °C. ¹H NMR (DMSO-*d*₆,
317 500 MHz) δ: 12.24 (br s, 2H, NH), 9.44 (s, 2H, CHO), 7.52 (s, 4H, ArH), 7.37 (d, 2H, *J* = 16.5
318 Hz, C=CH), 7.13 (d, 2H, *J* = 16.5 Hz, C=CH), 7.03 (dd, 2H, *J* = 2.0, 3.5 Hz, PyH), 6.58 (dd, 2H,
319 *J* = 2.0, 3.5 Hz, PyH) ppm. ¹³C NMR (DMSO-*d*₆, 125 MHz) δ: 178.5, 138.8, 136.3, 133.3, 129.4,
320 126.8, 118.0, 110.5 ppm (one signal missing). LRMS: 315.1 (M-H)⁻; HRMS calculated for
321 C₂₀H₁₅N₂O₂: 315.1139; found 315.1131. ε_{437nm} = 46,000; ε_{413nm} = 59,000 (DMSO).

322 **5,5'-((1*E*,1'*E*)-[1,1'-Biphenyl]-4,4'-diylbis(ethene-2,1-diyl))bis(1H-pyrrole-2-carbaldehyde)**
323 **(3c).** Compound **3c** was synthesized from **2c** (50 mg, 0.15 mmol) using **GP3** to give the title
324 compound (50 mg, 85% yield) as a dark yellow solid. M.p./d.p. > 250 °C. ¹H NMR (DMSO-*d*₆,
325 500 MHz) δ: 12.25 (br s, 2H, NH), 9.44 (s, 2H, CHO), 7.76 (d, 4H, *J* = 8.0 Hz, ArH), 7.60 (d, 4H,
326 *J* = 8.0 Hz, ArH), 7.42 (d, 2H, *J* = 16.5 Hz, C=CH), 7.17 (d, 2H, *J* = 16.5 Hz, C=CH), 7.04 (d, 2H,
327 *J* = 3.3 Hz, PyH), 6.60 (d, 2H, *J* = 3.3 Hz, PyH) ppm. ¹³C NMR (DMSO-*d*₆, 125 MHz) δ: 178.5,
328 138.7, 135.9, 133.2, 129.3, 127.1, 126.9, 126.8, 118.1, 110.4 ppm (one signal missing). LRMS:
329 393.2 (M+H)⁺; HRMS (APCI) calculated for C₂₆H₂₁N₂O₂: 393.1598; found 393.1596. ε_{401nm} =
330 81,000 (DMSO).

331 **5,5'-((1*E*,1'*E*)-Naphthalene-2,6-diylbis(ethene-2,1-diyl))bis(1H-pyrrole-2-carbaldehyde)**
332 **(3d).** Compound **3d** was synthesized from **2d** (60 mg, 0.19 mmol) using **GP3** to give the title
333 compound (54 mg, 76% yield) as a dark yellow solid. M.p./d.p. > 250 °C. ¹H NMR (DMSO-*d*₆,
334 500 MHz) δ: 12.29 (br s, 2H, NH), 9.46 (s, 2H, CHO), 7.93 (d, 2H, *J* = 9.3 Hz, ArH), 7.90 (s, 2H,
335 ArH), 7.75 (d, 2H, *J* = 9.3 Hz, ArH), 7.54 (d, 2H, *J* = 16.5 Hz, C=CH), 7.25 (d, 2H, *J* = 16.5 Hz,
336 C=CH), 7.06 (d, 2H, *J* = 3.9 Hz, PyH), 6.62 (d, 2H, *J* = 3.9 Hz, PyH) ppm. ¹³C NMR (DMSO-*d*₆,
337 125 MHz) δ: 178.6, 138.8, 134.5, 133.4, 132.9, 129.8, 128.6, 126.2, 123.8, 118.6, 110.6 ppm (one
338 signal missing). LRMS: 367.2 (M+H)⁺; HRMS (APCI) calculated for C₂₄H₁₈N₂O₂: 367.1441;
339 found 367.1431. ε_{433nm} = 26,000; ε_{408nm} = 31,000 (DMSO).

340 **5,5'-((1*E*,1'*E*)-Benzo[*c*][1,2,5]thiadiazole-4,7-diylbis(ethene-2,1-diyl))bis(1H-pyrrole-2-**
341 **carbaldehyde) (3e).** Compound **3e** was synthesized from **2e** (50 mg, 0.16 mmol) using **GP3** to
342 give the title compound (57 mg, 97% yield) as a dark red solid. M.p./d.p. > 250 °C. ¹H NMR (THF-
343 *d*₈, 500 MHz) δ: 11.57 (br s, 2H, NH), 9.48 (s, 2H, CHO), 8.13 (d, 2H, *J* = 16.3 Hz, C=CH), 7.68
344 (s, 2H, ArH), 7.64 (d, 2H, *J* = 16.3 Hz, C=CH), 6.94 (br s, 2H, PyH), 6.62 (br s, 2H, PyH) ppm.

345 ¹³C NMR (THF-*d*₈, 125 MHz) δ: 178.5, 154.7, 139.6, 135.4, 130.1, 129.0, 126.5, 124.0, 122.0,
346 111.5 ppm. LRMS: 375.1 (M+H)⁺; HRMS (APCI) calculated for C₂₀H₁₅N₄SO₂: 375.0910; found
347 375.0892. ε_{500nm} = 28,000; ε_{377nm} = 29,000 (DMSO).

348 **5,5'-((1*E*,1'*E*)-Anthracene-9,10-diylbis(ethene-2,1-diyl))bis(1*H*-pyrrole-2-carbaldehyde)**
349 **(3f)**. Compound **3f** was synthesized from **2f** (84 mg, 0.23 mmol) using **GP3** to give the title
350 compound (84 mg, 87% yield) as a dark yellow solid. M.p./d.p. > 250 °C. ¹H NMR (DMSO-*d*₆,
351 500 MHz) δ: 12.51 (br s, 2H, NH), 9.53 (s, 2H, CHO), 8.44–8.42 (m, 4H, ArH), 8.31 (d, 2H, *J* =
352 16.5 Hz, C=CH), 7.60–7.58 (m, 4H, ArH), 7.13–7.12 (m, 2H, PyH), 6.89 (d, 2H, *J* = 16.5 Hz,
353 C=CH), 6.78–6.77 (m, 2H, PyH) ppm. ¹³C NMR (DMSO-*d*₆, 125 MHz) δ: 178.9, 138.3, 133.5,
354 131.9, 128.8, 126.9, 126.1, 126.0, 125.8, 111.1 ppm (one signal missing). LRMS: 417.2 (M+H)⁺;
355 HRMS (APCI) calculated for C₂₈H₂₁N₂O₂: 417.1598; found 417.1581. ε_{431nm} = 19,000; ε_{334nm} =
356 22,000; ε_{306nm} = 20,000; ε_{264nm} = 62,000 (DMSO).

357 **5,5'-((1*E*,1'*E*)-(9*H*-Fluorene-2,7-diyl)bis(ethene-2,1-diyl))bis(1*H*-pyrrole-2-carbaldehyde)**
358 **(3g)**. Compound **3g** was synthesized from **2g** (97 mg, 0.28 mmol) using **GP3** to give the title
359 compound (106 mg, 94% yield) as a brown solid. M.p./d.p. > 250 °C. ¹H NMR (DMSO-*d*₆, 500
360 MHz) δ: 12.25 (br s, 2H, NH), 9.44 (s, 2H, CHO), 7.90 (d, 2H, *J* = 8.0 Hz, ArH), 7.74 (s, 2H,
361 ArH), 7.53 (d, 2H, *J* = 8.0 Hz, ArH), 7.46 (d, 2H, *J* = 16.5 Hz, C=CH), 7.17 (d, 2H, *J* = 16.5 Hz,
362 C=CH), 7.04 (d, 2H, *J* = 3.5 Hz, PyH), 6.59 (d, 2H, *J* = 3.5 Hz, PyH), 4.00 (s, 2H, CH₂) ppm. ¹³C
363 NMR (DMSO-*d*₆, 125 MHz) δ: 178.4, 144.2, 140.8, 139.0, 135.5, 133.2, 130.3, 125.8, 122.6,
364 120.5, 117.5, 110.3, 36.3 ppm (one signal missing). LRMS: 405.2 (M+H)⁺; HRMS (APCI)
365 calculated for C₂₇H₂₁N₂O₂: 405.1598; found 405.1580. ε_{436nm} = 55,000; ε_{412nm} = 70,000 (DMSO).

366 **5,5'-((1*E*,1'*E*)-Pyrene-1,6-diylbis(ethene-2,1-diyl))bis(1*H*-pyrrole-2-carbaldehyde) (3h).**
367 Compound **3h** was synthesized from **2h** (60 mg, 0.16 mmol) using **GP3** to give the title compound
368 (65 mg, 95% yield) as a brown solid. M.p./d.p. > 250 °C. ¹H NMR (DMSO-*d*₆, 500 MHz) δ: 12.56
369 (br s, 2H, NH), 9.51 (s, 2H, CHO), 8.80 (d, 2H, *J* = 9.3 Hz, ArH), 8.60 (d, 2H, *J* = 16.5 Hz, C=CH),
370 8.48 (d, 2H, *J* = 8.0 Hz, ArH), 8.32 (d, 2H, *J* = 8.0 Hz, ArH), 8.27 (d, 2H, *J* = 9.3 Hz, ArH), 7.48
371 (d, 2H, *J* = 16.5 Hz, C=CH), 7.11 (br s, 2H, PyH), 6.70 (br s, 2H, PyH) ppm. ¹³C NMR (DMSO-
372 *d*₆, 125 MHz) δ: 178.8, 139.1, 133.8, 131.3, 130.3, 128.5, 127.6, 125.6, 125.5, 124.7, 123.2, 122.9,
373 120.5, 112.5 ppm (one signal missing). LRMS: 441.2 (M+H)⁺; HRMS (APCI) calculated for
374 C₃₀H₂₁N₂O₂: 441.1598; found 441.1588. ε_{453nm} = 55,000; ε_{332nm} = 38,000; ε_{257nm} = 31,000
375 (DMSO).

376 **5,5'-((1*E*,1'*E*)-(Benzo[*c*][1,2,5]thiadiazole-4,7-diylbis(4,1-phenylene))bis(ethene-2,1-**
377 **diyl))bis(1*H*-pyrrole-2-carbaldehyde) (3i)**. Compound **3i** was synthesized from **2i** (44 mg, 0.11
378 mmol) using **GP3** to give the title compound (113 mg, 92% yield) as a brown solid. M.p./d.p. >
379 250 °C. ¹H NMR (DMSO-*d*₆, 500 MHz) δ: 12.30 (br s, 2H, NH), 9.46 (s, 2H, CHO), 8.11 (d, 2H,
380 *J* = 7.5 Hz, ArH), 8.03 (s, 2H, ArH), 7.70 (d, 2H, *J* = 7.5 Hz, ArH), 7.48 (d, 2H, *J* = 16.0 Hz,
381 C=CH), 7.23 (d, 2H, *J* = 16.0 Hz, C=CH), 7.06 (br s, 2H, PyH), 6.63 (br s, 2H, PyH) ppm. ¹³C
382 NMR (DMSO-*d*₆, 125 MHz) δ: 178.6, 153.4, 138.7, 136.7, 136.1, 133.4, 131.7, 129.6, 129.3,
383 128.1, 126.5, 118.7, 110.6 ppm (one signal missing). LRMS: 527.1 (M+H)⁺; HRMS (APCI)
384 calculated for C₃₂H₂₃N₄SO₂: 527.1536; found 527.1512. ε_{431nm} = 42,000; ε_{373nm} = 53,000 (DMSO).

385 **5,5'-(Benzo[*c*][1,2,5]thiadiazole-4,7-diyl)bis(1'-methyl-1*H*,1'*H*-[2,2'-bipyrrole]-5-**
386 **carbaldehyde) (3j)**. Compound **3j** was synthesized from **2j** (50 mg, 0.12 mmol) using **GP3** and

387 purified using column chromatography over silica eluting with 2:1:2 diethyl ether:THF:hexane to
388 give the title compound (47 mg, 84% yield) as a dark red solid. M.p./d.p. > 250 °C. ¹H NMR
389 (DMSO-*d*₆, 500 MHz) δ: 12.26 (br s, 2H, NH), 9.49 (s, 2H, CHO), 7.78 (s, 2H, ArH), 7.14 (d, 2H,
390 *J* = 3.5 Hz, PyH), 6.82 (d, 2H, *J* = 3.5 Hz, PyH), 6.62 (d, 2H, *J* = 3.5 Hz, PyH), 6.60 (d, 2H, *J* =
391 3.5 Hz, PyH), 3.71 (s, 6H, NMe) ppm. ¹³C NMR (DMSO-*d*₆, 125 MHz) δ: 178.4, 153.5, 133.0,
392 132.8, 132.5, 128.9, 128.1, 124.2, 112.3, 112.2, 110.1, 109.7, 35.1 ppm. LRMS: 481.1 (M+H)⁺;
393 HRMS calculated for C₂₆H₂₁N₆SO₂: 481.1441; found 481.1422. ε_{496nm} = 32,700; ε_{365nm} = 72,400
394 (DMSO).

395 **(*E*)-5,5'-(1,1'-Bis(2-ethylhexyl)-2,2'-dioxo-[3,3'-biindolinylidene]-6,6'-diyl)bis(1H-pyrrole-**
396 **2-carbaldehyde) (3k).** Compound **3k** was synthesized from **2k** (60 mg, 0.10 mmol) using **GP3** to
397 give the title compound (59 mg, 90% yield) as a dark purple/black solid. M.p./d.p. > 250 °C. ¹H
398 NMR (DMSO-*d*₆, 500 MHz) δ: 12.54 (br s, 2H, NH), 9.56 (s, 2H, CHO), 9.04 (d, 2H, *J* = 8.0 Hz,
399 ArH), 7.56 (d, 2H, *J* = 8.0 Hz, ArH), 7.48 (s, 2H, ArH), 7.16 (br s, 2H, PyH), 6.99 (br s, 2H, PyH),
400 3.62–3.55 (m, 4H, NCH₂), 1.91–1.83 (m, 2H, CH), 1.35–1.25 (m, 10H, CH₂), 1.25–1.17 (m, 6H,
401 CH₂), 0.85 (t, 6H, *J* = 6.8 Hz, CH₃), 0.84–0.78 (m, 6H, CH₃) ppm. ¹³C NMR (DMSO-*d*₆, 125
402 MHz) δ: 179.3, 167.6, 145.5, 139.0, 134.5, 134.4, 131.1, 129.4, 122.4, 120.4, 118.8, 110.7, 104.9,
403 43.5, 36.7, 29.8, 27.8, 23.3, 22.6, 13.9, 10.4 ppm. LRMS: 673.4 (M+H)⁺; HRMS calculated for
404 C₄₂H₄₉N₄O₄: 673.3748; found 673.3737. ε_{579nm} = 26,800; ε_{466nm} = 24,200; ε_{331nm} = 29,200
405 (DMSO).

406 **[Ru(3a)(bpy)₂]₂PF₆ complex salt (4a).** Complex salt **4a** was synthesized from ligand **3a** using
407 **GP4** and 1 equiv. *cis*-bis-(2,2'-bipyridine)dichlororuthenium(II) dihydrate for 1 hr to give the
408 corresponding bis(ruthenium(II)) hexafluorophosphate salt **4b** (50 mg, 96% yield) as a black
409 glittery solid following isolation by Millipore filtration. M.p. 170–175 °C. ¹H NMR (CDCl₃, 500
410 MHz) δ: 8.55 (s, 1H, CHO), 8.53 (d, 1H, *J* = 6.0 Hz, ArH), 8.39 (d, 1H, *J* = 8.0 Hz, ArH), 8.36 (t,
411 2H, *J* = 7.0 Hz, ArH), 8.30 (d, 1H, *J* = 8.0 Hz, ArH), 7.99 (t, 1H, *J* = 8.5 Hz, ArH), 7.94 (t, 1H, *J*
412 = 7.0 Hz, ArH), 7.91–7.87 (m, 2H, ArH), 7.85 (t, 1H, *J* = 7.5 Hz, ArH), 7.79 (t, 1H, *J* = 7.5 Hz,
413 ArH), 7.53–7.50 (m, 2H, ArH), 7.40 (t, 1H, *J* = 6.5 Hz, ArH), 7.28–7.21 (m, 3H, ArH), 7.18–7.15
414 (m, 3H, ArH), 6.82 (d, 1H, *J* = 16.5 Hz, CH=C), 6.73 (ad, 2H, *J* = 7.5 Hz, ArH), 6.70 (d, 1H, *J* =
415 4.5 Hz, ArH), 5.50 (d, 1H, *J* = 16.5 Hz, CH=C) ppm. ¹³C NMR (CDCl₃, 125 MHz) δ: 179.6, 159.4,
416 158.3, 158.1, 157.2, 155.0, 153.0, 151.9, 151.7, 150.6, 144.8, 136.8, 136.6, 135.9, 135.1, 132.0,
417 128.6, 128.1, 127.0, 126.9, 126.8, 126.7, 126.3, 125.8, 123.9, 123.5, 123.4, 120.6, 114.6 ppm (two
418 signals missing). LRMS: 610.1 (M)⁺; HRMS calculated for C₃₃H₂₆N₅ORu: 610.1175; found
419 610.1156. ε_{473nm} = 10,900; ε_{346nm} = 27,300; ε_{295nm} = 57,100 (CH₂Cl₂). The corresponding chloride
420 salt **5a** was obtained following **GP5**, after which the reaction mixture was concentrated *in vacuo*
421 and the residue was purified over basic alumina eluting with 10–40% methanol in ethyl acetate to
422 give **5a** (13 mg, 83%) as a red/brown solid. M.p./d.p. > 250 °C. LRMS: 610.1 (M)⁺; PF₆⁻ ion not
423 observed in negative mode.

424 **[Ru₂(3b)(bpy)₄](PF₆)₂ complex salt (4b).** Complex salt **4b** was synthesized from ligand **3b**
425 using **GP4** to give the corresponding bis(ruthenium(II)) hexafluorophosphate salt **4b** (56 mg, 86%
426 yield) as a black glittery solid. M.p./d.p. > 250 °C. ¹H NMR (CD₂Cl₂, 500 MHz) δ: 8.56 (s, 2H, 2
427 × CHO), 8.56–8.55 (m, 2H, ArH), 8.40–8.37 (m, 4H, ArH), 8.32 (d, 2H, *J* = 8.5 Hz, ArH), 8.24
428 (d, 2H, *J* = 8.0 Hz, ArH), 8.00–7.92 (m, 8H, ArH), 7.89–7.82 (m, 4H, ArH), 7.55–7.53 (m, 4H,
429 ArH), 7.44 (t, 2H, *J* = 6.5 Hz, ArH), 7.28–7.20 (m, 6H, ArH), 6.79 (d, 2H, *J* = 16.0 Hz, ArH), 6.70
430 (d, 2H, *J* = 4.0 Hz, ArH), 6.61 (s, 4H, ArH), 5.45 (d, 2H, *J* = 16.0 Hz, ArH) ppm. ¹³C NMR

431 (CD₂Cl₂, 125 MHz) δ : 180.2, 159.7, 158.8, 158.1, 157.6, 155.1, 153.4, 152.5, 152.0, 151.0, 145.3,
432 136.8, 136.5, 136.0, 135.3, 131.5, 127.4, 126.94, 126.86, 126.8, 126.6, 125.8, 124.0, 123.5, 123.4,
433 123.3, 120.94, 120.92, 114.9, 70.8 ppm. LRMS: 571.1 (M/2)⁺ and 145.0 (PF₆)⁻; HRMS calculated
434 for C₆₀H₄₆N₁₀O₂Ru₂: 571.0941; found 571.0917. $\epsilon_{489\text{nm}} = 41,000$; $\epsilon_{377\text{nm}} = 54,000$; $\epsilon_{294\text{nm}} = 112,000$
435 (CH₂Cl₂). The corresponding dichloride salt **5b** was obtained following **GP5** and isolated via
436 Millipore filtration (13 mg, 73%) as a red/brown solid. M.p./d.p. > 250 °C. LRMS: 571.1 (M/2)⁺;
437 PF₆⁻ ion not observed in negative mode.

438 **[Ru₂(3c)(bpy)₄](PF₆)₂ complex salt (4c).** Complex salt **4c** was synthesized from ligand **3c** using
439 **GP4** to give the corresponding bis(ruthenium(II)) hexafluorophosphate salt **4c** (22 mg, 61% yield)
440 as a deep red solid. M.p./d.p. > 250 °C; ¹H NMR (CD₂Cl₂, 500 MHz) δ : 8.59–8.56 (m, 2H, ArH),
441 8.56 (s, 2H, CHO), 8.45 (t, 2H, *J* = 7.3 Hz, ArH), 8.38–8.36 (m, 2H, ArH), 8.32 (d, 2H, *J* = 8.0
442 Hz, ArH), 8.25 (d, 2H, *J* = 8.0 Hz, ArH), 8.10 (t, 2H, *J* = 7.5 Hz, ArH), 7.99–7.95 (m, 6H, ArH),
443 7.91 (d, 2H, *J* = 5.5 Hz, ArH), 7.86–7.83 (m, 2H, ArH), 7.57–7.53 (m, 4H, ArH), 7.49 (d, 4H, *J* =
444 8.3 Hz, ArH), 7.44 (t, 2H, *J* = 6.0 Hz, ArH), 7.40–7.36 (m, 2H, ArH), 7.26 (d, 2H, *J* = 4.5 Hz,
445 PyH), 7.22 (t, 2H, *J* = 6.5 Hz, ArH), 6.87 (d, 2H, *J* = 16.0 Hz, C=CH), 6.81 (d, 4H, *J* = 8.3 Hz,
446 ArH), 6.73 (d, 2H, *J* = 4.5 Hz, PyH), 5.55 (d, 2H, *J* = 16.0 Hz, C=CH), 1.53 (br s, 8H, H₂O) ppm.
447 ¹³C NMR (CD₂Cl₂, 125 MHz) δ : 180.2, 159.6, 158.8, 158.2, 157.7, 155.1, 153.3, 152.6, 152.0,
448 151.1, 145.2, 139.7, 136.7, 136.5, 136.2, 136.1, 136.0, 131.4, 127.3 (2x C) 127.1 (2x C), 126.9 (2x
449 C), 125.9, 124.4, 123.4 (2x C), 123.3, 121.0, 114.7 ppm. LRMS: 609.1 (M/2)⁺ and 145.0 (PF₆)⁻;
450 HRMS calculated for C₆₆H₅₀N₁₀O₂Ru₂: 609.1097; found 609.1101. $\epsilon_{472\text{nm}} = 36,000$; $\epsilon_{430\text{nm}} =$
451 $42,000$; $\epsilon_{374\text{nm}} = 66,000$; $\epsilon_{294\text{nm}} = 106,000$ (CH₂Cl₂). The corresponding dichloride salt **5c** was
452 obtained following **GP5** and isolated via Millipore filtration (11 mg, 72%) as a red/brown solid.
453 M.p./d.p. > 250 °C. LRMS: 609.1 (M/2)⁺; PF₆⁻ ion not observed in negative mode.

454 **[Ru₂(3d)(bpy)₄](PF₆)₂ complex salt (4d).** Complex salt **4d** was synthesized from ligand **3d**
455 using **GP4** to give the corresponding bis(ruthenium(II)) hexafluorophosphate salt **4d** (18 mg, 42%
456 yield) as a deep red solid. M.p./d.p. > 250 °C. ¹H NMR (CD₂Cl₂, 500 MHz) δ : 8.57 (s, 2H, CHO),
457 8.57–8.56 (m, 2H, ArH), 8.51 (dd, 2H, *J* = 4.5, 8.0 Hz, ArH), 8.42 (dd, 2H, *J* = 4.0, 8.0 Hz, ArH),
458 8.31 (d, 2H, *J* = 8.5 Hz, ArH), 8.25 (d, 2H, *J* = 8.0 Hz, ArH), 8.03–7.93 (m, 10H, ArH), 7.86–7.83
459 (m, 2H, ArH), 7.57–7.52 (m, 6H, ArH), 7.45–7.42 (m, 2H, ArH), 7.37–7.33 (m, 2H, ArH), 7.27
460 (d, 2H, *J* = 4.0 Hz, ArH), 7.23–7.21 (m, 4H, ArH), 6.98 (dd, 2H, *J* = 2.0, 16.0 Hz, C=CH), 6.78–
461 6.76 (m, 4H, ArH), 5.59 (dd, 2H, *J* = 5.5, 16.0 Hz, C=CH), 1.53 (br s, 8H, H₂O) ppm. ¹³C NMR
462 (CD₂Cl₂, 125 MHz) δ : 180.3, 159.7, 158.8, 158.2, 157.7, 155.1, 153.4, 152.5, 152.0, 151.0, 145.3,
463 136.7, 136.5, 136.0, 135.8, 134.9, 133.3, 131.9, 128.2, 127.4, 127.2, 126.9 (2x C), 125.84, 125.79,
464 124.8, 124.4, 123.5, 123.4, 123.3, 121.5, 114.9 ppm. LRMS: 596.1 (M/2)⁺ and 145.0 (PF₆)⁻;
465 HRMS calculated for C₆₄H₄₈N₁₀O₂Ru₂: 596.1019; found 596.1005. $\epsilon_{481\text{nm}} = 42,000$; $\epsilon_{437\text{nm}} =$
466 $42,000$; $\epsilon_{380\text{nm}} = 58,000$; $\epsilon_{294\text{nm}} = 116,000$ (CH₂Cl₂). The corresponding dichloride salt **5d** was
467 obtained following **GP5** and isolated via Millipore filtration (7 mg, 78%) as a red/brown solid.
468 M.p./d.p. > 250 °C. LRMS: 596.1 (M/2)⁺; PF₆⁻ ion not observed in negative mode.

469 **[Ru₂(3e)(bpy)₄](PF₆)₂ complex salt (4e).** Complex salt **4e** was synthesized from ligand **3e** using
470 **GP4** to give the corresponding bis(ruthenium(II)) hexafluorophosphate salt **4e** (24 mg, 61% yield)
471 as a deep purple solid. M.p./d.p. > 250 °C. ¹H NMR (CD₂Cl₂, 500 MHz) δ : 8.62 (s, 2H, CHO),
472 8.52–8.50 (m, 2H, ArH), 8.46–8.39 (m, 4H, ArH), 8.32–8.29 (m, 2H, ArH), 8.24–8.22 (m, 2H,
473 ArH), 8.00–7.95 (m, 6H, ArH), 7.91–7.86 (m, 4H, ArH), 7.85–7.81 (m, 2H, ArH), 7.54–7.51 (m,
474 2H, ArH), 7.49 (d, 2H, *J* = 7.0 Hz, ArH), 7.45–7.41 (m, 2H, ArH), 7.34 (dd, 2H, *J* = 2.0, 16.0,

475 C=CH), 7.30 (d, 2H, $J = 5.0$ Hz, ArH), 7.24–7.17 (m, 4H, ArH), 6.93 (s, 2H, ArH), 6.86 (d, 2H, J
476 = 4.5 Hz, ArH), 6.39 (dd, 2H, $J = 2.0, 16.0$, C=CH), 1.54 (br s, 8H, H₂O) ppm. ¹³C NMR (CD₂Cl₂,
477 125 MHz) δ : 180.7, 159.5, 158.8, 158.2, 157.8, 155.4, 153.7, 153.3, 152.6, 151.8, 150.9, 145.9,
478 136.8, 136.5, 136.1, 135.6, 129.1, 128.0, 127.4, 127.3, 127.0, 126.9, 126.8, 125.8, 125.4, 124.2,
479 123.5, 123.31, 123.26, 115.4 ppm. LRMS: 600.1 (M/2)⁺ and 145.0 (PF₆)⁻; HRMS calculated for
480 C₆₀H₄₄N₁₂SO₂Ru₂: 600.0753; found 600.0733. $\epsilon_{525\text{nm}} = 42,000$; $\epsilon_{358\text{nm}} = 40,000$; $\epsilon_{295\text{nm}} = 114,000$
481 (CH₂Cl₂). The corresponding dichloride salt **5e** was obtained following **GP5** and isolated via
482 Millipore filtration (11 mg, 71%) as a brown solid. M.p./d.p. > 250 °C. LRMS: 600.1 (M/2)⁺; PF₆⁻
483 ion not observed in negative mode.

484 [**Ru₂(3f)(bpy)₄](PF₆)₂ complex salt (**4f**). Salt **4f** was synthesized from ligand **3f** using **GP4** to
485 give the corresponding bis(ruthenium(II)) hexafluorophosphate salt **4f** (24 mg, 45% yield) as a
486 deep red solid. M.p./d.p. > 250 °C. ¹H NMR (CD₂Cl₂, 500 MHz) δ : 8.64 (s, 2H, CHO), 8.59 (d,
487 2H, $J = 5.5$ Hz, ArH), 8.36 (d, 2H, $J = 8.0$ Hz, ArH), 8.31–8.25 (m, 4H, ArH), 8.19 (d, 2H, $J = 8.0$
488 Hz, ArH), 8.12–8.08 (m, 2H, ArH), 8.04–8.01 (m, 4H, ArH), 8.00–7.96 (m, 2H, ArH), 7.93–7.89
489 (m, 4H, ArH), 7.81–7.77 (m, 2H, ArH), 7.68 (d, 2H, $J = 16.0$ Hz, C=CH), 7.62–7.59 (m, 2H, ArH),
490 7.52–7.48 (m, 4H, ArH), 7.44–7.42 (m, 4H, ArH), 7.37–7.35 (m, 2H, ArH), 7.18–7.15 (m, 2H,
491 ArH), 6.99–6.95 (m, 2H, ArH), 6.54–6.49 (m, 2H, ArH), 6.10–6.04 (m, 2H, ArH), 5.04 (d, 2H, J
492 = 16.0 Hz, C=CH), 1.54 (br s, 8H, H₂O) ppm. ¹³C NMR (CD₂Cl₂, 125 MHz) δ : 181.0, 158.7,
493 158.2, 157.6, 154.4, 152.5, 152.4, 152.3, 152.00, 151.96, 151.0, 145.1, 136.7, 136.4, 136.3, 133.7,
494 132.4, 131.0, 129.2, 127.5, 127.3, 127.0, 126.8, 126.5, 125.8, 125.7, 125.6, 123.9, 123.5, 123.3,
495 114.5 ppm. LRMS: 621.1 (M/2)⁺ and 145.0 (PF₆)⁻; HRMS calculated for C₆₈H₅₀N₁₀O₂Ru₂:
496 621.1097; found 621.1074. $\epsilon_{508\text{nm}} = 30,000$; $\epsilon_{345\text{nm}} = 34,000$; $\epsilon_{295\text{nm}} = 110,000$ (CH₂Cl₂). The
497 corresponding dichloride salt **5f** was obtained following **GP5** and isolated via Millipore filtration
498 (9 mg, 52%) as a red/brown solid. M.p./d.p. > 250 °C. LRMS: 621.1 (M/2)⁺; PF₆⁻ ion not observed
499 in negative mode.**

500 [**Ru₂(3g)(bpy)₄](PF₆)₂ complex salt (**4g**). Complex salt **4g** was synthesized from ligand **3g** using
501 **GP4** to give the corresponding bis(ruthenium(II)) hexafluorophosphate salt **4g** (39 mg, 66% yield)
502 as a deep red solid. M.p./d.p. > 250 °C. ¹H NMR (CD₂Cl₂, 500 MHz) δ : 8.57 (d, 2H, $J = 5.5$ Hz,
503 ArH), 8.55 (s, 2H, CHO), 8.51 (d, 2H, $J = 8.0$ Hz, ArH), 8.41 (d, 2H, $J = 8.0$ Hz, ArH), 8.31 (d,
504 2H, $J = 8.0$ Hz, ArH), 8.25 (d, 2H, $J = 8.0$ Hz, ArH), 8.07 (t, 2H, $J = 8.0$ Hz, ArH), 7.99–7.94 (m,
505 8H, ArH), 7.86–7.83 (m, 2H, ArH), 7.59–7.53 (m, 6H, ArH), 7.44 (t, 2H, $J = 7.0$ Hz, ArH), 7.40–
506 7.37 (m, 2H, ArH), 7.26 (d, 2H, $J = 4.5$ Hz, ArH), 7.22 (t, 2H, $J = 6.0$ Hz, ArH), 6.93 (d, 2H, $J =$
507 16.5 Hz, C=CH), 6.88 (s, 2H, ArH), 6.85 (d, 2H, $J = 8.0$ Hz, ArH), 6.74 (d, 2H, $J = 4.5$ Hz, ArH),
508 5.57 (dd, 2H, $J = 6.0, 16.5$ Hz, C=CH), 3.81 (s, 2H, CH₂), 1.54 (br s, 8H, H₂O) ppm. ¹³C NMR
509 (CD₂Cl₂, 125 MHz) δ : 179.9, 159.7, 158.8, 158.2, 157.7, 155.3, 153.4, 152.5, 152.0, 151.0, 145.2,
510 144.4, 141.5, 136.7, 136.4, 136.0, 135.9, 135.7, 132.3, 127.3, 127.2, 126.9, 126.7, 125.9, 124.4,
511 123.5, 123.34, 123.26, 122.1, 120.5, 120.4, 120.2, 114.7, 36.6 ppm. LRMS: 615.1 (M/2)⁺ and
512 145.0 (PF₆)⁻; HRMS calculated for C₆₇H₅₀N₁₀O₂Ru₂: 615.1097; found 615.1084. $\epsilon_{477\text{nm}} = 49,000$;
513 $\epsilon_{435\text{nm}} = 54,000$; $\epsilon_{381\text{nm}} = 72,000$; $\epsilon_{294\text{nm}} = 124,000$ (CH₂Cl₂). The corresponding dichloride salt **5g**
514 was obtained following **GP5** and isolated via Millipore filtration (13 mg, 75%) as a red/brown
515 solid. M.p./d.p. > 250 °C. LRMS: 615.1 (M/2)⁺; PF₆⁻ ion not observed in negative mode.**

516 [**Ru₂(3h)(bpy)₄](PF₆)₂ complex salt (**4h**). Complex salt **4h** was synthesized from ligand **3h**
517 using **GP4** to give the corresponding bis(ruthenium(II)) hexafluorophosphate salt **4h** (39 mg, 69%
518 yield) as a deep red solid. M.p./d.p. > 250 °C. ¹H NMR (CD₂Cl₂, 500 MHz) δ : 8.62 (s, 2H, CHO),**

519 8.60 (d, 2H, $J = 5.5$ Hz, ArH), 8.38–8.30 (m, 8H, ArH), 8.27–8.24 (m, 4H, ArH), 8.04–8.03 (m,
520 2H, ArH), 8.02–7.95 (m, 6H, ArH), 7.92–7.91 (m, 2H, ArH), 7.88–7.84 (m, 4H, ArH), 7.77 (t, 2H,
521 $J = 7.5$ Hz, ArH), 7.59–7.56 (m, 4H, ArH), 7.46 (t, 2H, $J = 6.8$ Hz, ArH), 7.33 (d, 2H, $J = 4.5$ Hz,
522 ArH), 7.23 (t, 2H, $J = 6.3$ Hz, ArH), 7.17–7.12 (m, 4H, ArH), 6.94 (d, 2H, $J = 4.5$, ArH), 5.75 (d,
523 2H, $J = 16.0$ Hz, C=CH), 1.53 (br s, 8H, H₂O) ppm. ¹³C NMR (CD₂Cl₂, 125 MHz) δ : 180.6, 159.7,
524 158.8, 158.2, 157.6, 155.3, 153.3, 152.5, 152.0, 151.1, 145.4, 136.8, 136.6, 136.1, 135.3, 131.8,
525 131.0, 128.6, 128.3, 128.0, 127.4, 127.0, 126.9 (2x C), 126.0, 125.5, 125.2, 125.1, 124.2, 124.1,
526 123.8, 123.4, 123.3, 123.0, 114.9 ppm. LRMS: 633.1 (M/2)⁺ and 145.0 (PF₆)⁻; HRMS calculated
527 for C₇₀H₅₀N₁₀O₂Ru₂: 633.1097; found 633.1119. $\epsilon_{511\text{nm}} = 64,000$; $\epsilon_{401\text{nm}} = 40,000$; $\epsilon_{294\text{nm}} = 132,000$
528 (CH₂Cl₂). The corresponding dichloride salt **5h** was obtained following **GP5** and isolated via
529 Millipore filtration (15 mg, 83%) as a red/brown solid. M.p./d.p. > 250 °C. LRMS: 633.1 (M/2)⁺;
530 PF₆⁻ ion not observed in negative mode.

531 [**Ru₂(3i)(bpy)₄](PF₆)₂ complex salt (**4i**). Complex salt **4i** was synthesized from ligand **3i** using
532 **GP4** to give the corresponding bis(ruthenium(II)) hexafluorophosphate salt **4i** (46 mg, 72% yield)
533 as a deep red solid. M.p./d.p. > 250 °C. ¹H NMR (CD₂Cl₂, 500 MHz) δ : 8.59 (s, 2H, CHO), 8.60–
534 8.57 (m, 2H, ArH), 8.40–8.34 (m, 6H, ArH), 8.28 (d, 2H, $J = 8.0$ Hz, ArH), 8.01–7.96 (m, 10H,
535 ArH), 7.86 (at, 8H, $J = 8.3$ Hz, ArH), 7.58–7.55 (m, 4H, ArH), 7.45 (t, 2H, $J = 6.5$ Hz, ArH), 7.34
536 (t, 2H, $J = 6.8$ Hz, ArH), 7.28 (d, 2H, $J = 4.5$ Hz, ArH), 7.23 (t, 2H, $J = 6.5$ Hz, ArH), 6.96–6.91
537 (m, 6H, ArH), 6.77 (d, 2H, $J = 4.0$ Hz, ArH), 5.62 (d, 2H, $J = 16.5$ Hz, C=CH), 1.55 (br s, 4H,
538 H₂O) ppm. ¹³C NMR (CD₂Cl₂, 125 MHz) δ : 180.4, 159.8, 158.7, 158.2, 157.5, 155.0, 154.3, 153.4,
539 152.5, 152.0, 151.1, 145.3, 137.1, 137.0, 136.8, 136.6, 136.0, 135.4, 132.7, 131.3, 129.6 (2x C),
540 128.4, 127.4, 127.1, 126.9, 126.6 (2x C), 125.9, 124.1, 123.44, 123.37 (2x C), 121.6, 114.8 ppm
541 (one signal missing). LRMS: 676.1 (M/2)⁺ and 145.0 (PF₆)⁻; HRMS calculated for
542 C₇₂H₅₂N₁₂SO₂Ru₂: 676.1066; found 676.1039. $\epsilon_{475\text{nm}} = 47,000$; $\epsilon_{358\text{nm}} = 57,000$; $\epsilon_{295\text{nm}} = 122,000$
543 (CH₂Cl₂). The corresponding dichloride salt **5i** was obtained following **GP5** and isolated via
544 Millipore filtration (13 mg, 75%) as a red/brown solid. M.p./d.p. > 250 °C. LRMS: 676.1 (M/2)⁺;
545 PF₆⁻ ion not observed in negative mode.**

546 [**Ru₂(3j)(bpy)₄](PF₆)₂ complex salt (**4j**). Complex salt **4j** was synthesized from ligand **3j** using
547 **GP4** to give the corresponding bis(ruthenium(II)) hexafluorophosphate salt **4j** (30 mg, 62% yield)
548 as a deep red/black solid. M.p./d.p. > 250 °C. ¹H NMR (CD₂Cl₂, 500 MHz) δ : 8.73 (s, 2H, CHO),
549 8.54 (d, 2H, $J = 5.5$ Hz, ArH), 8.36–8.32 (m, 4H, ArH), 8.25–8.22 (m, 4H, ArH), 8.10 (t, 2H, $J =$
550 7.5 Hz, ArH), 8.03 (t, 2H, $J = 7.3$ Hz, ArH), 7.97 (t, 2H, $J = 7.8$ Hz, ArH), 7.80 (t, 2H, $J = 7.8$ Hz,
551 ArH), 7.63–7.59 (m, 2H, ArH), 7.59–7.56 (m, 2H, ArH), 7.55–7.53 (m, 4H, ArH), 7.50 (t, 2H, $J =$
552 6.5 Hz, ArH), 7.42 (s, 2H, ArH), 7.35 (d, 2H, $J = 4.0$ Hz, ArH), 7.16 (t, 2H, $J = 6.5$ Hz, ArH),
553 6.97–6.93 (m, 2H, ArH), 6.43 (dd, 2H, $J = 4.5, 1.0$ Hz, ArH), 5.88 (dd, 2H, $J = 3.5, 5.5$ Hz, ArH),
554 5.46 (t, 2H, $J = 3.0$ Hz, ArH), 2.95 (s, 6H, NMe) ppm. ¹³C NMR (CD₂Cl₂, 125 MHz) δ : 182.4,
555 158.9, 158.5, 158.4, 158.3, 154.4, 152.8, 152.6, 152.2, 150.9, 148.1, 144.7, 136.7, 136.13, 136.07,
556 135.4, 130.6, 130.4, 129.2, 127.2, 126.7, 126.5, 126.2, 125.0, 124.6, 123.30, 123.26, 123.2, 122.9,
557 119.8, 111.9, 110.1, 33.4 ppm. LRMS: 653.1 (M/2)⁺ and 145.0 (PF₆)⁻; HRMS calculated for
558 C₆₆H₅₀N₁₄SO₂Ru₂: 653.1019; found 653.1011. $\epsilon_{509\text{nm}} = 35,000$; $\epsilon_{356\text{nm}} = 35,000$; $\epsilon_{294\text{nm}} = 127,000$
559 (CH₂Cl₂). The corresponding dichloride salt **5j** was obtained following **GP5** with 10:1
560 acetone:hexanes, and isolated via Millipore filtration (8 mg, 93%) as a red/brown solid. M.p./d.p.
561 > 250 °C. LRMS: 653.1 (M/2)⁺; PF₆⁻ ion not observed in negative mode.**

562 **[Ru₂(3k)(bpy)₄](PF₆)₂ complex salt (4k).** Complex salt **4k** was synthesized from ligand **3k**
563 using **GP4** in 9:1 methanol:water for 1 hr to give the corresponding bis(ruthenium(II))
564 hexafluorophosphate salt **4k** (18 mg, 70% yield) as a dark brown/black solid. M.p./d.p. 208–213
565 °C. ¹H NMR (CD₂Cl₂, 500 MHz) δ: 8.76 (s, 2H, CHO), 8.60–8.58 (m, 2H, ArH), 8.51–8.48 (m,
566 2H, ArH), 8.35–8.29 (m, 4H, ArH), 8.22 (d, 2H, *J* = 7.0 Hz, ArH), 8.06–7.98 (m, 8H, ArH), 7.80
567 (t, 2H, *J* = 7.8 Hz, ArH), 7.58–7.55 (m, 2H, ArH), 7.51 (t, 2H, *J* = 6.3 Hz, ArH), 7.45–7.39 (m,
568 4H, ArH), 7.35–7.32 (m, 4H, ArH), 7.17 (t, 2H, *J* = 6.8 Hz, ArH), 6.79–6.71 (m, 2H, ArH), 6.46
569 (d, 2H, *J* = 4.0 Hz, ArH), 6.29–6.18 (m, 4H, ArH), 3.70–3.58 (m, 2H, NCH₂), 3.47–3.33 (m, 2H,
570 NCH₂), 1.69 (br s, 2H, *CH*Et), 1.35–1.17 (m, 16H, CH₂), 0.92–0.81 (m, 12H, CH₃) ppm. ¹³C NMR
571 (CD₂Cl₂, 125 MHz) δ: 182.9, 168.3, 158.9, 158.8, 158.5, 158.2, 157.0, 152.7, 152.3, 152.1, 151.3,
572 145.7, 144.7, 140.2, 136.8, 136.5, 136.1, 135.2, 132.4, 129.2, 127.3, 127.0, 126.6, 126.4, 126.2,
573 125.6, 123.5, 123.4, 123.0, 121.6, 120.8, 118.0, 107.6, 44.3, 37.9, 30.9, 29.0, 24.2, 23.4, 14.2, 10.7
574 ppm (some peaks were observed in duplicate suggesting diastereomeric effects). LRMS: 749.2
575 (M/2)⁺ and 144.9 (PF₆)⁻; HRMS calculated for C₈₂H₇₈N₁₂O₄Ru₂: 749.2173; found 749.2190. ε_{516nm}
576 = 30,100; ε_{377nm} = 32,400; ε_{295nm} = 118,400 (CH₂Cl₂). The corresponding dichloride salt **5k** was
577 obtained following **GP5** with 10:1 acetone:hexanes, stirring at room temperature for 30 min. The
578 reaction mixture was then concentrated *in vacuo* and the residue purified over neutral alumina,
579 eluting with 3–8% methanol in dichloromethane to give **5k** (14 mg, 84%) as a dark brown/black
580 solid. M.p./d.p. > 250 °C. LRMS: 749.2 (M/2)⁺; PF₆⁻ ion not observed in negative mode.

581

582 2.4 Methods

583 2.4.1 Photophysical measurements

584 Absorption and emission spectra were collected from dilute solutions (5 μM) in spectroscopic-
585 grade MeCN. Oxygen-free samples were prepared by sparging 4-mL solutions of PSs in long-neck
586 quartz cuvettes (Luzchem SC-10L) with argon (30 min, 50 ±10 mmHg) prior to spectroscopic
587 measurements. Luminescence quantum yields (Φ_{em}) were calculated according to eqn. 1 (*s* =
588 sample, *r* = reference) using [Ru(bpy)₃](PF₆)₂ as the reference (Φ_{em} = 0.012 in aerated MeCN,⁷³
589 0.062 in deoxygenated MeCN,²¹ and 0.38 at 77 K in 4:1 v/v ethanol-methanol glass²¹):

$$\Phi_s = \Phi_r \left(\frac{I_s}{A_s} \right) \left(\frac{A_r}{I_r} \right) \left(\frac{\eta_s^2}{\eta_r^2} \right) \quad (1)$$

590 Singlet oxygen quantum yields (Φ_Δ) were also estimated using eqn. 1 with [Ru(bpy)₃](PF₆)₂ as
591 the standard (Φ_Δ = 0.57 in aerated MeCN).⁷⁴ Absorption spectra were recorded using a Jasco V-
592 530 spectrophotometer, and luminescence spectra were collected using a PTI Quantamaster
593 equipped with a standard photomultiplier tube (K170B) and a Hamamatsu R5509-42
594 photomultiplier tube for NIR detection (<1400 nm). Luminescence lifetimes were measured using
595 a PTI LaserStrobe system incorporating a nitrogen-dye laser (GL-3300/GL-301) integrated with
596 an R928 stroboscopic detector. Emission was also probed by gated methods using a pulsed xenon
597 flash lamp and gated detector. Exponential curve fitting and corrections to the wavelength-
598 dependence of lamp output and detector response were done with PTI Felix32 software.

599 2.4.2 HL-60 cell culture

600 HL-60 cells (ATCC CCL-240) were cultured at 37 °C under 5% CO₂ in RPMI 1640 media
601 (Mediatech Media MT-10-040-CV) supplemented with 20% FBS (PAA Laboratories, A15-701)

602 and were passaged 3–4 times per week using standard aseptic technique. Cultures were started at
603 200,000 cells mL⁻¹ in 25-cm² tissue culture flasks and were subcultured when growth reached
604 approximately 1×10⁶ cells mL⁻¹. Cytotoxicity and photocytotoxicity assays were performed on
605 cells of mid-passage number (8–25 passages).

606 2.4.3 HL-60 cytotoxicity and photocytotoxicity assays

607 Cell viability experiments were performed in 96-well microtiter plates (Corning Costar, Acton,
608 MA) with each PS dose tested in triplicate. Microtiter plates were prepared in duplicate as follows
609 for dark and light treatments, respectively. Phosphate buffered saline (PBS) (200 μL)
610 supplemented with 2.68 mM potassium chloride, 1.47 mM potassium phosphate monobasic, 137
611 mM sodium chloride, and 8.10 mM sodium phosphate dibasic was added to non-sample wells
612 along the periphery of the plate to minimize evaporation from the inner sample wells. HL-60 cells
613 growing in log phase (approximately 8×10⁵ cells) were transferred in 50-μL aliquots to inner wells
614 containing 25 μL of warm complete culture medium and placed in a 37 °C, 5% CO₂ water-jacketed
615 incubator (Thermo Electron Corp., Forma Series II, Model 3110, HEPA Class 100) for 1 h to
616 equilibrate. Prewarmed aliquots (25 μL) of serially diluted ruthenium compounds (in
617 supplemented PBS solution) were added to the microplate sample wells, and the microplates were
618 incubated at 37 °C under 5% CO₂. A light treatment was delivered to one of the microplates at 1
619 or 16 h (drug-to-light interval (*t_{hv}*)) with unfiltered light (400–700 nm, 27.8 mW cm⁻²) from a 190
620 W BenQ MS510 overhead projector, visible light from a Luzchem LZC-4X photoreactor equipped
621 with 14 LES-Vis-01 bulbs (7.8 mW cm⁻²), or with red light (625 nm, 28.7 mW cm⁻²) from an LED
622 array (Photodynamic, Inc.). The irradiation time was varied to yield energy densities ranging from
623 5 to 100 J cm⁻². Both dark and PDT-treated microplates were incubated for a further 48 h at which
624 point prewarmed, 10-μL aliquots of Alamar Blue reagent (Life Technologies DAL 1025) were
625 added to all sample wells. Both microplates were incubated for 15–16 h at 37 °C under 5% CO₂
626 after addition of the indicator dye. Cell viability was determined based on the ability of the Alamar
627 Blue redox indicator to be metabolically converted to a fluorescent dye by live cells. Fluorescence
628 was quantified with a Cytofluor 4000 fluorescence microplate reader with the excitation filter set
629 at 530 ± 25 nm and emission filter set at 620 ± 40 nm. EC₅₀ values (effective concentration for
630 reducing cell viability to 50%) for cytotoxicity (dark microplates) and photocytotoxicity (light
631 microplates) were calculated from sigmoidal fits of the dose-response curves using Graph Pad
632 Prism 6.0 according to eqn. 2, where *y_i* and *y_f* are the initial and final fluorescence signal intensities,
633 respectively.

$$634 \quad \gamma = \gamma_i + \frac{\gamma_i - \gamma_f}{1 + 10^{(\log EC_{50} - x) \times (\text{Hill slope})}} \quad (2)$$

635
636 For cells growing in log phase and of similar passage number, EC₅₀ values were reproducible to
637 within ±25% in the submicromolar regime; ±10% below 10 μM; and ±5% above 10 μM.
638 Photocytotoxicity indices (PIs), a measure of the therapeutic window, were calculated from the
639 ratio of dark to light EC₅₀ values obtained from the dose–response curves.

640 2.4.4 HL-60 multicellular tumor spheroid cytotoxicity and photocytotoxicity assays

641 Multicellular 3D spheroids of HL-60 human promyelocytic leukemia cells (ATCC CCL-240)
642 were grown using a modified liquid overlay technique.⁷⁵ Briefly, 5×10⁴ cells in 200 μL RPMI
643 1640 (Mediatech Media MT-10-040-CV) supplemented with 20% FBS (PAA Laboratories, A15-
644 701) were delivered to the inner wells of 96-well microtiter plates (Corning Costar, Acton, MA)
645 coated with 1.5% agarose (Fisher Bioreagents, BP1356-100). The outer wells along the periphery

646 contained 200 μL Dulbecco's phosphate buffered saline (VWR International, CA45000-434) to
647 minimize evaporation from sample wells. One dark plate and a light plate for each irradiation
648 condition were prepared and maintained at 37 $^{\circ}\text{C}$ under 5% CO_2 incubation (Thermo Electron
649 Corp., Forma Series II, Model 3110, HEPA Class 100). The morphological structures and sizes of
650 HL-60 spheroids were confirmed at 40 \times total magnification using a Nikon inverted microscope
651 (Eclipse TE2000U). When the diameter of the spheroids reached approximately 600 μm (72–96
652 h), they were dosed with serially diluted PSs in 25 μL aliquots to yield final PS concentrations of
653 1 nM to 300 μM in the assay. Light plates were irradiated with visible light (7.8 mW cm^{-2} , 28 J
654 cm^{-2}) from a photoreactor (Luzchem LZC-4X), or with 625 nm light (32 mW cm^{-2} , 100 J cm^{-2})
655 from an LED array made in-house at a PS-to-light interval of 16 h. Dark assay plates were
656 maintained at 37 $^{\circ}\text{C}$ under 5% CO_2 incubator while light plates were irradiated. All plates were
657 incubated for an additional 48 h prior to adding 10 μL aliquots of Alamar blue reagent (Life
658 Technologies DAL 1025) to each well to assess cell viability. Fluorescence from the sample wells
659 was quantified 16 h post Alamar Blue addition using methods described for planktonic cultures
660 (below).

661 **2.4.5 Bacterial culture**

662 *S. mutans* (ATCC 25175) and *S. aureus* (ATCC 25923) cultures were started by suspending half
663 of the commercially-obtained freeze-dried pellets in 2 mL of tryptic soy broth (TSB) and
664 incubating for 24 h at 37 $^{\circ}\text{C}$. The bacterial cultures were pelleted, suspended in 5 mL of fresh TSB,
665 and aliquoted (0.5 mL) to 1.5-mL microfuge tubes containing 0.5 mL 70% glycerol in water. These
666 cultures were mixed thoroughly and stored at -80°C .

667 **2.4.6 Bacterial survival assays**

668 Photodynamic inactivation (PDI) of *S. mutans* and *S. aureus* growing as planktonic cultures was
669 probed using a standard broth microdilution method.⁷⁶ A standard curve of McFarland barium
670 sulfate standards 0.5, 1, 2, 3, 4, and 5 was made, according to a standard method,^{76,77} representing
671 approximately 1.5, 3, 6, 9, 12, 15 $\times 10^8$ bacterial concentration (CFU mL^{-1}). The absorbance values
672 of the barium sulfate standards (562 nm) was measured, the equation of the trendline was
673 extrapolated, and this was used to quantify the approximate bacterial concentration. On
674 experimental days, a bacterial stock solution was prepared by transferring several bacterial
675 colonies to 2–3 mL sterile water, vortexing well to mix, then reading the absorbance at 562 nm in
676 order to determine the approximate bacterial concentration. An inoculum dilution was then made
677 from the stock at 1×10^6 CFU mL^{-1} (relative to the established trendline of barium sulfate
678 standards) in fresh TSB. Dark and light experiments were each performed in duplicate in 96-well
679 microplates (Corning Costar 3595), where outer wells along the periphery contained 200 μL of
680 sterile distilled water to prevent evaporation. Cell-free control wells received 100 μL TSB, while
681 control cell wells and sample wells received 100 μL stock bacterial solution ($\sim 1 \times 10^6$ CFU mL^{-1}).
682 The plates were then placed in a 37 $^{\circ}\text{C}$ incubator for at least 30 min to equilibrate.

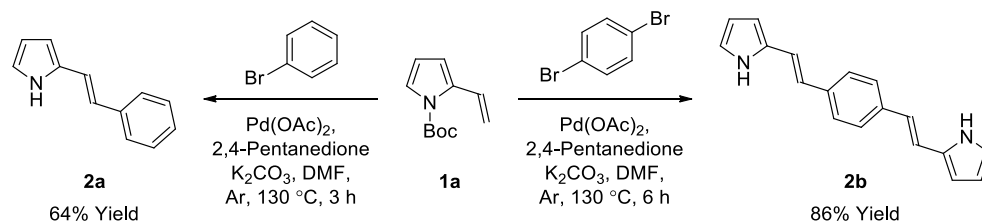
683 Serial dilutions of aqueous stock solutions of the Ru compounds were prepared in
684 microcentrifuge tubes in TSB at 2X the concentration needed (final concentrations in the wells
685 were 0.1 nM, 1 nM, 10 nM, 100 nM, 0.1 μM , 1 μM , 10 μM , and 50 μM). Prewarmed 100 μL
686 aliquots of compounds were added to the sample wells (prewarmed TSB to the controls) and final
687 assay volumes were 200 μL (final bacterial concentration $\sim 5 \times 10^5$ CFU mL^{-1}). The PS-to-light
688 interval was 1 hr. Dark treatment microplates were wrapped in foil and placed in a dark drawer,
689 while PDI-treated microplates were irradiated with visible light (400–700 nm, 40 ± 0.8 mW cm^{-2})
690 using a 190 W BenQ MS510 overhead projector or with red light (625 nm, 35 ± 1.3 mW cm^{-2})

691 from an LED array (Photodynamic Inc.). The irradiation time was 42 min and 48 min respectively,
692 to yield light doses of approximately 100 J cm⁻². Both dark and PDT-treated microplates were
693 incubated overnight. The sample wells were carefully pipetted up and down to mix well and the
694 absorbance at 562 nm was measured for all microplates with a BioTek EL800 plate reader. MIC₅₀
695 values (the minimum inhibitory concentration at which ≥ 50% of the bacteria is inhibited) for
696 antibiotic (dark) and antimicrobial PDI (light) activity were calculated from sigmoidal fits of the
697 dose response curves using Graph Pad Prism 6.0 according to eq. 2 (above), where y_i and y_f are
698 the initial and final absorbance intensities.
699

700 3. RESULTS AND DISCUSSION

701 3.1 Synthesis and Characterization

702 We have previously reported the first synthesis of heteroleptic pyrrolyl/2,2'-bipyridyl complexes
703 of ruthenium (II).⁶⁷ Considering the high stability and unusual UV/vis properties of these mono-
704 ruthenium complexes, we now explore the synthesis and properties of symmetric bis(ruthenium)
705 complexes of this type, with the goal of determining the effect of varying the extent of conjugation
706 in these bis[Ru(II)-pyrrolide] triads. Initial studies concerned the design and synthesis of a mono-
707 pyrrolic ligand bearing extended conjugation, with intent to optimize the synthetic protocol.^{67,78}
708 As such, *N*-Boc-2-vinyl pyrrole (**1a**)⁷⁹ was synthesized in a two-step procedure from 2-formyl
709 pyrrole and, following a modified procedure,⁸⁰ was successfully employed as a Heck substrate
710 with bromobenzene, providing the *in situ*-deprotected styryl-pyrrole **2a** in good yield (64%,
711 Scheme 1). Employing 1,4-dibromobenzene as the aryl halide along with 2 equivalents of vinyl-
712 pyrrole **1a** resulted in the conjugated, symmetric bis(pyrrole) **2b** in high yield (86%).



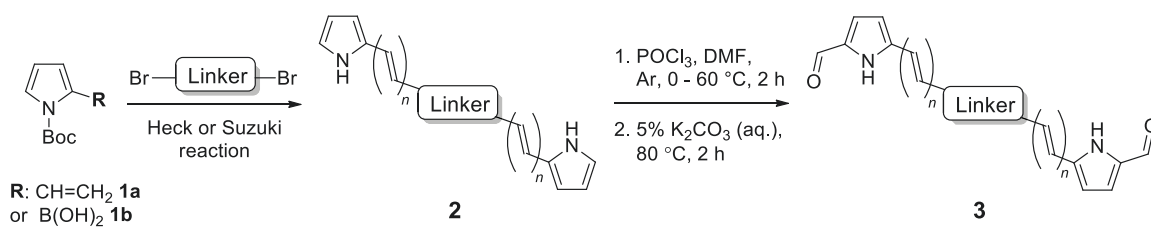
713

714 Scheme 1. Synthesis of conjugated pyrrole **2a** and bis(pyrrole) **2b** via Heck reaction

715 We then examined the scope of dibromoarene substrates in the double Heck reaction with vinyl
716 pyrrole **1a** (Table 1). A variety of linkers were selected for study, including bicyclic (entries 3 and
717 4), heterocyclic (entry 5), polycyclic compounds (entries 6–8), and linkers featuring extended
718 conjugation (entries 9–11). The majority of substrates examined were well tolerated, giving
719 bis(pyrrole)s **2b–i** in excellent isolated yields (86–100%). Bithiophene, pyrazine and binaphthyl
720 linkers were unsuccessful in this synthetic screen, as were extended linkers **j** and **k**. A double
721 Suzuki reaction with *N*-Boc-pyrrole-2-boronic acid (**1b**) was subsequently investigated for linkers
722 **j** and **k**, whereupon conditions were developed to generate the corresponding bis(pyrrole)s **2j** and
723 **2k** in yields of 85 and 53%, respectively (entries 10 and 11).

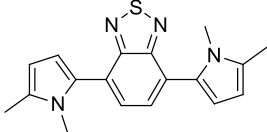
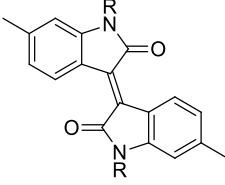
724

725

Table 1. Synthesis of a novel series of bis(pyrrolic) ligands (**3a–3k**)

726

Entry	Pyrrole	Linker	Structure	<i>n</i>	Yield of 2 (%) ^a	Yield of 3 (%) ^a
1	1a	a		1	64 (2a) ^b	86 (3a) ^f
2	1a	b		1	86 (2b) ^c	85 (3b) ^g
3	1a	c		1	94 (2c) ^c	85 (3c) ^g
4	1a	d		1	97 (2d) ^c	76 (3d) ^g
5	1a	e		1	91 (2e) ^c	97 (3e) ^g
6	1a	f		1	97 (2f) ^c	87 (3f) ^g
7	1a	g		1	100 (2g) ^c	94 (3g) ^g
8	1a	h		1	100 (2h) ^c	95 (3h) ^g
9	1a	i		1	100 (2i) ^c	92 (3i) ^g

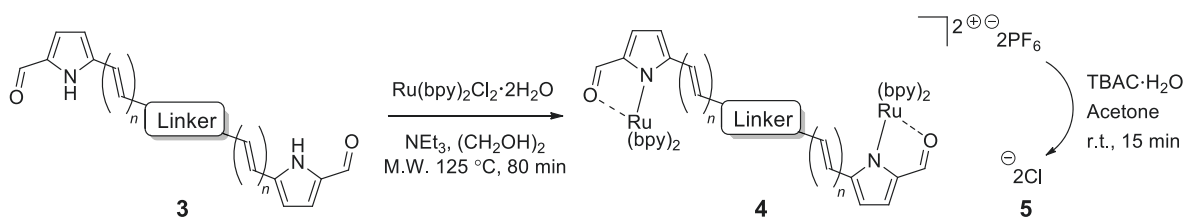
10	1b	j		0	85 (2j) ^d	84 (3j) ^g
11	1b	k	 R = 2-Et-hexyl	0	53 (2k) ^{d,e}	90 (3k) ^g

727 ^aIsolated Yield; ^bHeck Reaction conditions: 1 equiv. **1a**, Pd(OAc)₂, 2,4-pentanedione, K₂CO₃,
728 DMF, Ar, 130 °C, 3 h; ^cHeck Reaction, 2 equiv. **1a**, 6 h; ^dSuzuki Reaction conditions: Pd(PPh₃)₄,
729 K₂CO₃, DMF, 110 °C, 24 h; ^eSuzuki Reaction, 115 °C for 18 h then 125 °C for 5 h; ^fVilsmeier
730 Reaction, 1 equiv. POCl₃; ^gVilsmeier Reaction, 2 equiv. POCl₃.

731 Using mono-pyrrole **2a** as a model substrate, Vilsmeier-Haack formylation was found to be
732 successful in installing an α -formyl group,^{81,82} providing bidentate ligand **3a** in high yield (86%,
733 Table 1, entry 1). Bis(pyrrole)s **2b–2k** were subsequently subjected to Vilsmeier-Haack
734 formylation conditions,⁸³ employing 2 equivalents of phosphoryl chloride, whereby the
735 corresponding bis(bidentate) ligands **3b–3k** were isolated in good to excellent yields (76–97%,
736 entries 2–11) following isolation by precipitation in water.

737 Mono-pyrrolic ligand **3a** was again used as a model substrate for ruthenium complexation, using
738 a previously reported microwave-promoted procedure,^{67,84} whereupon heteroleptic
739 [Ru(**3a**)(bpy)₂]PF₆ complex salt **4a** was isolated following treatment with aqueous ammonium
740 hexafluorophosphate (96%, Table 2, entry 1). Complexation of bis(bidentate) ligands **3b–3j**, using
741 2 equivalents of [Ru(bpy)₂Cl₂]·2H₂O and slightly modified reaction conditions, was successful in
742 generating the corresponding bis(ruthenium) complex salts **4b–4j**, (42–86%, entries 2–10), which
743 were purified using column chromatography on neutral alumina. Difficulties were encountered
744 with ligand **3k**, which underwent complexation and concomitant reduction of the central double
745 bond of isoindigo linker **k**. This was thought to be an effect of the ethylene glycol solvent, which
746 is known to oxidize during heating in air to generate the reductant glycolaldehyde.⁸⁵ Altering the
747 reaction solvent to 9:1 methanol:water overcame this problem and allowed for isolation of the
748 desired complex salt **4k** (70%, entry 11). For the purpose of assessing the photobiological activity
749 of each bis[Ru(II)-pyrrolide] triad, salt conversion of the hexafluorophosphate salts (**4a–4k**) to the
750 water-soluble chloride salts (**5a–5k**) was carried out by treatment with tetrabutylammonium
751 chloride (TBAC) in acetone.⁸⁶

752

Table 2. Bis(Ruthenium) complexation of ligands **3b–3k**

753

Entry	Linker	<i>n</i>	Yield of 4 (%) ^a	Yield of 5 (%) ^a
1	a	1	96 (4a) ^b	83 (5a)
2	b	1	86 (4b) ^c	73 (5b)
3	c	1	61 (4c) ^c	72 (5c)
4	d	1	42 (4d) ^c	78 (5d)
5	e	1	61 (4e) ^c	71 (5e)
6	f	1	45 (4f) ^c	52 (5f)
7	g	1	66 (4g) ^c	75 (5g)
8	h	1	69 (4h) ^c	83 (5h)
9	i	1	72 (4i) ^c	75 (5i)
10	j	0	62 (4j) ^c	93 (5j) ^c
11	k	0	70 (4k) ^{c,d}	84 (5k) ^c

754 ^aIsolated yield; ^b1 equiv. $\text{Ru}(\text{bpy})_2\text{Cl}_2 \cdot 2\text{H}_2\text{O}$ with reaction time of 60 min; ^c2 equiv.
 755 $\text{Ru}(\text{bpy})_2\text{Cl}_2 \cdot 2\text{H}_2\text{O}$; ^dReaction solvent 9:1 Methanol:water; ^eReaction solvent 10:1
 756 acetone:hexanes.

757 3.2 Spectroscopic Properties

758 The MeCN-soluble PF_6^- salts of the complexes (**4a–k**) were used for all spectroscopic
 759 measurements, while the water-soluble Cl^- salts of the complexes (**5a–k**) were used for biological
 760 studies. The reason the MeCN was used as the solvent of choice for spectroscopy (instead of water
 761 or other aqueous solution) is that the water quenches the $^1\text{O}_2$ emission, precluding accurate

762 determination of the upper limit for $^1\text{O}_2$ quantum yields⁸⁷ and because MeCN is the solvent used
763 in many published spectroscopic studies.

764 3.2.1 Absorption

765 The electronic absorption properties of bis[Ru(II)-pyrrolide] triads **4b–k** (and their
766 corresponding ligands) and mononuclear **4a** were investigated in MeCN (Figure 1a–c, Table 1)
767 and analyzed in the context of the well-studied Ru(II) polypyridyl complexes.²¹ Ru(II) polypyridyl
768 complexes such as $[\text{Ru}(\text{bpy})_3]^{2+}$ typically display absorption spectra that are characterized by two
769 distinct regions in the UV and visible, respectively: (i) intense and sharp bands corresponding to
770 singlet intraligand $^1\pi\pi^*$ transitions below 300 nm that are localized to the polypyridyl ligands, and
771 (ii) much broader, lower-intensity bands corresponding to singlet metal-to-ligand charge transfer
772 ($^1\text{MLCT}$) transitions between 400 and 500 nm that involve charge transfer from the Ru($d\pi$) orbitals
773 to the π^* orbitals of the ligand(s). While the Ru(II) complexes in our study contain two polypyridyl
774 ligands, the third ligand is an extremely π -delocalized system that in some cases has significant
775 intraligand charge transfer (ILCT) character due to highly polarizable groups (e.g., **3e**, **3j–k**). In
776 addition, with respect to each Ru(II) center in the bis[Ru(II)-pyrrolide] triad, this symmetric third
777 ligand is further chelated to the second Ru(II) center which could alter further the character of
778 these transitions. It was expected that the absorption spectra of the target complexes would show
779 contributions from these novel ligands that would be influenced by their proximities to the two
780 Ru(II) metal centers.

781 The absorption spectra of the free ligands are shown in Figure 1a. For those ligands derived from
782 (poly)cyclic aromatic hydrocarbon linkers (**3b–d**, **3f–h**), the longest wavelength absorption
783 maxima mirrored the $^1\pi\pi^*$ transitions characteristic of the linker but with bathochromic shifts and
784 contributions arising from extended π -conjugation with the vinyl-appended 2-formyl pyrrolides.
785 For example, free pyrene has a longest-wavelength absorption maximum just below 350 nm,⁸⁸
786 whereas **3h**, with pyrene as the linker, had its longest-wavelength absorption maximum near 448
787 nm, with a shoulder at 489 nm (≥ 100 nm red-shift relative to free pyrene). Notably, this significant
788 bathochromic shift places the spectral window of the $^1\pi\pi^*$ transition of ligand **3h** in a similar
789 position as the $^1\text{MLCT}$ transition of $[\text{Ru}(\text{bpy})_3]^{2+}$ ($\lambda_{\text{max}}=448$ nm). The longest-wavelength
790 absorption maxima of **3e** and **3j–k**, with predicted ILCT contributions, are even more red-shifted,
791 appearing at wavelengths ≥ 500 nm ($\lambda_{\text{max}}=593$ nm for **3k**). It was anticipated that chelation of these
792 unique π -expanded ligands to Ru(II) to form the bis[Ru(II)-pyrrolide] triads would further widen
793 the visible spectral window and lead to enhanced molar extinction coefficients, especially at the
794 longer wavelengths.

795 The UV/Vis absorption spectrum of our previously reported 2-formyl pyrrolide Ru(II) complex
796 **6**,⁶⁷ representative of the core mononuclear N,O-coordinated system used in the triads but without
797 extended conjugation, is compared to $[\text{Ru}(\text{bpy})_3]^{2+}$, mononuclear **4a**, and bis[Ru(II)-pyrrolide] **4b**
798 in Figure 1b. Complex **6** was the first published example of a heteroleptic pyrrolide/2,2'-bipyridyl
799 Ru(II) complex. This simple mononuclear construct displays continuous absorption between 200
800 and 600 nm, with a longest-wavelength absorption maximum near 528 nm for the $^1\text{MLCT}$
801 transition, which is approximately 80 nm longer than that for $[\text{Ru}(\text{bpy})_3]^{2+}$. Red-shifts of almost
802 100 nm for the lowest-energy $^1\text{MLCT}$ transitions (relative to the corresponding Ru(II) systems
803 containing neutral diimine ligands) agrees with what we have previously observed for Ru(II)
804 complexes bearing anionic cyclometalating ligands, such as thionoester-substituted pyrrolides and
805 deprotonated phenylpyridines.^{55,57,67,78} Presumably, this shift of the $^1\text{MLCT}$ absorption band is a

806 direct result of a concomitant increase in the energy of the Ru($d\pi$) orbitals arising from the strong
807 N- σ (η^1) donation of the pyrrolide nitrogen.

808 The styryl substituted pyrrolide complex (**4a**) led to significant absorption past 500 nm ($\epsilon_{510} =$
809 $1.1 \times 10^4 \text{ M}^{-1} \text{ cm}^{-1}$) and doubled the extinction coefficients in this region compared to **6** (Figure
810 1b). The slight blue-shift of about 13 nm for the longest-wavelength absorption maximum for **4a**
811 could reflect the enhanced conjugation of the pyrrolide ligand and weaker N- σ (η^1) bonding to the
812 Ru(II) center. Nevertheless, the extended conjugation provided by the styryl group in combination
813 with the relatively strong N- σ donation of the N,O pyrrolide resulted in a Ru(II) complex that
814 absorbs green light ten times more strongly than the related $[\text{Ru}(\text{bpy})_3]^{2+}$ complex. In support of
815 our hypothesis that these properties could be improved further, incorporation of two metal
816 chromophores into a triad via two terminal 2-formylpyrrolyl ligands tethered to a central benzene
817 linker through alkenyl groups (**4b**) resulted in a four-fold increase in the longest wavelength
818 absorption maximum in comparison to its mononuclear counterpart **4a**, and 40-fold relative to the
819 parent $[\text{Ru}(\text{bpy})_3]^{2+}$.

820 The absorption spectrum of the bis[Ru(II)-pyrrolide] complex **4b** appeared to be more than a
821 simple linear combination of two mononuclear fragments and the free organic ligand, thereby
822 suggesting that the two metal centers are in conjugative communication mediated by the shared
823 organic linker. This notion is supported by the observation that the longest-wavelength absorption
824 maximum measured for the corresponding complex with a biphenyl linker (**4c**), which most likely
825 adopts a nonplanar dihedral angle and decouples the two metal centers, is blue-shifted and of
826 reduced intensity relative to both **4a** and **4b**. The other explored linkers can be structurally grouped
827 as follows: polycyclic aromatics (**4d**, **4f-h**), heterocycles based on benzothiadiazole (**4e**, **4i-j**), or
828 isoindigo (**4k**). Of all of the complexes, the pyrenyl linker (**4h**) exhibited the most intense
829 transitions at its longest-wavelength absorption maximum, while the benzothiadiazole (**4e**) and
830 isoindigo (**4k**) linkers yielded the longest-wavelength absorption maxima overall (albeit of
831 reduced intensity relative to **4h**). The absorption spectra of mononuclear **4a** and the ten bis[Ru(II)-
832 pyrrolide] complexes are compared in Figure 1c.

833 Generally, complexation of the respective novel ligand **3** to two Ru(II) centers to produce the
834 bis[Ru(II)-pyrrolide] triads **4** resulted in both a widening of the visible absorption window as well
835 as a noticeable hyperchromic shift at these wavelengths for all bis[Ru(II)-pyrrolide] triads except
836 for **4i** and **4j**. The longest-wavelength absorption bands in **4i** were very similar to **3i**, and in **4j**, the
837 free ligand was more absorptive at the longer wavelengths despite what appeared to be a longer
838 wavelength absorption maximum for its complex. Notably, for the benzothiadiazoles (**4e**, **4i-j**),
839 the groups on either side of the benzothiadiazole had a marked impact on the longest wavelength
840 transitions. For example, vinyl groups directly attached to the central benzothiadiazole group (**4e**)
841 led to a longest wavelength absorption maximum near 615 nm, which was among the longest in
842 the entire series. Adding phenyl groups between the benzothiadiazole and the vinyl groups (**5i**) or
843 replacing the vinyl groups with *N*-methyl pyrrole groups shifted these bands hypsochromically by
844 ≥ 100 nm. Clearly, there is much to be learned from these SARs and what they suggest in terms of
845 the polarizabilities and CT characters of the ligands and their resulting bis[Ru(II)-pyrrolide]
846 complexes, but the purpose of the present investigation was to provide a very general outline of
847 these observations.

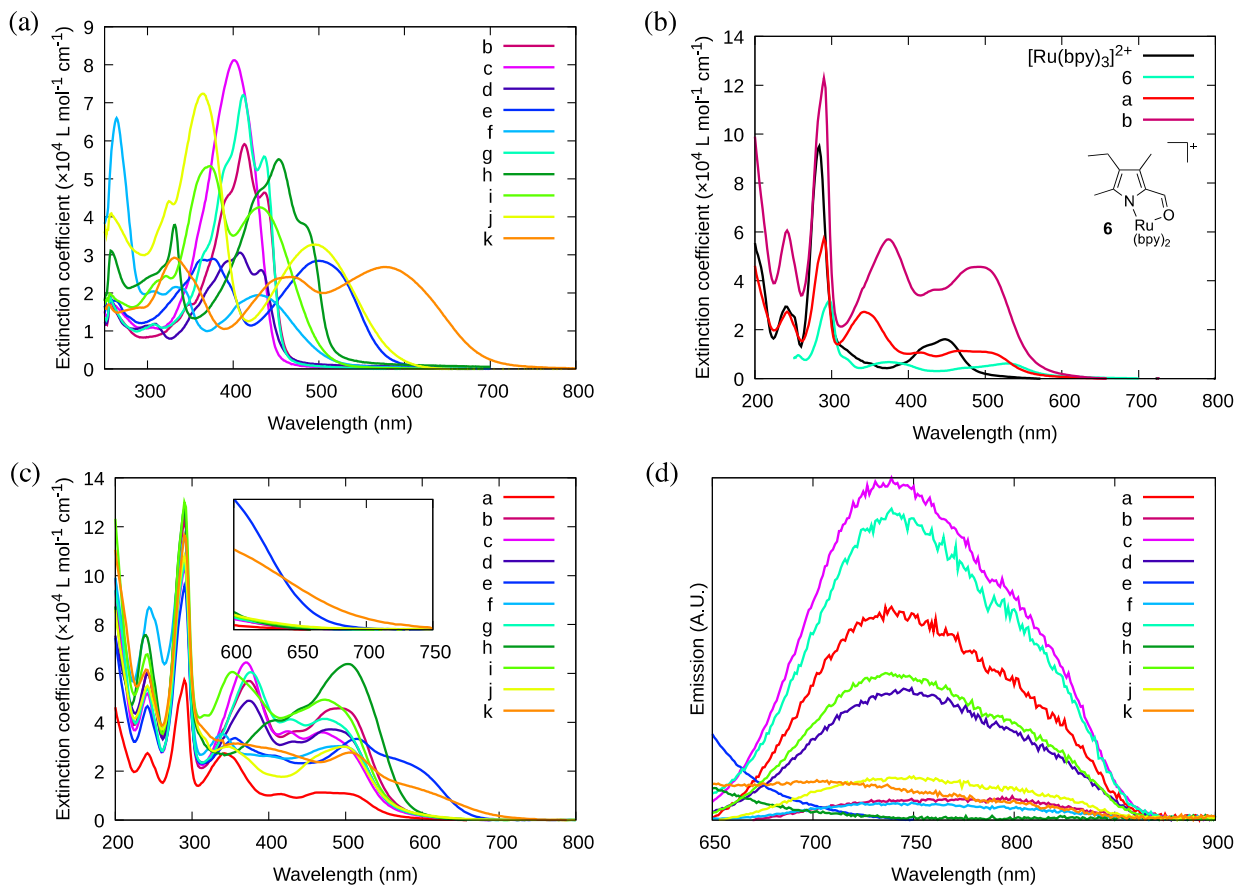
848 3.2.2 Emission

849 Mononuclear **4a** and the bis[Ru(II)-pyrrolide] complexes **4b–4k** did not phosphoresce at room
850 temperature under ambient oxygen conditions and very little phosphorescence was observed at
851 room temperature in an argon atmosphere (Figure 1d, Table 3). The largest phosphorescence
852 quantum yields (Φ_p) were only about 0.1%, but the signal for eight of the eleven complexes was
853 sufficient to identify discernable maxima for the $^3\text{MLCT}$ emission near 743 nm with a longer
854 wavelength shoulder near 800 nm (using the excitation maxima, which occurred near 465–485
855 nm). For the phosphorescence that was detectable, the various ligands and linkers had little
856 influence on the energy of the emitting $^3\text{MLCT}$ state, which likely involves π^* acceptor orbitals of
857 the bpy ligands, except for **4e** and **4h**. Complexes **4e** and **4h** did not yield any phosphorescence,
858 although the tail of their shorter wavelength ligand-centered fluorescence could be discerned in
859 the spectral observation window. While **4k** exhibited very weak phosphorescence, a value for Φ_p
860 was not determined due to the lack of a discrete peak. Collectively, the low phosphorescence
861 quantum yields (or absence of phosphorescence) for all of the compounds point toward other
862 efficient relaxation pathways that facilitate excited state decay even in the absence of oxygen.

863 3.2.3 Singlet oxygen quantum yields

864 In the presence of oxygen, mononuclear **4a** and the bis[Ru(II)-pyrrolide] complexes **4b–4k**
865 generated $^1\text{O}_2$ to varying degrees. The $^1\text{O}_2$ quantum yields (Φ_Δ) ranged from as low as 5–7% for
866 **4k** and **4f**, respectively, to as high as 77% for **4i** (Table 3). According to their Φ_Δ values, the
867 compounds clustered into three groups: (i) 5–13% (**4a**>**4f**>**4k**), (ii) 30–40% (**4g**=**4j**>**4e**), and (iii)
868 >50% (**4i**>**4b**≈**4h**>**4d**>**4c**). With the exception of **4i** (benzothiadiazole flanked by two phenyl
869 groups), the compounds with the largest $^1\text{O}_2$ quantum yields were those with phenyl, biphenyl, or
870 polycyclic aromatic hydrocarbon (pyrenyl and naphthalene) linkers. Anthracene as the central
871 linker (**4f**) was among the poorest $^1\text{O}_2$ generators of the group ($\Phi_\Delta=7\%$), and fluorene (**4g**) was
872 near the middle ($\Phi_\Delta=37\%$). Whether the $^3\text{MLCT}$ state(s), observed in the emission measurements,
873 contributed to $^1\text{O}_2$ production remains unknown but it is anticipated that non-emissive $^3\text{IL}/^3\text{ILCT}$
874 states may play a role with regard to the more highly photosensitizing systems. It was anticipated
875 that compounds with the higher $^1\text{O}_2$ quantum yields might act as PDT agents so we next
876 investigated their cytotoxicities toward cancer cells with light activation, and compared to their
877 dark cytotoxicities.

878



879

880 Figure 1. UV/Vis absorption spectra of (a) ligands **3b–k**; (b) previously reported **6** and
 881 $[\text{Ru}(\text{bpy})_3]^{2+}$ as reference complexes for mononuclear **4a** and bis[Ru(II)-pyrrolide] triad **4b**; and
 882 (c) mononuclear **4a** and bis[Ru(II)-pyrrolide] triads **4b–k**. (d) Phosphorescence emission spectra
 883 for mononuclear **4a** and bis[Ru(II)-pyrrolide] triads **4b–k** (collected in Ar using $\lambda_{\text{ex max}}$).
 884 Absorption and emission spectra were collected on the PF_6^- salts of the complexes (5 μM) in
 885 MeCN.

886

887 Table 3. Spectroscopic properties

Cmpd	Abs _{max} /nm (log ε)	$\lambda_{\text{em max}}$ (λ_{ex}) / nm ^a	Φ_{p}^a (1×10^{-3})	Φ_{Δ}
5a	244 (4.43), 284 (4.70), 290 (4.76), 340 (4.44), 416 (4.02), 464 (4.04), 514 (3.99)	743 (466)	1.07	0.13
5b	242 (4.78), 284 (5.04), 290 (5.09), 378 (4.75), 434 (4.56), 494 (4.66), 515 (4.60)	760 (500)	0.10	0.69

5c	244 (4.70), 284 (4.96), 290 (5.02), 372 (4.81), 428 (4.56), 470 (4.56), 504 (4.47)	743 (470)	1.20	0.57
5d	244 (4.77), 284 (4.99), 288 (5.02), 376 (4.69), 436 (4.50), 484 (4.57)	750 (484)	0.52	0.61
5e	244 (4.66), 282 (4.90), 290 (4.98), 360 (4.52), 414 (4.41), 518 (4.52), 602 (4.29)	— ^b	— ^b	0.32
5f	248 (4.93), 252 (4.91), 284 (5.02), 290 (5.07), 340 (4.55), 404 (4.42), 472 (4.47), 514 (4.44)	765 (495)	0.067	0.07
5g	206 (4.91), 244 (4.72), 284 (4.97), 290 (5.02), 378 (4.78), 430 (4.61), 474 (4.62), 502 (4.56)	743 (475)	0.69	0.37
5h	240 (4.88), 290 (5.11), 406 (4.61), 442 (4.66), 508 (4.80)	— ^b	— ^b	0.68
5i	242 (4.83), 292 (5.11), 318 (4.63), 354 (4.78), 476 (4.69), 510 (4.60)	738 (474)	0.68	0.77
5j	244 (4.73), 290 (5.03), 316 (4.53), 352 (4.47), 438 (4.30), 504 (4.47)	746 (500)	0.28	0.33
5k	242 (4.79), 292 (5.06), 398 (4.47), 510 (4.44), 618 (4.02)	715 (507)	— ^c	0.05

888 ^a298 K, Ar; ^bemission from the ³MLCT state at 298 K was not observed (the tail of ¹LC emission
889 was observed); ^cvery weak ³MLCT emission that was continuous over the observation window.

890 3.3 Photobiological Activity

891 3.3.1 HL-60 cytotoxicity and photocytotoxicity assays for the series

892 3.3.1.1 Cellular assays

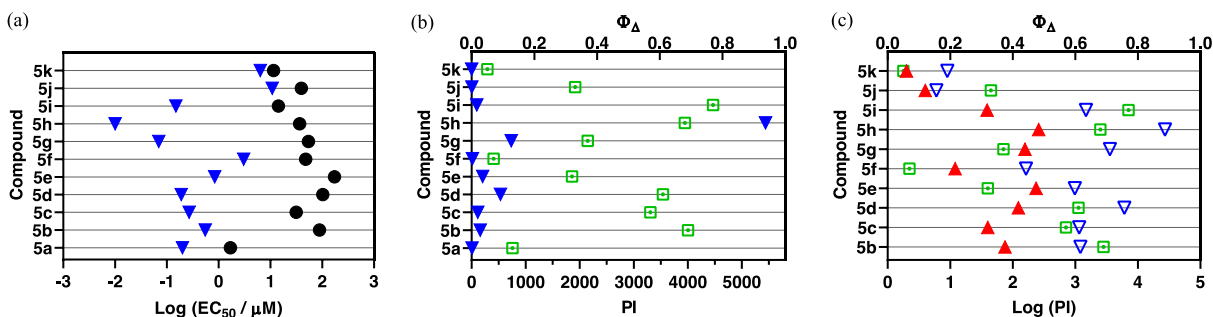
893 The water-soluble Cl⁻ salts (**5a–k**) were used for the biological experiments. The dark
894 cytotoxicities of the reference compound mononuclear **5a** and the bis[Ru(II)-pyrrolide] triads **5b–**
895 **5k** were determined using a human leukemia (HL-60) cell line. This cell line was chosen because
896 it grows as a suspension rather than an adherent monolayer, thus eliminating some additional
897 variability in the cellular assay that arises when treating differentially formed monolayers. Briefly,
898 cells growing in log phase were dosed with the compounds at concentrations between 1 nM and
899 300 μM and assessed for viability after approximately 64 h using the Alamar Blue reagent. The
900 photocytotoxicities were determined in an analogous manner except that a light treatment was
901 delivered approximately 16 h after the cells were dosed with compound. The cell viability was
902 quantified from dose-response curve fits to yield the effective concentration required to reduce cell
903 viability by 50% (EC₅₀) in the dark (dark EC₅₀) and with the light treatment (light EC₅₀). The
904 phototherapeutic indices (PIs) were calculated as the ratios of the dark EC₅₀ and light EC₅₀ values,

905 and represent the amplification of the cytotoxic effect with the light trigger. All cellular assays
 906 were carried out in triplicate under normoxic conditions, with representative data compiled in
 907 Table 4.

908
 909 Table 4. Compilation of the dark cytotoxicities and photocytotoxicities of **5a–5k** toward HL-60
 910 cancer cells.
 911

Complex	Dark EC ₅₀ (μM)	Vis light^a EC ₅₀ (μM)	Vis PI^b	Red light^c EC ₅₀ (μM)	Red PI^b
5a	1.69 ± 0.06	0.20 ± 0.01	8	0.29 ± 0.07	6
5b	89.1 ± 0.8	0.55 ± 0.02	161	1.20 ± 0.03	74
5c	31.6 ± 1.7	0.27 ± 0.04	115	0.79 ± 0.04	40
5d	103 ± 0.6	0.19 ± 0.01	534	0.84 ± 0.02	123
5e	173 ± 6	0.84 ± 0.01	206	0.73 ± 0.02	237
5f	48.1 ± 0.4	3.05 ± 0.21	16	4.06 ± 0.09	12
5g	54.4 ± 0.9	0.07 ± 0.01	734	0.35 ± 0.02	157
5h	36.8 ± 2.9	0.01 ± 0.01	5,439	0.14 ± 0.01	261
5i	14.3 ± 0.4	0.15 ± 0.01	95	0.37 ± 0.05	39
5j	39.8 ± 0.9	10.8 ± 0.3	4	10.2 ± 0.1	4
5k	11.5 ± 0.3	6.36 ± 0.14	2	6.48 ± 0.16	2

912 ^aVis condition: 16 h DLI followed by broadband visible light irradiation (28 J cm⁻², 7.8 mW
 913 cm⁻²), ^bPI = phototherapeutic index (ratio of dark EC₅₀ to visible-light EC₅₀), ^cRed condition: 16
 914 h DLI followed by light irradiation with 625-nm LEDs (100 J cm⁻², 42 mW cm⁻²).



915
 916 Figure 2. (a) Activity plot for **5a–5k** showing cytotoxicities in the dark (●) and with light
 917 activation using broadband visible light (▼, 28 J cm^{-2} , 7.8 mW cm^{-2}); (b) activity plot for **5a–5k**
 918 highlighting phototherapeutic indices (PIs) under the same light conditions as in (a), as well as $^1\text{O}_2$
 919 quantum yields (□); and (c) activity plot for the bis[Ru(II)-pyrrolide] triads **5b–5k** showing their
 920 log PI values with visible (▼, 100 J cm^{-2} , 28 mW cm^{-2}) or 625-nm red (▲, 100 J cm^{-2} , 42 mW
 921 cm^{-2}) light.

922

923 3.3.1.2 Dark cytotoxicity

924 The dark cytotoxicities of the compounds investigated varied over two orders of magnitude from
 925 approximately $1.7 \mu\text{M}$ for the mononuclear **5a** to just over $170 \mu\text{M}$ for the bis-Ru(II) triad **5e**
 926 (Table 4, Figure 2a). Notably, the mononuclear compound **5a** was distinctly more cytotoxic than
 927 its triad counterparts, being seven-fold more cytotoxic than the most dark cytotoxic triad **5k** (dark
 928 $\text{EC}_{50}=11.5 \mu\text{M}$). There was a ten-fold variation among the Ru(II) triads that clustered into roughly
 929 three groups: least cytotoxic with dark EC_{50} values near 100 or more (**5b**, **5d–e**), moderately
 930 cytotoxic with values near $30\text{–}50 \mu\text{M}$ (**5c**, **5f–h**, **5j**), and cytotoxic with values between $10\text{–}15 \mu\text{M}$
 931 (**5i**, **5k**).

932 Structurally, the bis[Ru(II)-pyrrolide] systems can be divided into three classes: (i) those with
 933 aromatic hydrocarbon linkers that vary in the extent π -conjugation (**5b–d**, **5f–h**), (ii) those with
 934 benzothiadiazole linkers with or without conjugated groups (**5e**, **5i–j**), and (iii) one with an
 935 isoindigo linker (**5k**). The dark cytotoxicities of class (i) varied from 32 to $103 \mu\text{M}$, while those
 936 for class (ii) varied from 14 to $173 \mu\text{M}$. Complex **5k** with the isoindigo linker was the most
 937 cytotoxic at $11.5 \mu\text{M}$, and **5e** with the benzothiadiazole linker was the least at $173 \mu\text{M}$.
 938 Interestingly, incorporation of phenyl rings (**5i**) or N-Me pyrrole rings (**5j**) on either side of the
 939 benzothiadiazole group led to increased cytotoxicity relative to the parent **5e**. Likewise, there was
 940 a substantial difference between incorporation of one phenyl ring (**5b**) as the linker and two (**5c**),
 941 with the latter resulting in elevated cytotoxicity. The incorporation of two fused rings, as in
 942 naphthalene (**5d**), resulted in a slightly reduced cytotoxicity relative to **5b**.

943 Parameters such as lipophilicity and cellular uptake and distribution were not investigated as part
 944 of this study so it would be premature to speculate on reasons behind the observed differences in
 945 cytotoxicity. Rather, our intention here is to highlight the breadth of cytotoxic activity that can be
 946 obtained in a relatively small structural family of a new compound class and to also use the dark
 947 EC_{50} values as a reference point for assessing phototoxic effects and corresponding PIs. This
 948 significant variation within and between the classes underscores that the linker unit is an important

949 point of variation for manipulating the inherent cytotoxicity of bis[Ru(II)-pyrrolide] triads, which
950 could prove advantageous for optimization of PI values.

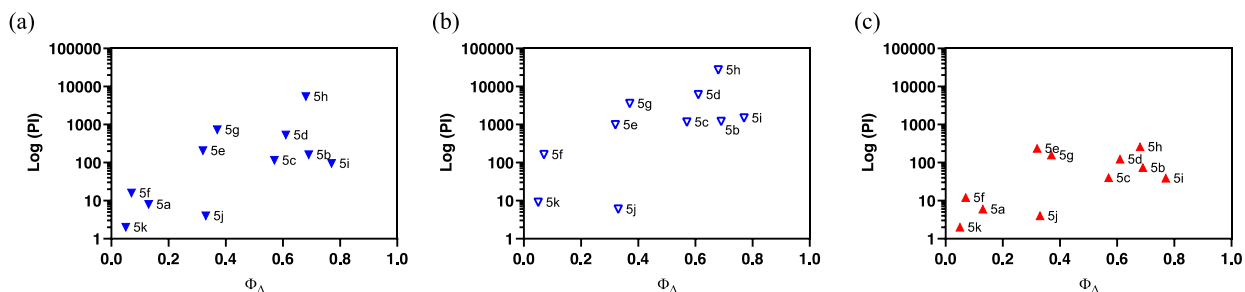
951 3.3.1.3 Photocytotoxicity

952 The photocytotoxicities of mononuclear **5a** along with the bis[Ru(II)-pyrrolide] triads were
953 determined with broadband visible light (28 J cm^{-2} , 7.8 mW cm^{-2}) and with 625-nm red light (100
954 J cm^{-2} , 42 mW cm^{-2}) (Figure 2a, Table 4). Their visible light EC_{50} values under this condition
955 varied by just over three orders of magnitude, ranging from approximately 3–11 μM for the least
956 phototoxic systems (**5f**, **5j–k**) to 10–70 nM for the most potent phototoxic compounds (**5g**, **5h**).
957 Other family members clustered near 150–270 nM (**5a**, **5c–d**, **5i**), with **5b** and **5e** much closer to
958 1 μM .

959 Because the light EC_{50} values contain contributions from the baseline dark cytotoxicity, the true
960 phototoxic effects were assessed as PI values, or fold-amplification between the dark and light
961 condition (Figure 2b, Table 4). According to their PIs, the compounds could be grouped by having
962 (i) very little phototherapeutic effect with PIs $\ll 100$ (**5a**, **5f**, **5j–k**), (ii) marginal effects with PIs
963 near 100–200 (**5b–c**, **5e**, **5i**), or (iii) very good effects with PIs > 100 (**5d**, **5g**, **5h**). Bis[Ru(II)-
964 pyrrolide] **5h**, exhibiting one of the larger $^1\text{O}_2$ quantum yields, stood out from the rest with its
965 visible PI exceeding 5,000 using this relatively soft light dose. The PIs generally correlated with
966 $^1\text{O}_2$ quantum yields across the series (Figure 3a), but the correlation was not strict when comparing
967 individual compounds. For example, **5h** had a much larger PI than the other family members (best
968 emphasized in Figure 3b), yet it did not have the largest $^1\text{O}_2$ yield of the series. Certainly, other
969 ROS and other phototoxic mechanisms could be at play, the cell-free $^1\text{O}_2$ quantum yields may not
970 reflect the cellular $^1\text{O}_2$ quantum yields, and/or the subcellular targets may have a larger impact on
971 the PI than the precise $^1\text{O}_2$ quantum yield. Nevertheless, this compound class can be considered a
972 new source of PSs for PDT.

973 Structurally, the largest PIs were observed for the bis[Ru(II)-pyrrolide] systems with conjugated
974 aromatic hydrocarbon linkers in the order: pyrene (**5h**) $>$ fluorene (**5g**) $>$ naphthalene (**5d**). The
975 smallest PIs were obtained for the mononuclear **5a**, which had very high dark cytotoxicity, and the
976 bis[Ru(II)-pyrrolide] triads with anthracene (**5f**), isoindigo (**5k**), and bis(NMePy)benzothiadiazole
977 (**5j**) as central linkers. The family members with intermediate and similar PIs contained phenyl
978 and biphenyl linkers, (**5b**) and (**5c**), respectively, as well as benzothiadiazole and
979 diphenylbenzothiadiazole linkers, (**5e**) and (**5i**), respectively. It is tempting to speculate that linkers
980 with the requisite triplet state energies to act as excited state reservoirs might lead to increased
981 sensitivity to oxygen (and other excited state quenchers) in these triads and thus larger PIs.
982 However, as triplet state energies of the free ligands (and the corresponding $^3\text{IL}/^3\text{ILCT}$ energies of
983 the complexes) form part of a future extensive spectroscopic study we will not speculate at this
984 time.

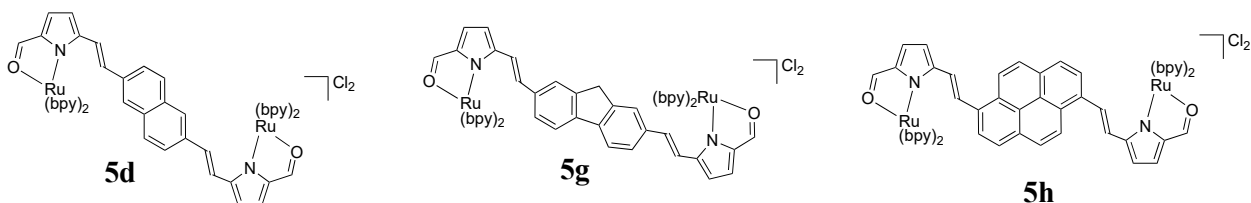
985



986

987 Figure 3. Plots correlating PI value with the $^1\text{O}_2$ quantum yield for each complex under three
 988 different light conditions: (a) broadband visible (\blacktriangledown , 28 J cm^{-2} , 7.8 mW cm^{-2}) for **5a–k**, (b)
 989 broadband visible (∇ , 100 J cm^{-2} , 28 mW cm^{-2}) for **5b–k**, and 625-nm red (\blacktriangle , 100 J cm^{-2} , 42
 990 mW cm^{-2}) for **5a–k**.

991 The photocytotoxicities and PIs for the bis[Ru(II)-pyrrolide] triads were also measured using a
 992 slightly stronger broadband visible light dose (100 J cm^{-2} , 28 mW cm^{-2}) from a different light
 993 source to cross-confirm the phototoxic effects across the series (Figure 2c and Figure 3b). The
 994 difference in light fluence or irradiance between the two experiments was almost four-fold, and
 995 the resulting PIs did not scale linearly with this change. However, the compounds clustered in the
 996 same groups based on their PIs and $^1\text{O}_2$ quantum yields (Figure 3b). The PI differences between
 997 the two visible light conditions were compound-dependent, ranging from two-fold (**5j**) to sixteen-
 998 fold (**5i**). Differences near ten-fold (**5b–d** and **5f**) or five-fold (**5e**, **5g–h**, **5k**) were measured for
 999 the rest of the family. Notably, **5h** had a visible EC_{50} value near 1 nM and $\text{PI} > 27,000$, while the
 1000 PI values for **5d** and **5g** were $>6,000$ and $>3,500$, respectively. **5h** has one of the larger PI reported
 1001 to date (Figure 4).

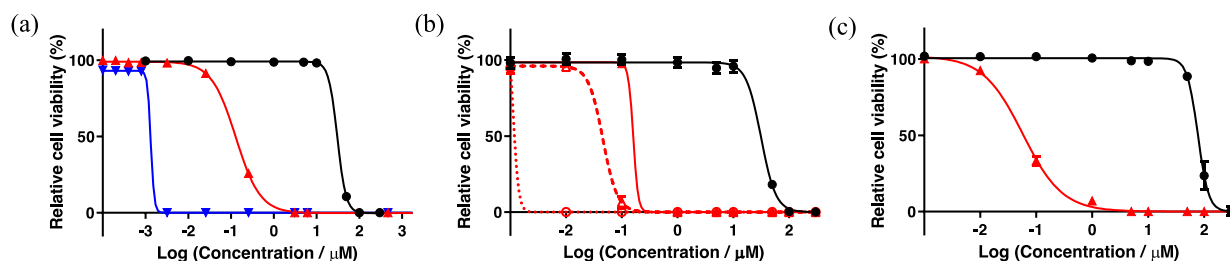


1002

1003 Figure 4. Molecular structures of the bis[Ru(II)-pyrrolides] with the largest PIs.

1004 Since mononuclear **5a** and the bis[Ru(II)-pyrrolide] systems display longest-wavelength
 1005 absorption maxima that are red-shifted compared to many well-studied Ru(II) polypyridyl
 1006 complexes,²¹ their photocytotoxicities and PIs were also investigated using 625-nm red LEDs (100
 1007 J cm^{-2} , 42 mW cm^{-2}). As observed for the two different visible light treatments, the compounds
 1008 clustered in the same groups based on their PIs and $^1\text{O}_2$ quantum yields (Figure 3c), but their PIs
 1009 were attenuated. The red PIs ranged from 2 for the least photoactive compound (**5k**) to 260 for the
 1010 most photoactive system (**5h**) (Table 4), with four of the triads maintaining PIs > 100 (**5d–e**, **5g–**
 1011 **5h**). The visible- and red-light treatments with a fluence of 100 J cm^{-2} (but different irradiances)
 1012 are compared in Figure 2c. The PIs for the bis[Ru(II)-pyrrolide] triads were attenuated to different
 1013 extents using lower-energy red light, from 100-fold for **5h** to two-fold with **5j**. The order of
 1014 attenuation appeared to parallel the magnitudes of the PIs with visible light rather than the molar
 1015 extinction coefficients at 625 nm, with the more photoactive compounds being the most affected.
 1016 Of the compounds considered most active under all three illumination conditions investigated,
 1017 only **5e** absorbs red light significantly ($\log \epsilon_{625 \text{ nm}} = 4.08$) yet **5h** ($\log \epsilon_{625 \text{ nm}} = 2.93$) had a larger

1018 PI. The only other compound that absorbs light substantially at 625 nm is **5k** ($\log \epsilon_{625 \text{ nm}} = 3.97$),
1019 which was dark cytotoxic and considered relatively non-phototoxic under all light conditions
1020 explored. These variances present intriguing launch points for future investigation.



1021
1022 Figure 5. (a) Wide concentration range dark/light cytotoxicity assay performed with **5h** using the
1023 HL-60 cell line. Cells dosed with **5h** received a dark (black) or light treatment with red (625-nm
1024 LEDs, red) or broadband visible (blue) light (100 J cm^{-2} , 29 mW cm^{-2}) with a DLI of 1 h. (b)
1025 Cytotoxicity (black) and photocytotoxicity (red) using the three 625-nm red light conditions: the
1026 red light dose used in (a) but with different concentrations of **5h** (—); 100 J cm^{-2} (29 mW cm^{-2})
1027 delivered in four 25 J cm^{-2} fractions separated by 15 min (---); and 200 J cm^{-2} delivered in two
1028 fractions of 100 J cm^{-2} separated by 1 h (···). (c) HL60 multicellular 3D spheroid cytotoxicity
1029 (black) and photocytotoxicity (red) assay with **5h** using the red light condition described for (a).

1030 3.3.2 Selected assays to investigate the scope of activity for bis[Ru(II)-pyrrolide] **5h**.

1031 3.3.2.1 Wide concentration range photocytotoxicity assay

1032 The visible light condition with a fluence of 100 J cm^{-2} described above yielded an EC_{50} value
1033 for **5h** near 1 nM, which was the lowest concentration tested in that assay. To gain more insight
1034 regarding the visible light EC_{50} value with 100 J cm^{-2} , we rescreened **5h** starting at 100 pM and
1035 reduced the drug-to-light (DLI) interval from 16 h to 1 h (Figure 5a). This new condition yielded
1036 a visible-light EC_{50} value for **5h** of 1.33 nM (PI=24,100). The PI was slightly reduced in this assay
1037 due to a higher dark cytotoxicity of $30.8 \mu\text{M}$ (versus $36.8 \mu\text{M}$ in the narrower range screen). In
1038 parallel, we also used red light (625 nm, 100 J cm^{-2} , 29 mW cm^{-2}) and obtained a red light EC_{50}
1039 value of 129 nM (PI=239), which was similar to what was determined in the narrower
1040 concentration range assay.

1041 3.3.2.2 Optimization of the red-light PI

1042 Given that bis[Ru(II)-pyrrolide] **5h** clearly emerged as a compound of interest for further
1043 investigation due to its unprecedented visible PI with both the high and low light fluences tested,
1044 we wondered whether the attenuated red-light PIs of ~240–260 obtained with a fluence of 100 J cm^{-2}
1045 could be improved. The light parameter offers a unique opportunity to optimize the PI as the
1046 wavelength, fluence, irradiance, DLI, and dosing regimen can be manipulated. While the optimal
1047 light dosimetry parameters are not absolute and most certainly are compound-dependent, simple
1048 changes such as increasing the fluence and dosing interval are straightforward. We optimized the
1049 PI for 625-nm red light (100 J cm^{-2} , 29 mW cm^{-2}) with a 16 h DLI, where the red EC_{50} value in
1050 this assay was 161 nM and the PI was 195 (Figure 5b). These unoptimized values differ slightly
1051 between assays¹⁶ so the reference condition was always run in parallel for comparison. Delivering
1052 the same total fluence but in four 25 J cm^{-2} intervals separated by 15 min increased the potency
1053 by almost four-fold (red EC_{50} =45.7 nM, PI=690). Increasing the light fluence to 200 J cm^{-2}
1054 delivered in two intervals of 100 J cm^{-2} separated by 1 h led to subnanomolar potency: red

1055 EC₅₀=630 pM and PI=50,000 (Figure 5b). The superior potency with this light regimen exceeded
1056 even that of the visible light condition that yielded a PI >27,000. PIs of these magnitudes have not
1057 been reported. This very limited optimization study underscores how the light regimen can
1058 compensate for marginal extinction coefficients at the activation wavelength. In this preliminary
1059 investigation, we did not investigate the mechanism behind this improved response as part of this
1060 study, but it is known that fractionated dosing can (in some cases) improve response.¹²

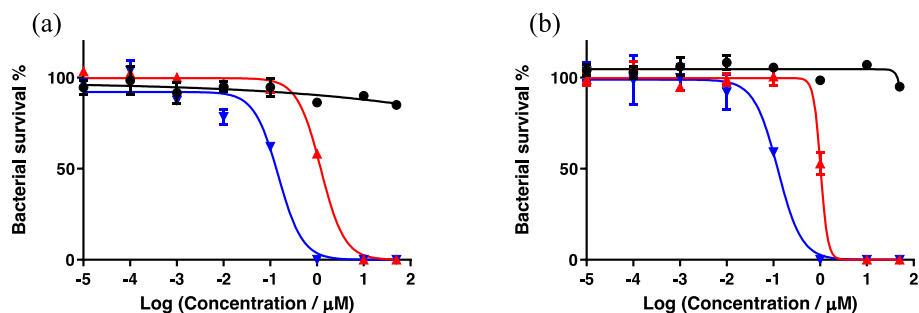
1061 3.3.2.3 Multicellular 3D tumor spheroid assay

1062 The 3D multicellular tumor spheroid model can be exploited to mimic the highly plastic
1063 migratory/invasive tumor phenotypes that characterize some of the most aggressive conditions in
1064 vivo.⁸⁹ For instance, they have hard-to-reach hypoxic regions that impart drug resistance. To test
1065 whether **5h** could maintain potency against tumor spheroids of the same cell line used for the 2D
1066 suspension assays (HL-60), spheroids were grown to sizes of about 600 μm in diameter and treated
1067 with **5h** in the concentration range of 1 nM to 300 μM. The spheroids were either kept in the dark
1068 or treated with 625-nm red light (100 J cm⁻², 29 mW cm⁻²) with a 16 h DLI. As expected the HL-
1069 60 tumor spheroids were greater than two-fold more resistant to **5h** in the dark (compared to 2D
1070 HL-60 cultures), with a dark EC₅₀ of approximately 77 μM. Surprisingly, however, the
1071 photocytotoxicity was greater against the 3D tumor spheroids, with a red-light EC₅₀ value of 60
1072 nM and PI>1,200. We did not examine the source of this enhanced photocytotoxicity in the 3D
1073 tumor spheroid model, which should be scrutinized more closely across spheroids of different sizes
1074 and of different cell lines to assess whether this is a general property of **5h**.

1075 3.3.2.4 Bacterial survival assays

1076 The ability of **5h** to act as a photocytotoxic compound toward bacteria was briefly explored. Two
1077 bacterial species were grown as planktonic cultures and treated with **5h** in the concentration range
1078 of 10 pM to 50 μM, where no dark cytotoxicity was apparent. Further treatment with either
1079 broadband visible or 625-nm red light (100 J cm⁻², 28 mW cm⁻²) using a DLI of 1 h resulted in
1080 phototoxic effects toward both *S. mutans* and *S. aureus* (Figure 6). There was no selectivity for
1081 either bacterial species, with visible EC₅₀ values on the order of 130 to 160 nM and PIs >300 (PIs
1082 not determined because there was no dark cytotoxicity at the concentrations investigated). As
1083 observed with the HL-60 cells, the photocytotoxicity was attenuated upon moving to the use of
1084 red light, rather than visible light of the same fluence and irradiance. The reduction was
1085 approximately eight-fold, yielding PIs >40–50. This result confirms that the phototoxic effect
1086 exhibited by **5h** extends to other types of cells and that this new class of bis[Ru(II)-pyrrolide] triad
1087 shows potential for use as photoactive antimicrobials.

1088



1089
 1090 Figure 6. In vitro cytotoxic effects of **5h** against *S. mutans* (a) and *S. aureus* (b) growing as
 1091 planktonic cultures in the dark (black) or with a light treatment. The light treatments were
 1092 broadband visible (blue) or 625-nm red (red) light (100 J cm^{-2} , 28 mW cm^{-2}) with a DLI of 1 h.

1093

1094 4. CONCLUDING REMARKS

1095 In summary, the ten new bis[Ru(II)-pyrrolide] triads demonstrated unequivocally that the central
 1096 organic linker plays a pivotal role in determining the spectroscopic, biological, and photobiological
 1097 properties of the metal-organic systems and that these properties in many cases are improved
 1098 relative to the mononuclear counterpart **5a**. The compounds demonstrated a large breadth of
 1099 activity as exemplified by a very wide range for $^1\text{O}_2$ quantum yields, dark cytotoxicities, and PIs.
 1100 Simple variation of the central organic chromophore resulted in some compounds being excellent
 1101 in vitro phototoxic agents, while others exhibited almost no photoactivity and could be considered
 1102 traditional cytotoxic agents. The source of higher dark cytotoxicity for certain compounds is not
 1103 known but could be related to their lipophilicities and resulting cellular uptake and/or localization.

1104 Since the excited state dynamics were not probed, it is not possible to conclude from this study
 1105 which complexes have accessible ^3IL and/or $^3\text{ILCT}$ states of suitable energies and whether these
 1106 are responsible for the larger $^1\text{O}_2$ quantum yields and PIs associated with certain complexes such
 1107 as **5h**. Given that the linkers are not isolated organic chromophores, but are presumed to be heavily
 1108 conjugated throughout the styryl-pyrrolide π -system, a fundamental investigation of the
 1109 photophysical dynamics of these new ligands is a necessary prerequisite for understanding the
 1110 behavior of the much more complex bis[Ru(II)-pyrrolide] triads. Moreover, the generation of $^1\text{O}_2$
 1111 under the cell-free condition does not establish ROS as the definitive mediator of photocytotoxicity.
 1112 Although we presume PDT effects are responsible, the excited state dynamics and redox
 1113 characteristics of the complexes must be explored in order to propose a mechanism(s).

1114 However, the fact that **5h** with the central pyrenyl group emerged as an extremely potent
 1115 photosensitizer for in vitro PDT and that the triplet state energy of the isolated pyrenyl group is in
 1116 energetic proximity to that of many well-studied $^3\text{MLCT}$ states suggests at least a tentative role
 1117 for $^3\text{IL}/^3\text{ILCT}$ states in producing the larger $^1\text{O}_2$ quantum yield and greater in vitro PDT potency
 1118 toward cancer cells. At the time **5h** was evaluated, PIs of such magnitude had not been reported
 1119 and the opportunity to use interval dosing to achieve PIs $>27,000$ had not been explored by groups
 1120 developing new PSs. Compound **5h** was also highly active toward the more resistant tumor
 1121 spheroid model, which is characterized by multicellular resistance and regions of hypoxia, and
 1122 also toward bacteria. The versatility of this new photosensitizer for both light-mediated anticancer
 1123 and antimicrobial applications highlights the potential utility of the bis[Ru(II)-pyrrolide] scaffold

1124 for photobiological applications and introduces a new platform for further optimization of these
1125 important light-responsive agents.

1126

1127 **5. ASSOCIATED CONTENT**

1128 **5.1 Supporting Information**

1129 Additional synthetic procedures for the synthesis of pyrrole **1a** and aryl dibromides **i**, **j** and **k**.
1130 Figures giving ¹H and ¹³C NMR spectra and UV/vis absorption spectra for all bis(pyrrole)s (**2**),
1131 ligands (**3**) and bis(ruthenium) complex salts (**4**). This material is available free of charge via the
1132 Internet at <http://pubs.acs.org>.

1133 **5.2 Author Information**

1134 **5.2.1 Corresponding authors**

1135 *To whom correspondence should be addressed. A.T. <alison.thompson@dal.ca>, ORCID 0000-
1136 0003-4231-3446; S.A.M. <sherri.mcfarland@uta.edu>, ORCID 0000-0002-8028-5055

1137 **5.2.2 Author contributions**

1138 The manuscript was written through contributions of all authors. All authors have given approval
1139 to the final version of the manuscript.

1140 **5.2.3 Notes**

1141 S.A.M. has a potential research conflict of interest due to a financial interest with Theralase
1142 Technologies, Inc. and PhotoDynamic, Inc. A management plan has been created to preserve
1143 objectivity in research in accordance with UTA policy.

1144 **5.2.4 Acknowledgments**

1145 S.A.M. and A.T. thank the Natural Sciences and Engineering Research Council of Canada
1146 (NSERC) for financial support. S.A.M. and C.G.C. thank the National Cancer Institute (NCI) of
1147 the National Institutes of Health (NIH) (Award R01CA222227) for partial support of this work.
1148 The content in this review is solely the responsibility of the authors and does not necessarily
1149 represent the official views of the National Institutes of Health. The TOC graphic was made using
1150 Biorender.com.

1151 **6. REFERENCES**

- 1152 (1) Bonnett, R. *Chemical Aspects of Photodynamic Therapy*; Advanced chemistry texts; Gordon
1153 and Breach Science Publishers: Amsterdam, The Netherlands, 2000.
- 1154 (2) DeRosa, M. Photosensitized Singlet Oxygen and Its Applications. *Coord. Chem. Rev.* **2002**,
1155 *233–234*, 351–371. [https://doi.org/10.1016/S0010-8545\(02\)00034-6](https://doi.org/10.1016/S0010-8545(02)00034-6).
- 1156 (3) Schlotthauer, T.; Schroot, R.; Glover, S.; Hammarström, L.; Jäger, M.; Schubert, U. S. A
1157 Multidonor–Photosensitizer–Multiacceptor Triad for Long-Lived Directional Charge
1158 Separation. *Phys. Chem. Chem. Phys.* **2017**, *19* (42), 28572–28578.
1159 <https://doi.org/10.1039/C7CP05593E>.
- 1160 (4) Gollnick, S. O.; Vaughan, L.; Henderson, B. W. Generation of Effective Antitumor Vaccines
1161 Using Photodynamic Therapy. *Cancer Res.* **2002**, *62* (6), 1604–1608.
- 1162 (5) Castano, A. P.; Mroz, P.; Hamblin, M. R. Photodynamic Therapy and Anti-Tumour
1163 Immunity. *Nat. Rev. Cancer* **2006**, *6* (7), 535–545. <https://doi.org/10.1038/nrc1894>.

- 1164 (6) Mroz, P.; Hashmi, J. T.; Huang, Y.-Y.; Lange, N.; Hamblin, M. R. Stimulation of Anti-Tumor
1165 Immunity by Photodynamic Therapy. *Expert Rev. Clin. Immunol.* **2011**, *7* (1), 75–91.
1166 <https://doi.org/10.1586/eci.10.81>.
- 1167 (7) Gollnick, S. O.; Brackett, C. M. Enhancement of Anti-Tumor Immunity by Photodynamic
1168 Therapy. *Immunol Res* **2010**, *46* (1–3), 216–226. [https://doi.org/10.1007/s12026-009-8119-](https://doi.org/10.1007/s12026-009-8119-4)
1169 [4](https://doi.org/10.1007/s12026-009-8119-4).
- 1170 (8) Gollnick, S. O. Photodynamic Therapy and Antitumor Immunity. *J Natl Compr Canc Netw*
1171 **2012**, *10 Suppl 2*, S40–43.
- 1172 (9) Shams, M.; Owczarczak, B.; Manderscheid-Kern, P.; Bellnier, D. A.; Gollnick, S. O.
1173 Development of Photodynamic Therapy Regimens That Control Primary Tumor Growth and
1174 Inhibit Secondary Disease. *Cancer Immunol. Immunother. CII* **2015**, *64* (3), 287–297.
1175 <https://doi.org/10.1007/s00262-014-1633-9>.
- 1176 (10) Anzengruber, F.; Avci, P.; de Freitas, L. F.; Hamblin, M. R. T-Cell Mediated Anti-Tumor
1177 Immunity after Photodynamic Therapy: Why Does It Not Always Work and How Can We
1178 Improve It? *Photochem. Photobiol. Sci. Off. J. Eur. Photochem. Assoc. Eur. Soc. Photobiol.*
1179 **2015**, *14* (8), 1492–1509. <https://doi.org/10.1039/c4pp00455h>.
- 1180 (11) Vatansever, F.; Hamblin, M. R. Photodynamic Therapy and Antitumor Immune Response.
1181 In *Cancer Immunology*; Rezaei, N., Ed.; Springer Berlin Heidelberg: Berlin, Heidelberg,
1182 2015; pp 383–399. https://doi.org/10.1007/978-3-662-44946-2_21.
- 1183 (12) van Straten, D.; Mashayekhi, V.; de Bruijn, H.; Oliveira, S.; Robinson, D. Oncologic
1184 Photodynamic Therapy: Basic Principles, Current Clinical Status and Future Directions.
1185 *Cancers* **2017**, *9* (12), 19. <https://doi.org/10.3390/cancers9020019>.
- 1186 (13) Dougherty, T. J.; Gomer, C. J.; Henderson, B. W.; Jori, G.; Kessel, D.; Korbek, M.; Moan,
1187 J.; Peng, Q. Photodynamic Therapy. *JNCI J. Natl. Cancer Inst.* **1998**, *90* (12), 889–905.
1188 <https://doi.org/10.1093/jnci/90.12.889>.
- 1189 (14) Levy, J.; Levy, E. Photofrin-PDT from Bench to Bedside: Some Lessons Learned. In
1190 *Handbook of photodynamic therapy: updates on recent applications of porphyrin-based*
1191 *compounds*; Pandey, R. K., Kessel, D., Dougherty, T. J., Eds.; World Scientific: New Jersey,
1192 2016.
- 1193 (15) Kessel, D. Thomas J. Dougherty: An Appreciation. *Photochem. Photobiol.* **2020**, *96* (3), 454–
1194 457. <https://doi.org/10.1111/php.13144>.
- 1195 (16) Monroe, S.; Colón, K. L.; Yin, H.; Roque, J.; Konda, P.; Gujar, S.; Thummel, R. P.; Lilge, L.;
1196 Cameron, C. G.; McFarland, S. A. Transition Metal Complexes and Photodynamic Therapy
1197 from a Tumor-Centered Approach: Challenges, Opportunities, and Highlights from the
1198 Development of TLD1433. *Chem. Rev.* **2019**, *119* (2), 797–828.
1199 <https://doi.org/10.1021/acs.chemrev.8b00211>.
- 1200 (17) McFarland, S. A.; Mandel, A.; Dumoulin-White, R.; Gasser, G. Metal-Based
1201 Photosensitizers for Photodynamic Therapy: The Future of Multimodal Oncology? *Curr.*
1202 *Opin. Chem. Biol.* **2020**, *56*, 23–27. <https://doi.org/10.1016/j.cbpa.2019.10.004>.
- 1203 (18) Glazer, E. C. Light-Activated Metal Complexes That Covalently Modify DNA. *Isr. J. Chem.*
1204 **2013**, *53* (6–7), 391–400. <https://doi.org/10.1002/ijch.201300019>.
- 1205 (19) Smith, N. A.; Sadler, P. J. Photoactivatable Metal Complexes: From Theory to Applications
1206 in Biotechnology and Medicine. *Philos. Trans. R. Soc. Math. Phys. Eng. Sci.* **2013**, *371*
1207 (1995), 20120519. <https://doi.org/10.1098/rsta.2012.0519>.

- 1208 (20) Balzani, V.; Juris, A. Photochemistry and Photophysics of Ru(II) polypyridine Complexes
1209 in the Bologna Group. From Early Studies to Recent Developments. *Coord. Chem. Rev.* **2001**,
1210 *211* (1), 97–115. [https://doi.org/10.1016/S0010-8545\(00\)00274-5](https://doi.org/10.1016/S0010-8545(00)00274-5).
- 1211 (21) Juris, A.; Balzani, V.; Barigelletti, F.; Campagna, S.; Belser, P.; von Zelewsky, A. Ru(II)
1212 Polypyridine Complexes: Photophysics, Photochemistry, Electrochemistry, and
1213 Chemiluminescence. *Coord. Chem. Rev.* **1988**, *84*, 85–277. [https://doi.org/10.1016/0010-8545\(88\)80032-8](https://doi.org/10.1016/0010-8545(88)80032-8).
- 1215 (22) Howerton, B. S.; Heidary, D. K.; Glazer, E. C. Strained Ruthenium Complexes Are Potent
1216 Light-Activated Anticancer Agents. *J. Am. Chem. Soc.* **2012**, *134* (20), 8324–8327.
1217 <https://doi.org/10.1021/ja3009677>.
- 1218 (23) Wachter, E.; Heidary, D. K.; Howerton, B. S.; Parkin, S.; Glazer, E. C. Light-Activated
1219 Ruthenium Complexes Photobind DNA and Are Cytotoxic in the Photodynamic Therapy
1220 Window. *Chem. Commun.* **2012**, *48* (77), 9649. <https://doi.org/10.1039/c2cc33359g>.
- 1221 (24) Wachter, E.; Glazer, E. C. Mechanistic Study on the Photochemical “Light Switch” Behavior
1222 of [Ru(Bpy)₂Dmdppz]²⁺. *J. Phys. Chem. A* **2014**, *118* (45), 10474–10486.
1223 <https://doi.org/10.1021/jp504249a>.
- 1224 (25) Sun, Y.; Joyce, L. E.; Dickson, N. M.; Turro, C. Efficient DNA Photocleavage by
1225 [Ru(Bpy)₂(Dppn)]²⁺ with Visible Light. *Chem. Commun.* **2010**, *46* (14), 2426.
1226 <https://doi.org/10.1039/b925574e>.
- 1227 (26) Lincoln, R.; Kohler, L.; Monroe, S.; Yin, H.; Stephenson, M.; Zong, R.; Chouai, A.; Dorsey,
1228 C.; Hennigar, R.; Thummel, R. P.; McFarland, S. A. Exploitation of Long-Lived ³IL Excited
1229 States for Metal–Organic Photodynamic Therapy: Verification in a Metastatic Melanoma
1230 Model. *J. Am. Chem. Soc.* **2013**, *135* (45), 17161–17175. <https://doi.org/10.1021/ja408426z>.
- 1231 (27) Yin, H.; Stephenson, M.; Gibson, J.; Sampson, E.; Shi, G.; Sainuddin, T.; Monroe, S.;
1232 McFarland, S. A. *In Vitro* Multiwavelength PDT with ³IL States: Teaching Old Molecules
1233 New Tricks. *Inorg. Chem.* **2014**, *53* (9), 4548–4559. <https://doi.org/10.1021/ic5002368>.
- 1234 (28) Moorlag, C.; Sarkar, B.; Sanrame, C. N.; Bäuerle, P.; Kaim, W.; Wolf, M. O. Conjugation
1235 Length Dependent Ground and Excited State Electronic Behavior in Oligoethynyl Ru
1236 Complexes. *Inorg. Chem.* **2006**, *45* (18), 7044–7046. <https://doi.org/10.1021/ic060912n>.
- 1237 (29) Majewski, M. B.; Tacconi, N. R. de; MacDonnell, F. M.; Wolf, M. O. Ligand-Triplet-Fueled
1238 Long-Lived Charge Separation in Ruthenium(II) Complexes with Bithienyl-Functionalized
1239 Ligands. *Inorg. Chem.* **2011**, *50* (20), 9939–9941. <https://doi.org/10.1021/ic201895y>.
- 1240 (30) Majewski, M. B.; de Tacconi, N. R.; MacDonnell, F. M.; Wolf, M. O. Long-Lived,
1241 Directional Photoinduced Charge Separation in Ru^{II} Complexes Bearing Laminate
1242 Polypyridyl Ligands. *Chem. - Eur. J.* **2013**, *19* (25), 8331–8341.
1243 <https://doi.org/10.1002/chem.201203786>.
- 1244 (31) Han, X.; Wu, L.-Z.; Si, G.; Pan, J.; Yang, Q.-Z.; Zhang, L.-P.; Tung, C.-H. Switching
1245 between Ligand-to-Ligand Charge-Transfer, Intraligand Charge-Transfer, and Metal-to-
1246 Ligand Charge-Transfer Excited States in Platinum(II) Terpyridyl Acetylde Complexes
1247 Induced by PH Change and Metal Ions. *Chem. - Eur. J.* **2007**, *13* (4), 1231–1239.
1248 <https://doi.org/10.1002/chem.200600769>.
- 1249 (32) Verma, S.; Kar, P.; Das, A.; Ghosh, H. N. Photophysical Properties of Ligand Localized
1250 Excited State in Ruthenium(II) Polypyridyl Complexes: A Combined Effect of Electron
1251 Donor–Acceptor Ligand. *Dalton Trans.* **2011**, *40* (38), 9765.
1252 <https://doi.org/10.1039/c1dt10266d>.

- 1253 (33) Keniley, L. K.; Dupont, N.; Ray, L.; Ding, J.; Kovnir, K.; Hoyt, J. M.; Hauser, A.; Shatruck,
1254 M. Complexes with Redox-Active Ligands: Synthesis, Structure, and Electrochemical and
1255 Photophysical Behavior of the Ru(II) Complex with TTF-Annulated Phenanthroline. *Inorg.*
1256 *Chem.* **2013**, *52* (14), 8040–8052. <https://doi.org/10.1021/ic4006949>.
- 1257 (34) Zhao, Y.; Woods, J. A.; Farrer, N. J.; Robinson, K. S.; Pracharova, J.; Kasparikova, J.;
1258 Novakova, O.; Li, H.; Salassa, L.; Pizarro, A. M.; Clarkson, G. J.; Song, L.; Brabec, V.;
1259 Sadler, P. J. Diazido Mixed-Amine Platinum(IV) Anticancer Complexes Activatable by
1260 Visible-Light Form Novel DNA Adducts. *Chem. - Eur. J.* **2013**, *19* (29), 9578–9591.
1261 <https://doi.org/10.1002/chem.201300374>.
- 1262 (35) Swavey, S.; Fang, Z.; Brewer, K. J. Mixed-Metal Supramolecular Complexes Coupling
1263 Phosphine-Containing Ru(II) Light Absorbers to a Reactive Pt(II) through Polyazine
1264 Bridging Ligands. *Inorg. Chem.* **2002**, *41* (9), 2598–2607. <https://doi.org/10.1021/ic010806f>.
- 1265 (36) Holder, A. A.; Swavey, S.; Brewer, K. J. Design Aspects for the Development of Mixed-
1266 Metal Supramolecular Complexes Capable of Visible Light Induced Photocleavage of DNA.
1267 *Inorg. Chem.* **2004**, *43* (1), 303–308. <https://doi.org/10.1021/ic035029t>.
- 1268 (37) Holder, A. A.; Zigler, D. F.; Tarrago-Trani, M. T.; Storrie, B.; Brewer, K. J. Photobiological
1269 Impact of [{(Bpy)₂Ru(Dpp)}₂RhCl₂]Cl₅ and [{(Bpy)₂Os(Dpp)}₂RhCl₂]Cl₅ [Bpy =
1270 2,2'-Bipyridine; Dpp = 2,3-Bis(2-Pyridyl)Pyrazine] on Vero Cells. *Inorg. Chem.* **2007**, *46*
1271 (12), 4760–4762. <https://doi.org/10.1021/ic0619916>.
- 1272 (38) Zigler, D. F.; Mongelli, M. T.; Jeletic, M.; Brewer, K. J. A Trimetallic Supramolecular
1273 Complex of Osmium(II) and Rhodium(III) Displaying MLCT Transitions in the near-IR.
1274 *Inorg. Chem. Commun.* **2007**, *10* (3), 295–298. <https://doi.org/10.1016/j.inoche.2006.10.024>.
- 1275 (39) Havrylyuk, D.; Stevens, K.; Parkin, S.; Glazer, E. C. Toward Optimal Ru(II) Photocages:
1276 Balancing Photochemistry, Stability, and Biocompatibility Through Fine Tuning of Steric,
1277 Electronic, and Physicochemical Features. *Inorg. Chem.* **2020**, *59* (2), 1006–1013.
1278 <https://doi.org/10.1021/acs.inorgchem.9b02065>.
- 1279 (40) Albani, B. A.; Durr, C. B.; Turro, C. Selective Photoinduced Ligand Exchange in a New
1280 Tris-Heteroleptic Ru(II) Complex. *J. Phys. Chem. A* **2013**, *117* (50), 13885–13892.
1281 <https://doi.org/10.1021/jp4085684>.
- 1282 (41) Knoll, J. D.; Albani, B. A.; Durr, C. B.; Turro, C. Unusually Efficient Pyridine
1283 Photodissociation from Ru(II) Complexes with Sterically Bulky Bidentate Ancillary Ligands.
1284 *J. Phys. Chem. A* **2014**, *118* (45), 10603–10610. <https://doi.org/10.1021/jp5057732>.
- 1285 (42) Li, A.; Turro, C.; Kodanko, J. J. Ru(II) Polypyridyl Complexes as Photocages for Bioactive
1286 Compounds Containing Nitriles and Aromatic Heterocycles. *Chem. Commun.* **2018**, *54* (11),
1287 1280–1290. <https://doi.org/10.1039/C7CC09000E>.
- 1288 (43) Göttle, A. J.; Alary, F.; Boggio-Pasqua, M.; Dixon, I. M.; Heully, J.-L.; Bahreman, A.; Askes,
1289 S. H. C.; Bonnet, S. Pivotal Role of a Pentacoordinate ³MC State on the Photocleavage
1290 Efficiency of a Thioether Ligand in Ruthenium(II) Complexes: A Theoretical Mechanistic
1291 Study. *Inorg. Chem.* **2016**, *55* (9), 4448–4456.
1292 <https://doi.org/10.1021/acs.inorgchem.6b00268>.
- 1293 (44) Lameijer, L. N.; Ernst, D.; Hopkins, S. L.; Meijer, M. S.; Askes, S. H. C.; Le Dévédec, S. E.;
1294 Bonnet, S. A Red-Light-Activated Ruthenium-Caged NAMPT Inhibitor Remains Phototoxic
1295 in Hypoxic Cancer Cells. *Angew. Chem. Int. Ed.* **2017**, *56* (38), 11549–11553.
1296 <https://doi.org/10.1002/anie.201703890>.
- 1297 (45) van Rixel, V. H. S.; Ramu, V.; Auyeung, A. B.; Beztsinna, N.; Leger, D. Y.; Lameijer, L. N.;
1298 Hilt, S. T.; Le Dévédec, S. E.; Yildiz, T.; Betancourt, T.; Gildner, M. B.; Hudnall, T. W.; Sol,

1299 V.; Liagre, B.; Kornienko, A.; Bonnet, S. Photo-Uncaging of a Microtubule-Targeted Rigidin
1300 Analogue in Hypoxic Cancer Cells and in a Xenograft Mouse Model. *J. Am. Chem. Soc.*
1301 **2019**, *141* (46), 18444–18454. <https://doi.org/10.1021/jacs.9b07225>.

1302 (46) Bonnet, S. Why Develop Photoactivated Chemotherapy? *Dalton Trans.* **2018**, *47* (31),
1303 10330–10343. <https://doi.org/10.1039/C8DT01585F>.

1304 (47) Stephenson, M.; Reichardt, C.; Pinto, M.; Wächtler, M.; Sainuddin, T.; Shi, G.; Yin, H.;
1305 Monroe, S.; Sampson, E.; Dietzek, B.; McFarland, S. A. Ru(II) Dyads Derived from 2-(1-
1306 Pyrenyl)-1 *H* -Imidazo[4,5- *f*][1,10]Phenanthroline: Versatile Photosensitizers for
1307 Photodynamic Applications. *J. Phys. Chem. A* **2014**, *118* (45), 10507–10521.
1308 <https://doi.org/10.1021/jp504330s>.

1309 (48) Shi, G.; Monroe, S.; Hennigar, R.; Colpitts, J.; Fong, J.; Kasimova, K.; Yin, H.; DeCoste, R.;
1310 Spencer, C.; Chamberlain, L.; Mandel, A.; Lilge, L.; McFarland, S. A. Ru(II) Dyads Derived
1311 from α -Oligothiophenes: A New Class of Potent and Versatile Photosensitizers for PDT.
1312 *Coord. Chem. Rev.* **2015**, 282–283, 127–138. <https://doi.org/10.1016/j.ccr.2014.04.012>.

1313 (49) Reichardt, C.; Pinto, M.; Wächtler, M.; Stephenson, M.; Kupfer, S.; Sainuddin, T.;
1314 Guthmuller, J.; McFarland, S. A.; Dietzek, B. Photophysics of Ru(II) Dyads Derived from
1315 Pyrenyl-Substituted Imidazo[4,5- *f*][1,10]Phenanthroline Ligands. *J. Phys. Chem. A* **2015**,
1316 *119* (17), 3986–3994. <https://doi.org/10.1021/acs.jpca.5b01737>.

1317 (50) Reichardt, C.; Sainuddin, T.; Wächtler, M.; Monroe, S.; Kupfer, S.; Guthmuller, J.; Gräfe, S.;
1318 McFarland, S.; Dietzek, B. Influence of Protonation State on the Excited State Dynamics of
1319 a Photobiologically Active Ru(II) Dyad. *J. Phys. Chem. A* **2016**, *120* (32), 6379–6388.
1320 <https://doi.org/10.1021/acs.jpca.6b05957>.

1321 (51) Reichardt, C.; Schneider, K. R. A.; Sainuddin, T.; Wächtler, M.; McFarland, S. A.; Dietzek,
1322 B. Excited State Dynamics of a Photobiologically Active Ru(II) Dyad Are Altered in
1323 Biologically Relevant Environments. *J. Phys. Chem. A* **2017**, *121* (30), 5635–5644.
1324 <https://doi.org/10.1021/acs.jpca.7b04670>.

1325 (52) Reichardt, C.; Monroe, S.; Sobotta, F. H.; Colón, K. L.; Sainuddin, T.; Stephenson, M.;
1326 Sampson, E.; Roque, J.; Yin, H.; Brendel, J. C.; Cameron, C. G.; McFarland, S.; Dietzek, B.
1327 Predictive Strength of Photophysical Measurements for in Vitro Photobiological Activity in
1328 a Series of Ru(II) Polypyridyl Complexes Derived from π -Extended Ligands. *Inorg. Chem.*
1329 **2019**, *58* (5), 3156–3166. <https://doi.org/10.1021/acs.inorgchem.8b03223>.

1330 (53) Arenas, Y.; Monroe, S.; Shi, G.; Mandel, A.; McFarland, S.; Lilge, L. Photodynamic
1331 Inactivation of Staphylococcus Aureus and Methicillin-Resistant Staphylococcus Aureus
1332 with Ru(II)-Based Type I/Type II Photosensitizers. *Photodiag Photodyn Ther* **2013**, *10*, 615–
1333 625. <https://doi.org/10.1016/j.pdpdt.2013.07.001>.

1334 (54) Sainuddin, T.; Pinto, M.; Yin, H.; Hetu, M.; Colpitts, J.; McFarland, S. A. Strained
1335 Ruthenium Metal–Organic Dyads as Photocisplatin Agents with Dual Action. *J. Inorg.*
1336 *Biochem.* **2016**, *158*, 45–54. <https://doi.org/10.1016/j.jinorgbio.2016.01.009>.

1337 (55) Ghosh, G.; Colón, K. L.; Fuller, A.; Sainuddin, T.; Bradner, E.; McCain, J.; Monroe, S. M. A.;
1338 Yin, H.; Hetu, M. W.; Cameron, C. G.; McFarland, S. A. Cyclometalated Ruthenium(II)
1339 Complexes Derived from α -Oligothiophenes as Highly Selective Cytotoxic or
1340 Photocytotoxic Agents. *Inorg. Chem.* **2018**, *57* (13), 7694–7712.
1341 <https://doi.org/10.1021/acs.inorgchem.8b00689>.

1342 (56) Monroe, S.; Cameron, C. G.; Zhu, X.; Colón, K. L.; Yin, H.; Sainuddin, T.; Hetu, M.; Pinto,
1343 M.; Fuller, A.; Bennett, L.; Roque, J.; Sun, W.; McFarland, S. A. Synthesis, Characterization
1344 and Photobiological Studies of Ru(II) Dyads Derived from α -Oligothiophene Derivatives of

- 1,10-Phenanthroline. *Photochem. Photobiol.* **2019**, *95* (1), 267–279. <https://doi.org/10.1111/php.13012>.
- (57) McCain, J.; Colón, K. L.; Barrett, P. C.; Monroe, S. M. A.; Sainuddin, T.; Roque III, J.; Pinto, M.; Yin, H.; Cameron, C. G.; McFarland, S. A. Photophysical Properties and Photobiological Activities of Ruthenium(II) Complexes Bearing π -Expansive Cyclometalating Ligands with Thienyl Groups. *Inorg. Chem.* **2019**, *58* (16), 10778–10790. <https://doi.org/10.1021/acs.inorgchem.9b01044>.
- (58) Roque III, J.; Barrett, P. C.; Cole, H. D.; Lifshits, L. M.; Shi, G.; Monroe, S.; von Dohlen, D.; Kim, S.; Russo, N.; Deep, G.; Cameron, C. G.; Alberto, M. E.; McFarland, S. A. Breaking the Barrier: An Osmium Photosensitizer with Unprecedented Hypoxic Phototoxicity for Real World Photodynamic Therapy. *Chem. Sci.* **2020**, (*In review*).
- (59) Lifshits, L.; Roque III, J.; Cole, H. D.; Thummel, R. P.; Cameron, C. G.; McFarland, S. A. Synthesis, Characterization and Photobiological Activity of NIR-Absorbing Ru(II) Complexes Containing α -Oligothiophenes for Applications in Photodynamic Therapy. *ChemBioChem* **2020**, (*Submitted manuscript*).
- (60) Roque III, J. A.; Barrett, P. C.; Cole, H. D.; Lifshits, L. M.; Bradner, E.; Shi, G.; von Dohlen, D.; Kim, S.; Deep, G.; Cameron, C. G.; Alberto, M. E.; McFarland, S. A. Photophysical and Photodynamic Properties of Thiophene-Appended, Hypoxia-Active, Osmium Complexes: The Coligands Are Not Innocent. *Inorg. Chem.* **2020**, (*To Submit*).
- (61) Chen, Q.; Ramu, V.; Aydar, Y.; Groenewoud, A.; Zhou, X.-Q.; Jager, M. J.; Cole, H.; Cameron, C. G.; McFarland, S. A.; Bonnet, S.; Snaar-Jagalska, B. E. TLD1433 Photosensitizer Inhibits Conjunctival Melanoma Cells in Zebrafish Ectopic and Orthotopic Tumour Models. *Cancers* **2020**, *12* (3), 587. <https://doi.org/10.3390/cancers12030587>.
- (62) Fong, J.; Kasimova, K.; Arenas, Y.; Kaspler, P.; Lazic, S.; Mandel, A.; Lilge, L. A Novel Class of Ruthenium-Based Photosensitizers Effectively Kills in Vitro Cancer Cells and in Vivo Tumors. *Photochem. Photobiol. Sci.* **2015**, *14* (11), 2014–2023. <https://doi.org/10.1039/C4PP00438H>.
- (63) Kaspler, P.; Lazic, S.; Forward, S.; Arenas, Y.; Mandel, A.; Lilge, L. A Ruthenium(II) Based Photosensitizer and Transferrin Complexes Enhance Photo-Physical Properties, Cell Uptake, and Photodynamic Therapy Safety and Efficacy. *Photochem. Photobiol. Sci.* **2016**, *15* (4), 481–495. <https://doi.org/10.1039/C5PP00450K>.
- (64) Munegowda, M. A.; Fisher, C.; Molehuis, D.; Foltz, W.; Roufaiel, M.; Bassan, J.; Nitz, M.; Mandel, A.; Lilge, L. Efficacy of Ruthenium Coordination Complex–Based Rutherrin in a Preclinical Rat Glioblastoma Model. *Neuro-Oncol. Adv.* **2019**, *1* (1), vdz006. <https://doi.org/10.1093/noajnl/vdz006>.
- (65) Lilge, L.; Roufaiel, M.; Lazic, S.; Kaspler, P.; Munegowda, M. A.; Nitz, M.; Bassan, J.; Mandel, A. Evaluation of a Ruthenium Coordination Complex as Photosensitizer for PDT of Bladder Cancer: Cellular Response, Tissue Selectivity and in Vivo Response. *Transl. Biophotonics* **2020**, *2* (1–2). <https://doi.org/10.1002/tbio.201900032>.
- (66) Lilge, L.; Wu, J.; Xu, Y.; Manalac, A.; Molehuis, D.; Schwiegelshohn, F.; Vesselov, L.; Embree, W.; Nesbit, M.; Betz, V.; Mandel, A.; Jewett, M. A. S.; Kulkarni, G. S. Minimal Required PDT Light Dosimetry for Nonmuscle Invasive Bladder Cancer. *J. Biomed. Opt.* **2020**, *25* (6), 1–13. <https://doi.org/10.1117/1.JBO.25.6.068001>.
- (67) Lundrigan, T.; Jackson, C. L. M.; Uddin, Md. I.; Tucker, L. A.; Ali, A. A.-S.; Linden, A.; Cameron, T. S.; Thompson, A. Synthesis of Heteroleptic Pyrrolide/Bipyridyl Complexes of Ruthenium(II). *Can. J. Chem.* **2012**, *90* (8), 693–700. <https://doi.org/10.1139/v2012-045>.

- 1391 (68) Spaggiari, A.; Vaccari, D.; Davoli, P.; Prati, F. The Triphenyl Phosphite-Chlorine Reagent in
1392 the Synthesis of Pyrroles from *N*-Allylamides. *Synthesis* **2006**, No. 6, 995–998.
1393 <https://doi.org/10.1055/s-2006-926365>.
- 1394 (69) Liu, J.; Bu, L.; Dong, J.; Zhou, Q.; Geng, Y.; Ma, D.; Wang, L.; Jing, X.; Wang, F. Green
1395 Light-Emitting Polyfluorenes with Improved Color Purity Incorporated with 4,7-Diphenyl-
1396 2,1,3-Benzothiadiazole Moieties. *J. Mater. Chem.* **2007**, *17* (27), 2832.
1397 <https://doi.org/10.1039/b700004a>.
- 1398 (70) Sun, M.; Lan, L.; Wang, L.; Peng, J.; Cao, Y. Synthesis of Novel Conjugated Polyelectrolytes
1399 for Organic Field-Effect Transistors Gate Dielectric Materials. *Macromol. Chem. Phys.* **2008**,
1400 *209* (24), 2504–2509. <https://doi.org/10.1002/macp.200800420>.
- 1401 (71) Mei, J.; Graham, K. R.; Stalder, R.; Reynolds, J. R. Synthesis of Isoindigo-Based
1402 Oligothiophenes for Molecular Bulk Heterojunction Solar Cells. *Org. Lett.* **2010**, *12* (4), 660–
1403 663. <https://doi.org/10.1021/ol902512x>.
- 1404 (72) Kang, H. C.; Haugland, R. P. Dibenzopyrrometheneboron Difluoride Dyes. US5433896, July
1405 18, 1995.
- 1406 (73) Foxon, S. P.; Metcalfe, C.; Adams, H.; Webb, M.; Thomas, J. A. Electrochemical and
1407 Photophysical Properties of DNA Metallo-Intercalators Containing the Ruthenium(II) Tris(1-
1408 Pyrazolyl)Methane Unit. *Inorg. Chem.* **2007**, *46* (2), 409–416.
1409 <https://doi.org/10.1021/ic0607134>.
- 1410 (74) Abdel-Shafi, A. A.; Beer, P. D.; Mortimer, R. J.; Wilkinson, F. Photosensitized Generation
1411 of Singlet Oxygen from Ruthenium(II)-Substituted Benzoaza-Crown-Bipyridine Complexes.
1412 *Phys. Chem. Chem. Phys.* **2000**, *2* (14), 3137–3144. <https://doi.org/10.1039/b002884n>.
- 1413 (75) Ho, W. Y.; Yeap, S. K.; Ho, C. L.; Rahim, R. A.; Alitheen, N. B. Development of
1414 Multicellular Tumor Spheroid (MCTS) Culture from Breast Cancer Cell and a High
1415 Throughput Screening Method Using the MTT Assay. *PLoS ONE* **2012**, *7* (9), e44640.
1416 <https://doi.org/10.1371/journal.pone.0044640>.
- 1417 (76) *Methods for Dilution Antimicrobial Susceptibility Tests for Bacteria That Grow Aerobically:*
1418 *Approved Standard*, 7. ed.; Ferraro, M. J., Clinical and Laboratory Standards Institute, Eds.;
1419 Clinical and Laboratory Standards series; CLSI: Wayne, PA, 2006.
- 1420 (77) *Clinical Microbiology Procedures Handbook*, 2nd ed.; Isenberg, H. D., American Society for
1421 Microbiology, Eds.; ASM Press: Washington, D.C, 2004.
- 1422 (78) Smithen, D. A.; Yin, H.; Beh, M. H. R.; Hetu, M.; Cameron, T. S.; McFarland, S. A.;
1423 Thompson, A. Synthesis and Photobiological Activity of Ru(II) Dyads Derived from Pyrrole-
1424 2-Carboxylate Thionoesters. *Inorg. Chem.* **2017**, *56* (7), 4121–4132.
1425 <https://doi.org/10.1021/acs.inorgchem.7b00072>.
- 1426 (79) Waser, J.; Gaspar, B.; Nambu, H.; Carreira, E. M. Hydrazines and Azides via the Metal-
1427 Catalyzed Hydrohydrazination and Hydroazidation of Olefins. *J. Am. Chem. Soc.* **2006**, *128*
1428 (35), 11693–11712. <https://doi.org/10.1021/ja062355+>.
- 1429 (80) Cui, X.; Li, J.; Liu, L.; Guo, Q. X. 1,3-Dicarbonyl Compounds as Phosphine-Free Ligands
1430 for Pd-Catalyzed Heck and Suzuki Reactions. *Chin. Chem. Lett.* **2007**, *18* (6), 625–628.
1431 <https://doi.org/10.1016/j.ccllet.2007.04.014>.
- 1432 (81) Silverstein, R. M.; Ryskiewicz, E. E.; Willard, C. 2-PYRROLEALDEHYDE. *Org. Synth.*
1433 **1956**, *36*, 74. <https://doi.org/10.15227/orgsyn.036.0074>.
- 1434 (82) Haugland, R. P.; Kang, H. C. Chemically Reactive Dipyrrometheneboron Difluoride Dyes.
1435 US4774339A, September 27, 1988.

- 1436 (83) Setsune, J.; Watanabe, K. Cryptand-like Porphyrinoid Assembled with Three
1437 Dipyrrylpyridine Chains: Synthesis, Structure, and Homotropic Positive Allosteric Binding
1438 of Carboxylic Acids. *J. Am. Chem. Soc.* **2008**, *130* (8), 2404–2405.
1439 <https://doi.org/10.1021/ja710424n>.
- 1440 (84) Smalley, S. J.; Waterland, M. R.; Telfer, S. G. Heteroleptic Dipyrrin/Bipyridine Complexes
1441 of Ruthenium(II). *Inorg. Chem.* **2009**, *48* (1), 13–15. <https://doi.org/10.1021/ic8016497>.
- 1442 (85) Skrabalak, S. E.; Wiley, B. J.; Kim, M.; Formo, E. V.; Xia, Y. On the Polyol Synthesis of
1443 Silver Nanostructures: Glycolaldehyde as a Reducing Agent. *Nano Lett.* **2008**, *8* (7), 2077–
1444 2081. <https://doi.org/10.1021/nl800910d>.
- 1445 (86) Mariappan, M.; Suenaga, M.; Mukhopadhyay, A.; Raghavaiah, P.; Maiya, B. G. Synthesis,
1446 Structure, DNA Binding and Photocleavage Activity of a Ruthenium(II) Complex with 11-
1447 (9-Acridinyl)Dipyrido[3,2-a:2',3'-c]Phenazine Ligand. *Inorganica Chim. Acta* **2011**, *376* (1),
1448 340–349. <https://doi.org/10.1016/j.ica.2011.06.042>.
- 1449 (87) Ogilby, P. R.; Foote, C. S. Chemistry of Singlet Oxygen. 42. Effect of Solvent, Solvent
1450 Isotopic Substitution, and Temperature on the Lifetime of Singlet Molecular Oxygen
1451 (1.DELTA.g). *J. Am. Chem. Soc.* **1983**, *105* (11), 3423–3430.
1452 <https://doi.org/10.1021/ja00349a007>.
- 1453 (88) Birks, J. B. *Photophysics of Aromatic Molecules*; Wiley monographs in chemical physics;
1454 Wiley-Interscience: London, New York, 1970.
- 1455 (89) Sant, S.; Johnston, P. A. The Production of 3D Tumor Spheroids for Cancer Drug Discovery.
1456 *Drug Discov. Today Technol.* **2017**, *23*, 27–36. <https://doi.org/10.1016/j.ddtec.2017.03.002>.
1457

MS_Ru-pyrrolide-triads_200724.pdf (1.16 MiB)

[view on ChemRxiv](#) • [download file](#)

Bis[Pyrrolyl Ru(II)] Triads: a New Class of Photosensitizers for Metal-Organic Photodynamic Therapy

Deborah A. Smithen,^a Susan Monro,^b Mitch Pinto^b, John Roque III,^{c,d} Roberto M. Diaz-Rodriguez,^a Huimin Yin,^b Colin G. Cameron,^{c,d} Alison Thompson,^{a,*} and Sherri A. McFarland^{d,*}

^aDepartment of Chemistry, Dalhousie University, P.O. Box 15000, Halifax, NS, Canada, B3H 4R2

^bDepartment of Chemistry, Acadia University, Wolfville, NS, Canada, B4P 2R6

^cDepartment of Chemistry and Biochemistry, The University of North Carolina at Greensboro, PO Box 26170, Greensboro, NC 27402-6170 USA

^dDepartment of Chemistry and Biochemistry, The University of Texas at Arlington, 700 Planetarium Pl, Arlington, TX 76019-0065 USA

*Corresponding authors: A.T. <alison.thompson@dal.ca>, ORCID 0000-0003-4231-3446; S.A.M.

<sherri.mcfarland@uta.edu>, ORCID 0000-0002-8028-5055

Supporting Information

Table of Contents:

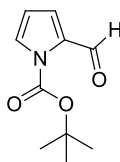
Additional Experimental Procedures	4
2-Formyl- <i>N</i> -Boc-pyrrole ¹	4
2-Vinyl- <i>N</i> -Boc-pyrrole (1a) ¹	4
4,7-Diphenylbenzo[<i>c</i>][1,2,5]thiadiazole ²	5
4,7-Bis(4-bromophenyl)benzo[<i>c</i>][1,2,5]thiadiazole (i) ²	6
4,7-Bis(1-methyl-1H-pyrrol-2-yl)benzo[<i>c</i>][1,2,5]thiadiazole ³	6
4,7-Bis(5-bromo-1-methyl-1H-pyrrol-2-yl)benzo[<i>c</i>][1,2,5]thiadiazole (j) ³	7
6,6'-Dibromoisindigo ⁴	7
<i>N,N'</i> -Bis(2-ethylhexyl)-6,6'-dibromoisindigo (k) ⁴	8
NMR Spectra	9
2-Formyl- <i>N</i> -Boc-pyrrole	9
2-Vinyl- <i>N</i> -Boc-pyrrole (1a)	9
4,7-Diphenylbenzo[<i>c</i>][1,2,5]thiadiazole	10
4,7-Bis(4-bromophenyl)benzo[<i>c</i>][1,2,5]thiadiazole (i)	11
4,7-Bis(1-methyl-1H-pyrrol-2-yl)benzo[<i>c</i>][1,2,5]thiadiazole	12
4,7-Bis(5-bromo-1-methyl-1H-pyrrol-2-yl)benzo[<i>c</i>][1,2,5]thiadiazole (j)	13

6,6'-Dibromoisindigo	14
<i>N,N'</i> -Bis(2-ethylhexyl)-6,6'-dibromoisindigo (k)	15
<i>Bis(pyrroles)(2)</i>	16
(<i>E</i>)-2-styryl-1H-pyrrole (2a).	16
1,4-Bis((<i>E</i>)-2-(1H-pyrrol-2-yl)vinyl)benzene (2b)	17
4,4'-Bis((<i>E</i>)-2-(1H-pyrrol-2-yl)vinyl)-1,1'-biphenyl (2c)	18
2,6-Bis((<i>E</i>)-2-(1H-pyrrol-2-yl)vinyl)naphthalene (2d)	19
4,7-Bis((<i>E</i>)-2-(1H-pyrrol-2-yl)vinyl)benzo[<i>c</i>][1,2,5]thiadiazole (2e)	20
9,10-Bis((<i>E</i>)-2-(1H-pyrrol-2-yl)vinyl)anthracene (2f)	21
2,7-Bis((<i>E</i>)-2-(1H-pyrrol-2-yl)vinyl)-9H-fluorene (2g)	22
1,6-Bis((<i>E</i>)-2-(1H-pyrrol-2-yl)vinyl)pyrene (2h)	23
4,7-Bis(4-((<i>E</i>)-2-(1H-pyrrol-2-yl)vinyl)phenyl)benzo[<i>c</i>][1,2,5]thiadiazole (2i)	24
4,7-Bis(1-methyl-1H,1'H-[2,2'-bipyrrol]-5-yl)benzo[<i>c</i>][1,2,5]thiadiazole (2j)	25
<i>N,N'</i> -Bis(2-ethylhexyl)-6,6'-Bis(1H-pyrrol-2-yl)isindigo (2k)	26
<i>Bis(formylpyrroles) (3)</i>	27
(<i>E</i>)-5-Styryl-1H-pyrrole-2-carbaldehyde (3a)	27
5,5'-((1 <i>E</i> ,1' <i>E</i>)-1,4-Phenylenebis(ethene-2,1-diyl))bis(1H-pyrrole-2-carbaldehyde) (3b)	28
5,5'-((1 <i>E</i> ,1' <i>E</i>)-[1,1'-biphenyl]-4,4'-diylbis(ethene-2,1-diyl))bis(1H-pyrrole-2-carbaldehyde) (3c)	29
5,5'-((1 <i>E</i> ,1' <i>E</i>)-naphthalene-2,6-diylbis(ethene-2,1-diyl))bis(1H-pyrrole-2-carbaldehyde) (3d)	30
5,5'-((1 <i>E</i> ,1' <i>E</i>)-benzo[<i>c</i>][1,2,5]thiadiazole-4,7-diylbis(ethene-2,1-diyl))bis(1H-pyrrole-2-carbaldehyde) (3e)	31
5,5'-((1 <i>E</i> ,1' <i>E</i>)-Anthracene-9,10-diylbis(ethene-2,1-diyl))bis(1H-pyrrole-2-carbaldehyde) (3f)	32
5,5'-((1 <i>E</i> ,1' <i>E</i>)-(9H-Fluorene-2,7-diyl)bis(ethene-2,1-diyl))bis(1H-pyrrole-2-carbaldehyde) (3g)	33
5,5'-((1 <i>E</i> ,1' <i>E</i>)-Pyrene-1,6-diylbis(ethene-2,1-diyl))bis(1H-pyrrole-2-carbaldehyde) (3h)	34
5,5'-((1 <i>E</i> ,1' <i>E</i>)-(Benzo[<i>c</i>][1,2,5]thiadiazole-4,7-diylbis(4,1-phenylene))bis(ethene-2,1-diyl))bis(1H-pyrrole-2-carbaldehyde) (3i)	35

5',5'''-(Benzo[<i>c</i>][1,2,5]thiadiazole-4,7-diyl)bis(1'-methyl-1H,1'H-[2,2'-bipyrrole]-5-carbaldehyde) (3j)	36
(<i>E</i>)-5,5'-(1,1'-Bis(2-ethylhexyl)-2,2'-dioxo-[3,3'-biindolinylidene]-6,6'-diyl)bis(1H-pyrrole-2-carbaldehyde) (3k)	37
<i>Bis(ruthenium) Complex Salts (4)</i>	38
[Ru(3a)(bpy) ₂](PF ₆) complex salt (4a)	38
[Ru ₂ (3b)(bpy) ₄](PF ₆) ₂ complex salt (4b)	39
[Ru ₂ (3c)(bpy) ₄](PF ₆) ₂ complex salt (4c)	40
[Ru ₂ (3d)(bpy) ₄](PF ₆) ₂ complex salt (4d)	41
[Ru ₂ (3e)(bpy) ₄](PF ₆) ₂ complex salt (4e)	42
[Ru ₂ (3f)(bpy) ₄](PF ₆) ₂ complex salt (4f)	43
[Ru ₂ (3g)(bpy) ₄](PF ₆) ₂ complex salt (4g)	44
[Ru ₂ (3h)(bpy) ₄](PF ₆) ₂ complex salt (4h)	45
[Ru ₂ (3i)(bpy) ₄](PF ₆) ₂ complex salt (4i)	46
[Ru ₂ (3j)(bpy) ₄](PF ₆) ₂ complex salt (4j)	47
[Ru ₂ (3k)(bpy) ₄](PF ₆) ₂ complex salt (4k)	48
UV Spectra	49
<i>Bis(pyrroles)</i>	49
<i>Bis(formylpyrroles)</i>	50
<i>Bis(ruthenium) Complex Salts</i>	51
References	52

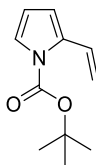
Additional Experimental Procedures

2-Formyl-*N*-Boc-pyrrole¹



A solution of 2-formyl pyrrole (2.0 g, 21.03 mmol) in anhydrous THF (20 mL) was added drop-wise, over 20 minutes, to a stirred suspension of sodium hydride (60% dispersion in mineral oil, 1.01 g, 25.23 mmol) in anhydrous THF (120 mL) under argon, with continued stirring at room temperature for 1 hour. (Boc)₂O (5.05 g, 23.13 mmol) was then added, as a solid in one portion, and the reaction was left to stir at room temperature overnight. After quenching with saturated aqueous ammonium chloride solution (20 mL), the reaction mixture was diluted with water (100 mL) and extracted with diethyl ether (3 x 100 mL). The combined organic extracts were washed with water (100 mL) and brine (100 mL), dried over anhydrous magnesium sulfate and concentrated to give the crude product, which was purified using column chromatography on silica, eluting with 20% ethyl acetate in hexanes, to give the title compound (3.63 g, 88% yield) as a pale yellow oil. ¹H NMR (CDCl₃, 500 MHz) δ 10.31 (s, 1H, CHO), 7.42 (dd, 1H, *J* = 1.5, 3.0 Hz), 7.17 (dd, 1H, *J* = 1.5, 3.5 Hz), 6.27 (at, 1H, *J* = 3.0 Hz), 1.63 (s, 9H, ^tBu) ppm; ¹³C NMR (CDCl₃, 125 MHz) δ 182.4, 148.5, 134.8, 127.4, 121.3, 111.8, 85.9, 28.0 ppm; LRMS: 218.1 (M+Na)⁺; HRMS: 218.0788 Found, 218.0788 Calculated for C₁₀H₁₃NO₃Na.

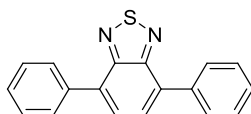
2-Vinyl-*N*-Boc-pyrrole (1a)¹



n-BuLi (1.6 M in hexanes, 5.28 mL, 8.45 mmol) was added to a stirred suspension of methyl triphenylphosphonium bromide (3.29 g, 9.22 mmol) in anhydrous THF (70 mL), at 0 °C under argon. After 2 hours, the mixture was cooled to -78 °C and a solution of 2-formyl-*N*-Boc-pyrrole (1.5 g, 7.68 mmol) in THF (10 mL) was added drop-wise over 15 minutes, with stirring overnight warming to room temperature. The reaction mixture was then diluted with water (100 mL) and

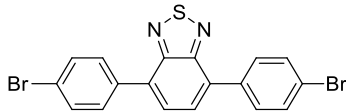
extracted with diethyl ether (3 x 100 mL). The combined organic extracts were washed with water (100 mL) and brine (100 mL), dried over anhydrous magnesium sulfate and concentrated to give the crude product, which was purified using column chromatography on silica, eluting with 10% ethyl acetate in hexanes, to give the product **1** (949 mg, 64% yield) as a yellow oil. ¹H NMR (CDCl₃, 500 MHz) δ 7.26-7.20 (m, 2H), 6.42-6.43 (m, 1H), 6.14 (at, 1H, *J* = 3.5 Hz), 5.53 (dd, 1H, *J* = 1.5, 17.5 Hz), 5.12 (dd, 1H, *J* = 1.5, 11.0 Hz), 1.60 (s, 9H, ^tBu) ppm; ¹³C NMR (CDCl₃, 125 MHz) δ 149.5, 134.6, 128.1, 122.0, 113.5, 110.9, 110.86, 83.9, 28.1 ppm; LRMS: 216.1 (M+Na)⁺; HRMS: 216.0990 Found, 216.0995 Calculated for C₁₁H₁₅NO₂Na.

4,7-Diphenylbenzo[*c*][1,2,5]thiadiazole²



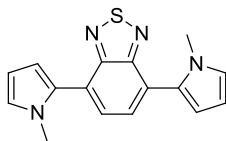
Potassium carbonate (564 mg, 4.08 mmol) and tetrakis(triphenylphosphine)palladium (118 mg, 0.102 mmol) were added to a stirred solution of 4,7-dibromobenzothiadiazole (300 mg, 1.02 mmol) and phenylboronic acid (275 mg, 2.14 mmol) in toluene (5 mL) and the resulting solution was bubbled with nitrogen for 10 minutes. Degassed (N₂) water (2 mL) was then added and the reaction mixture was heated to 90 °C, with stirring under nitrogen for 5 hours. After cooling to room temperature, the reaction mixture was separated between dichloromethane (50 mL) and water (50 mL). The aqueous phase was extracted with dichloromethane (3 x 50 mL) and the combined organic extracts were washed with water (100 mL) and brine (100 mL), dried over anhydrous sodium sulfate and concentrated to give the crude product, which was purified using column chromatography on silica, eluting with 20% diethyl ether in hexanes, to give the title compound (236 mg, 80% yield) as a pale yellow solid. M.p. 130–132 °C; ¹H NMR (CDCl₃, 500 MHz) δ 7.97 (d, 4H, *J* = 7.5, ArH), 7.80 (s, 2H, ArH), 7.57 (at, 4H, *J* = 7.5, ArH), 7.48 (t, 2H, *J* = 7.5 Hz, ArH) ppm; ¹³C NMR (CDCl₃, 125 MHz) δ 154.2, 137.6, 133.5, 129.4, 128.8, 128.5, 128.3 ppm; NMR data matches that previously reported for this compound.²

4,7-Bis(4-bromophenyl)benzo[*c*][1,2,5]thiadiazole (**i**)²



A solution of bromine (0.83 mL, 16.23 mmol) in anhydrous chloroform (1 mL) was added drop wise, over 5 minutes, to a solution of 4,7-diphenylbenzo[*c*][1,2,5]thiadiazole (200 mg, 0.694 mmol) and iodine (10 mg, 0.04 mmol) in anhydrous chloroform (3 mL), with stirring at room temperature under nitrogen for 16 hours. The reaction was quenched by the addition of 1 M aq. KOH solution (4 mL), with stirring for 1 hour, before separating between chloroform (200 mL) and water (150 mL). The organic phase was washed with 5% aq. Na₂SO₃ (150 mL) and brine (150 mL), dried over anhydrous sodium sulfate and concentrated to give the crude product, which was purified by trituration with toluene, to give the title compound (**i**) (250 mg, 83% yield) as a yellow solid. M.p. 274–278 °C; ¹H NMR (CDCl₃, 500 MHz) δ 7.86 (d, 4H, *J* = 8.3, ArH), 7.78 (s, 2H, ArH), 7.69 (d, 4H, *J* = 8.3, ArH) ppm; ¹³C NMR (CDCl₃, 125 MHz) δ 153.9, 136.2, 132.6, 132.0, 130.9, 128.1, 123.0 ppm; NMR data matches that previously reported for this compound.²

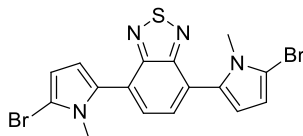
4,7-Bis(1-methyl-1H-pyrrol-2-yl)benzo[*c*][1,2,5]thiadiazole³



A solution of 4,7-dibromobenzothiadiazole (400 mg, 1.36 mmol), 1-methyl-2-pyrroleboronic acid pinacol ester (845 mg, 4.08 mmol) and sodium carbonate (577 mg, 5.44 mmol) in anhydrous DMF (12 mL) was bubbled with nitrogen for 10 minutes in a 5-20 mL capacity microwave vial. Tetrakis(triphenylphosphine)palladium (157 mg, 0.136 mmol) was then added with stirring and the vial was sealed and placed in a microwave reactor, with heating at 180 °C for 90 minutes. On completion of the reaction, the mixture was separated between dichloromethane (100 mL) and water (100 mL). The aqueous phase was extracted with dichloromethane (2 x 80 mL) and the combined organic extracts were washed with water (3 x 200 mL) and brine (200 mL), dried over anhydrous sodium sulfate and concentrated to give the crude product, which was purified by column chromatography on silica eluting with 15-20% diethyl ether in hexanes, to give the title compound (279 mg, 70% yield) as a deep red solid. M.p. 108–110 °C; ¹H NMR (CDCl₃, 500 MHz)

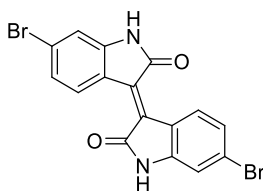
δ 7.58 (s, 2H, ArH), 6.88 (br s, 2H, PyH), 6.57 (br s, 2H, PyH), 6.33 (t, 2H, $J = 3.0$ Hz, PyH), 3.72 (s, 6H, 2 x CH₃) ppm; ¹³C NMR (CDCl₃, 125 MHz) δ 154.4, 130.2, 128.8, 125.5, 125.1, 112.0, 108.5, 35.9 ppm; LRMS: 317.1 (M+Na)⁺; HRMS: 217.0845 Found, 217.0831 Calculated for C₁₆H₁₄N₄SNa

4,7-Bis(5-bromo-1-methyl-1H-pyrrol-2-yl)benzo[*c*][1,2,5]thiadiazole (**j**)³



N-Bromosuccinimide (411 mg, 2.31 mmol) was added in one portion to a stirred solution of 4,7-bis(1-methyl-1H-pyrrol-2-yl)benzo[*c*][1,2,5]thiadiazole (340 mg, 1.155) in anhydrous THF (10 mL), with stirring at -10 °C (ice-salt bath), under nitrogen, for 3 hours. The reaction mixture was then separated between 2:1 diethyl ether:THF (90 mL) and water (90 mL). The aqueous phase was extracted with 2:1 diethyl ether:THF (2 x 90 mL) and the combined organic extracts were washed with water (200 mL) and brine (200 mL), dried over anhydrous magnesium sulfate and filtered through a short pad of silica, washing with diethyl ether, to give the title compound (**j**) (523 mg, 100% yield) as an orange solid, without the need for further purification. M.p. 130–135 °C; ¹H NMR (THF-*d*₈, 500 MHz) δ 7.63 (s, 2H, ArH), 6.47 (d, 2H, $J = 4.0$ Hz, PyH), 6.28 (d, 2H, $J = 4.0$ Hz, PyH), 3.60 (s, 6H, 2 x NMe) ppm; ¹³C NMR (THF-*d*₈, 125 MHz) δ 154.9, 132.6, 129.7, 126.6, 112.9, 111.6, 106.0, 34.9 ppm. **Note:** this compound was observed to be unstable in both dichloromethane and chloroform and will decompose very quickly in these solvents.

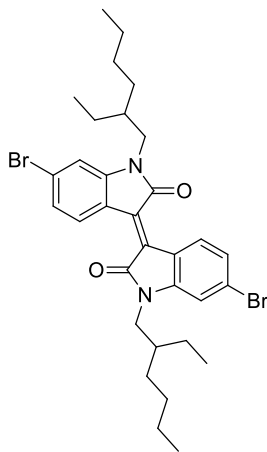
6,6'-Dibromoisindigo⁴



Concentrated HCl (0.1 mL) was added drop wise to a suspension of 6-bromoisatin (533 mg, 2.36 mmol) and 6-bromooxindole (500 mg, 2.36 mmol) in glacial acetic acid (15 mL) and the reaction mixture was heated to reflux temperature with stirring under nitrogen for 24 hours. After cooling to room temperature, the reaction mixture was filtered and the solid material washed sequentially

with water, ethanol and ethyl acetate until the washings were colourless, before drying in a vacuum oven to give 6,6'-dibromoisindigo (759 mg, 77% yield) as a dark brown solid. M.p./D.p. >250 °C; ¹H NMR (DMF-*d*₇, 500 MHz) δ 11.06 (br s, 2H, NH), 9.11 (d, 2H, *J* = 8.5 Hz, ArH), 7.21 (dd, 2H, *J* = 8.5, 1.5 Hz, ArH), 7.12 (d, 2H, *J* = 1.5 Hz, ArH) ppm; ¹³C NMR (DMF-*d*₇, 125 MHz) δ 169.8, 146.6, 133.6, 131.8, 126.6, 124.8, 122.0, 113.3 ppm; LRMS: 420.9 (M+H)⁺; HRMS: 420.9001 Found, 420.9025 Calculated for C₁₆H₉N₂O₂Br₂

***N,N'*-Bis(2-ethylhexyl)-6,6'-dibromoisindigo (k)⁴**

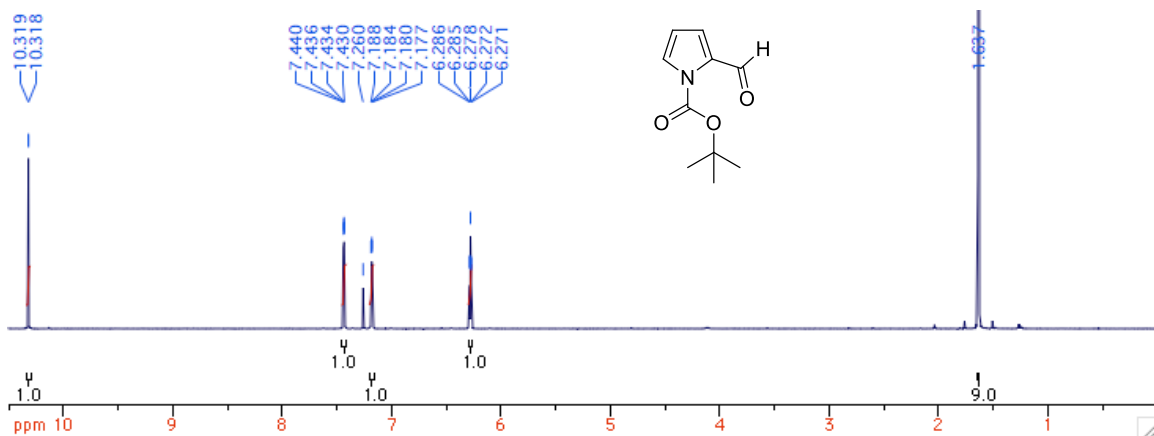


2-Ethylhexyl bromide (1.37 mL, 7.70 mmol) was added drop-wise, over 5 minutes, to a suspension of 6,6'-dibromoisindigo (1.47 g, 3.50 mmol) and potassium carbonate (2.9 g, 20.99 mmol) in anhydrous DMF (40 mL), with stirring under nitrogen. The reaction mixture was then heated to 100 °C, with stirring for 18 hours, before cooling to room temperature, pouring into water (200 mL) and extracting with dichloromethane (3 x 150 mL). The combined organic extracts were washed with water (2 x 500 mL) and brine (500 mL), dried over anhydrous sodium sulfate and concentrated to give the crude product, which was purified using column chromatography over silica, eluting with 40% hexanes in dichloromethane, to give the title compound (**k**, 1.847 g, 82% yield) as a dark red solid. M.p. 94–96 °C; ¹H NMR (CDCl₃, 500 MHz) δ 9.04 (d, 2H, *J* = 8.5 Hz, ArH), 7.16 (dd, 2H, *J* = 8.5, 2.0 Hz, ArH), 6.89 (d, 2H, *J* = 2.0 Hz, ArH), 3.67-3.57 (m, 4H), 1.86-1.79 (m, 2H), 1.41-1.25 (m, 16H), 0.93 (t, 6H, *J* = 7.5 Hz, 2 x CH₃), 0.90 (t, 6H, *J* = 7.0 Hz, 2 x CH₃) ppm; ¹³C NMR (CDCl₃, 125 MHz) δ 168.3, 146.3, 132.7, 131.1, 126.8, 125.3, 120.5, 111.7, 44.5, 37.6, 30.7, 28.7, 24.1, 23.2, 14.2, 10.8 ppm.

NMR Spectra

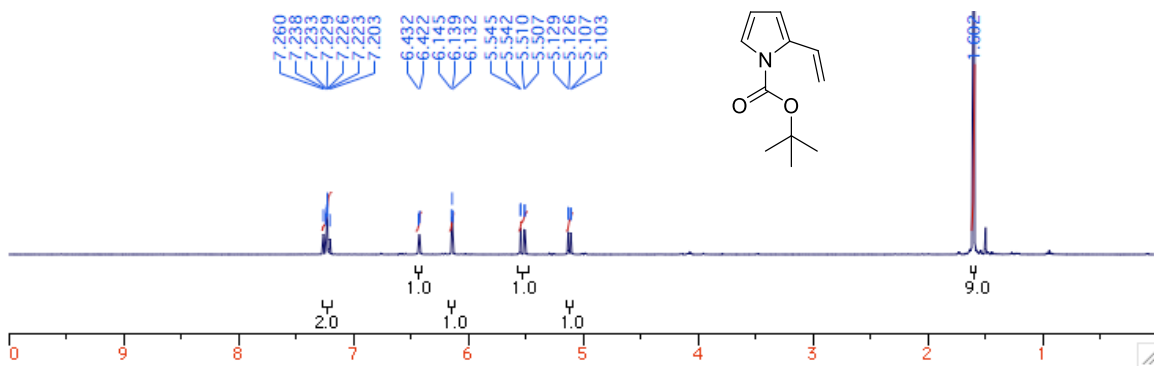
2-Formyl-N-Boc-pyrrole

¹H NMR (CDCl₃, 500 MHz):

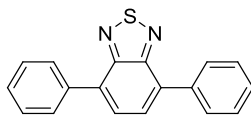


2-Vinyl-N-Boc-pyrrole (1a)

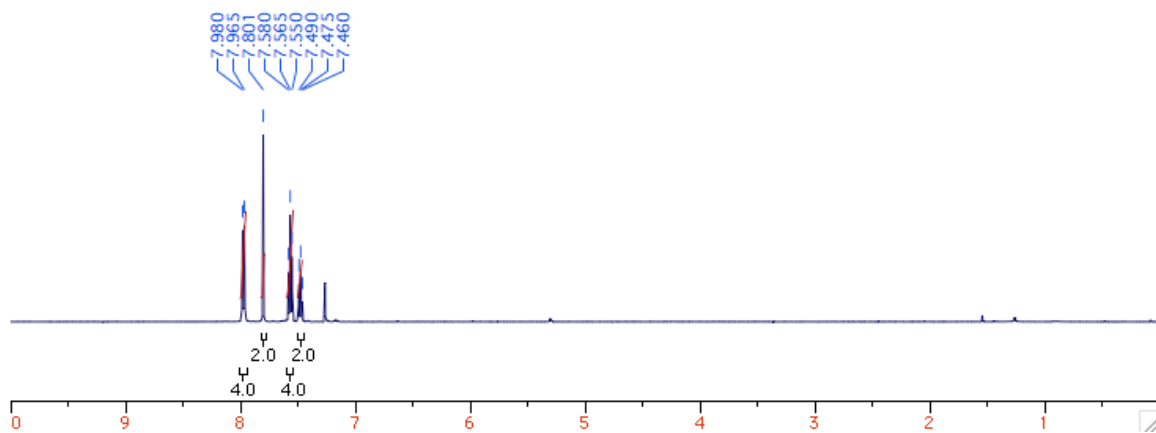
¹H NMR (CDCl₃, 500 MHz):



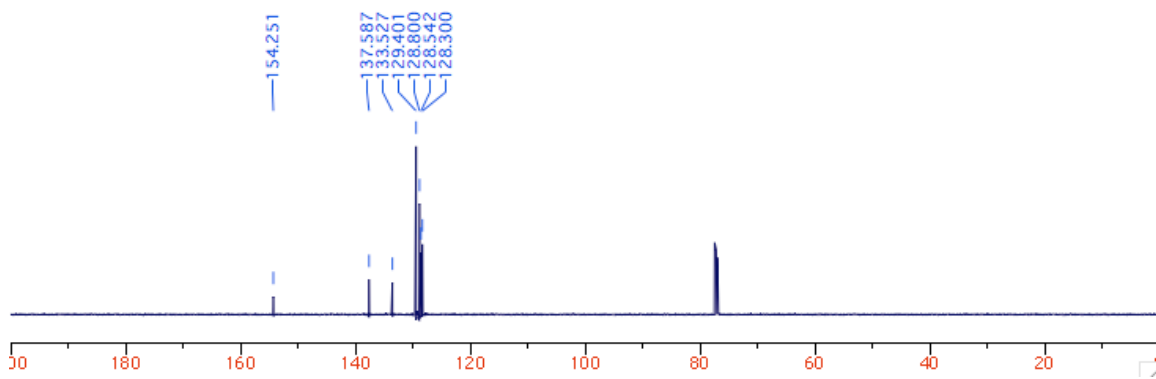
4,7-Diphenylbenzo[*c*][1,2,5]thiadiazole



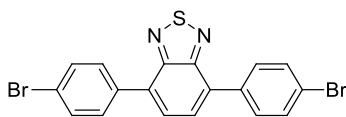
¹H NMR (CDCl₃, 500 MHz):



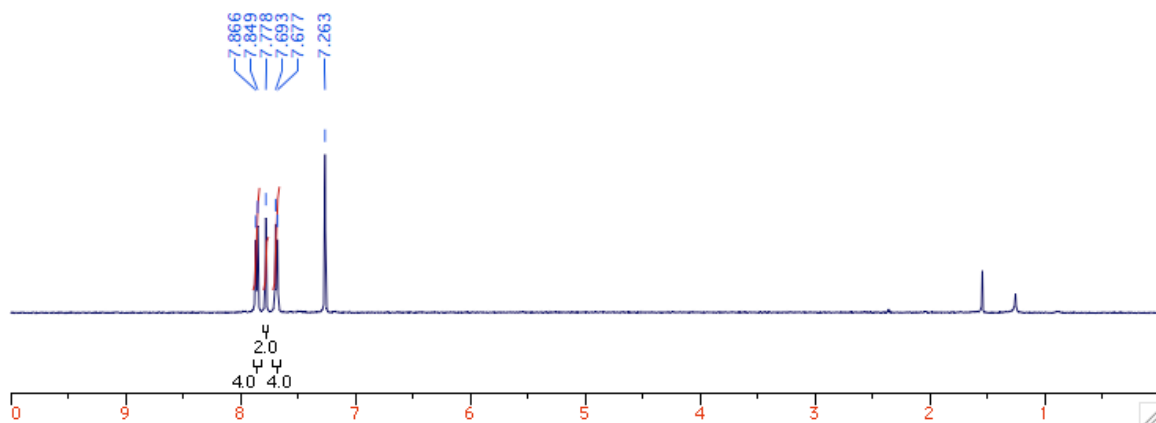
¹³C NMR (CDCl₃, 125 MHz):



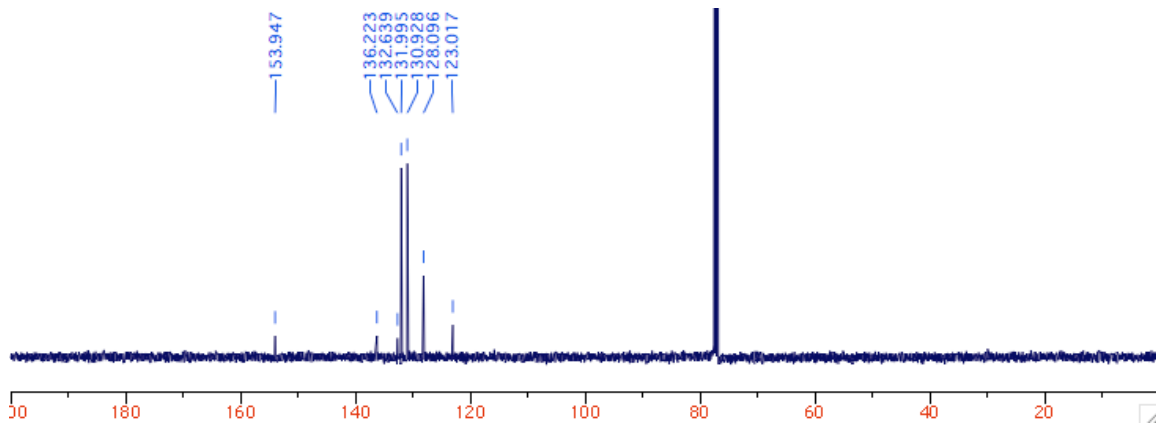
4,7-Bis(4-bromophenyl)benzo[*c*][1,2,5]thiadiazole (i)



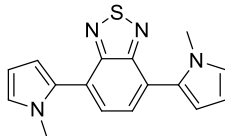
¹H NMR (CDCl₃, 500 MHz):



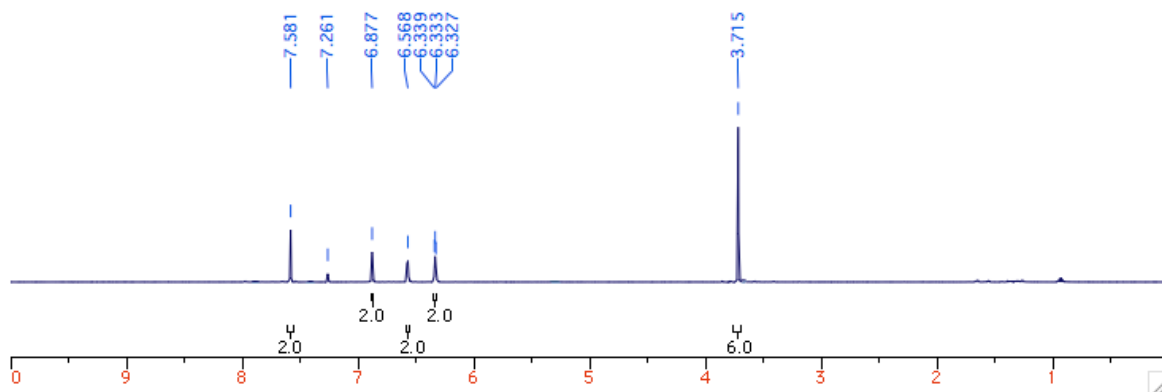
¹³C NMR (CDCl₃, 125 MHz):



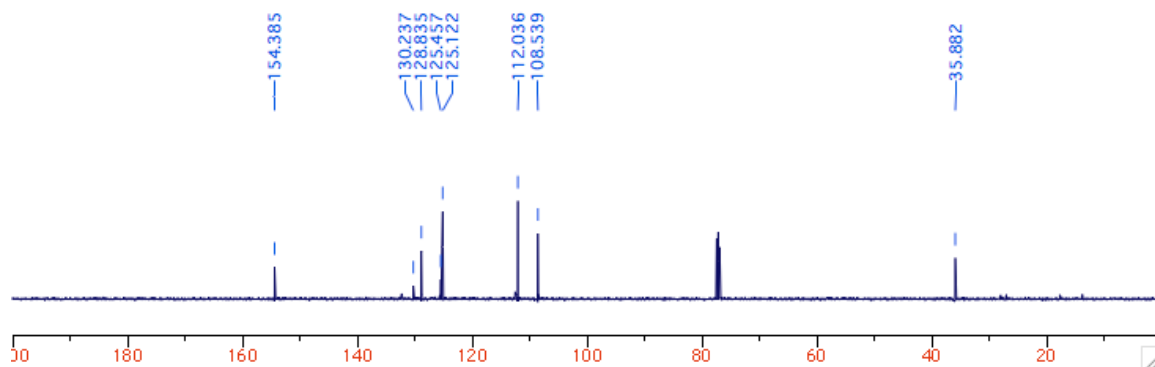
4,7-Bis(1-methyl-1H-pyrrol-2-yl)benzo[*c*][1,2,5]thiadiazole



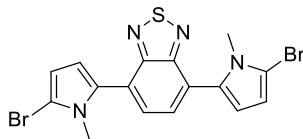
^1H NMR (CDCl_3 , 500 MHz):



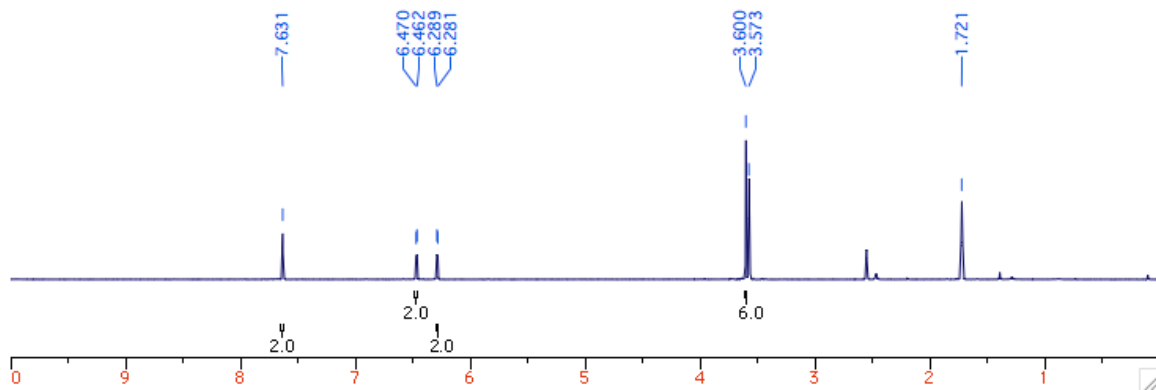
^{13}C NMR (CDCl_3 , 125 MHz):



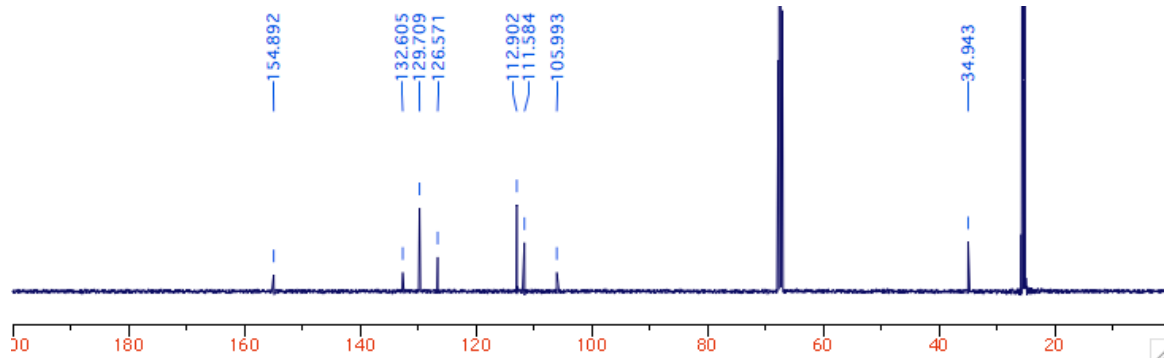
4,7-Bis(5-bromo-1-methyl-1H-pyrrol-2-yl)benzo[c][1,2,5]thiadiazole (j)



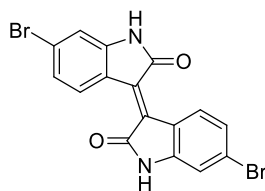
^1H NMR (THF- d_8 , 500 MHz):



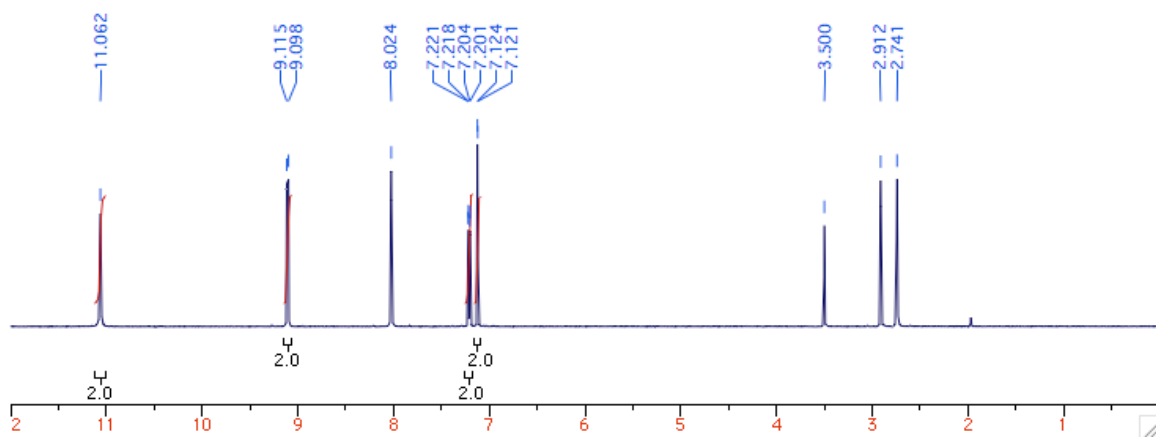
^{13}C NMR (THF- d_8 , 125 MHz):



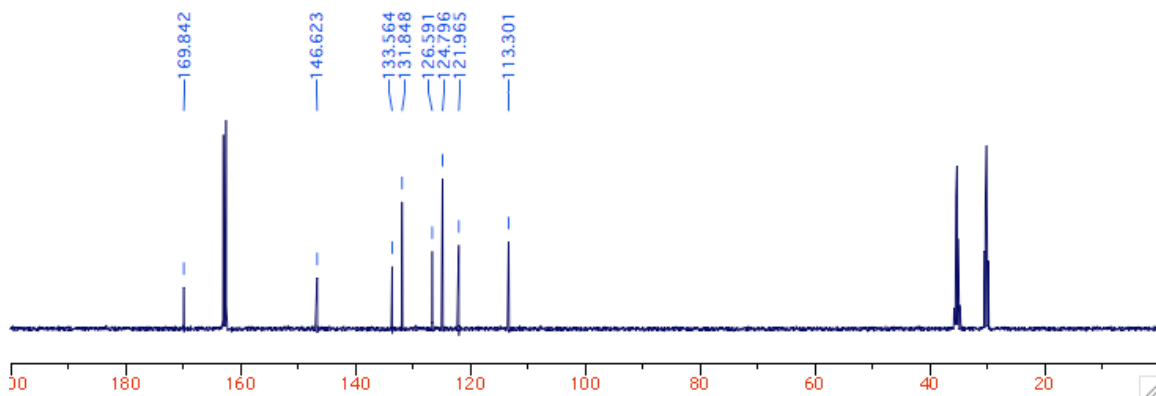
6,6'-Dibromoisoindigo



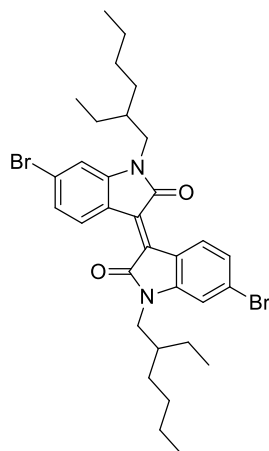
^1H NMR (DMF- d_7 , 500 MHz):



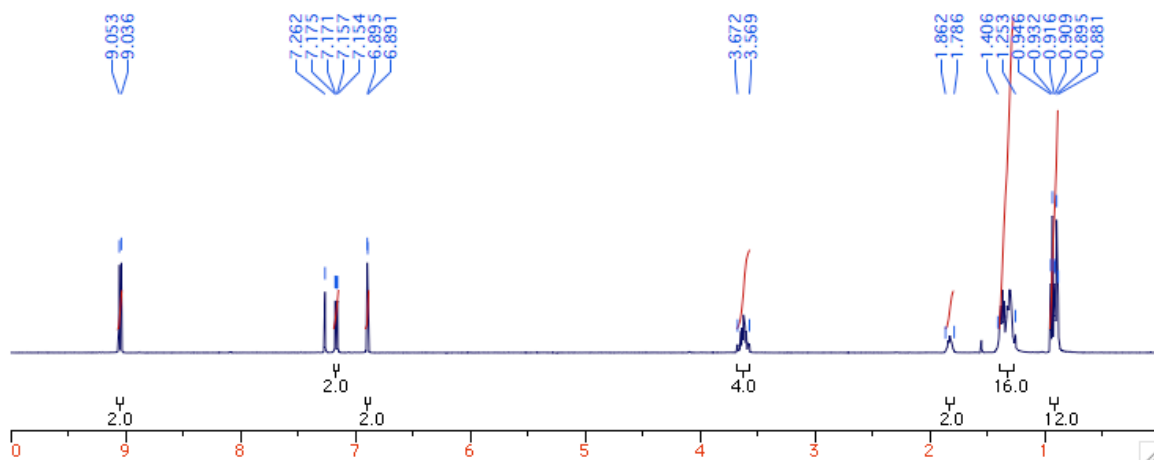
^{13}C udefr NMR (DMF- d_7 , 125 MHz):



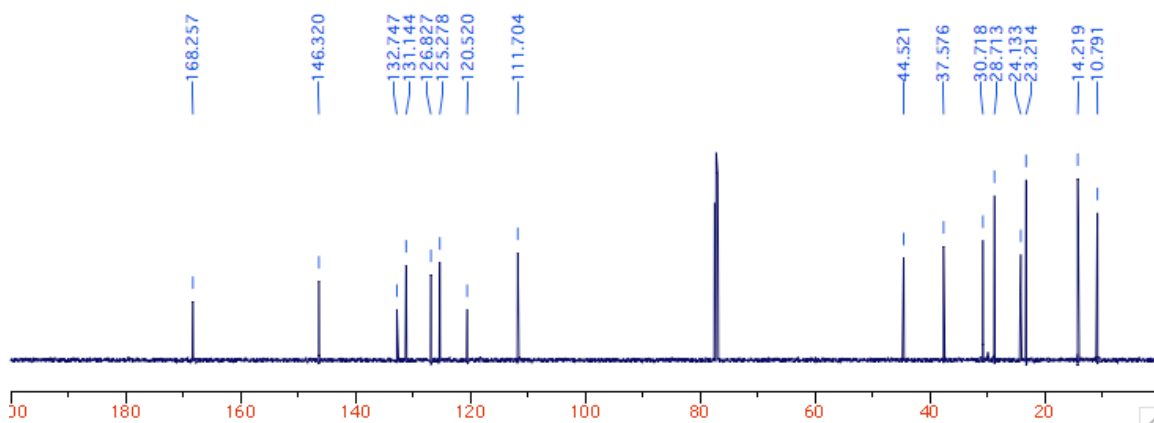
***N,N'*-Bis(2-ethylhexyl)-6,6'-dibromoindigo (k)**



¹H NMR (CDCl₃, 500 MHz):

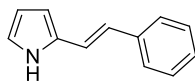


¹³C NMR (CDCl₃, 125 MHz):

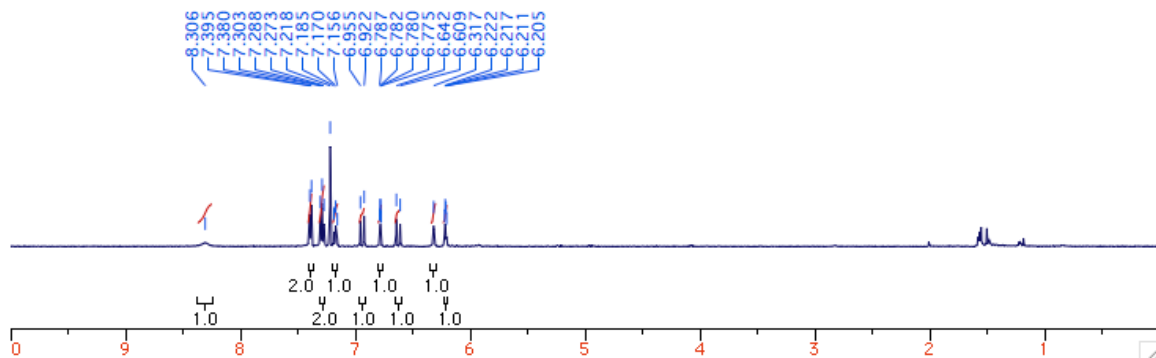


Bis(pyrroles)(2)

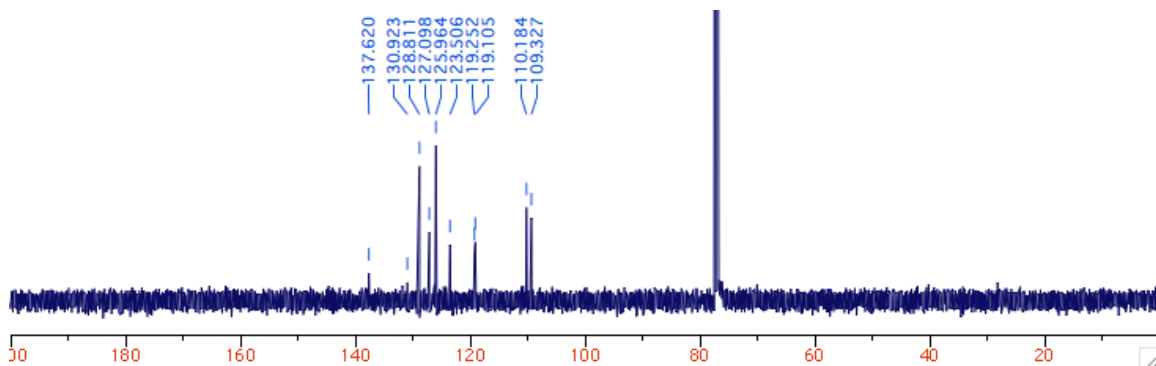
(E)-2-styryl-1H-pyrrole (2a).



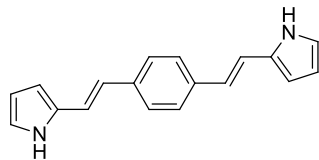
¹H NMR (CDCl₃, 500 MHz):



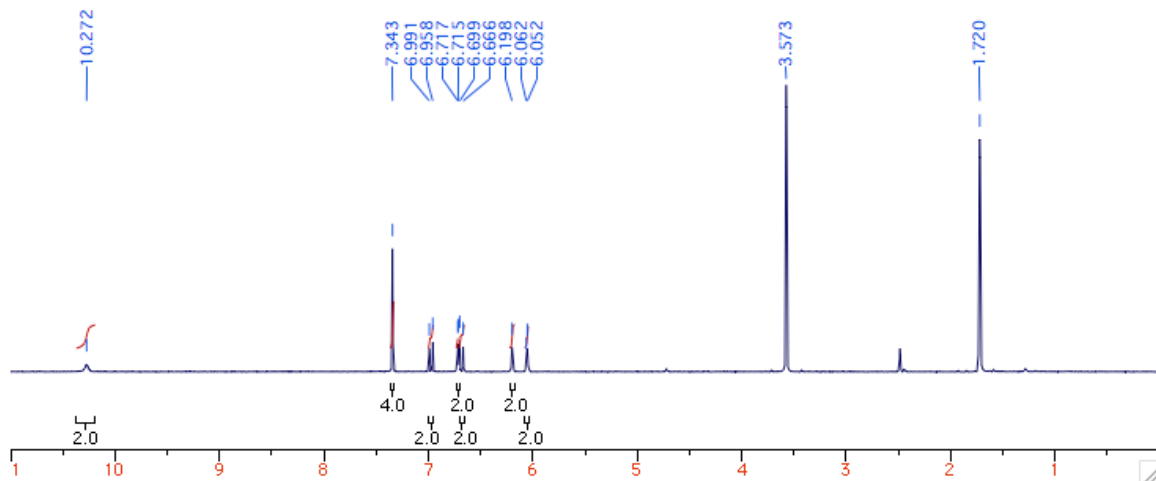
¹³C NMR (THF-d₈, 125 MHz):



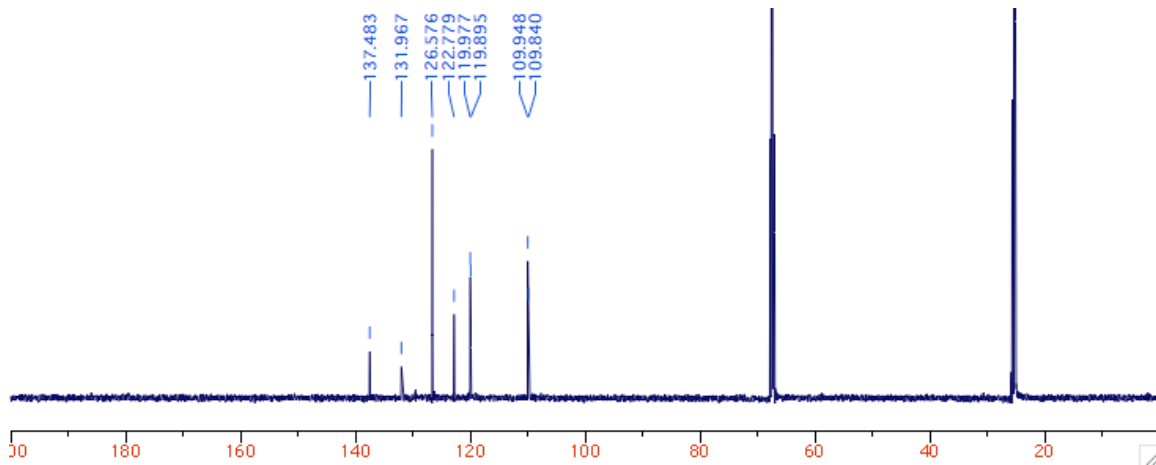
1,4-Bis((E)-2-(1H-pyrrol-2-yl)vinyl)benzene (2b)



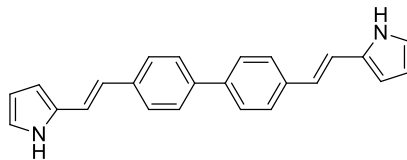
¹H NMR (THF-d₈, 500 MHz):



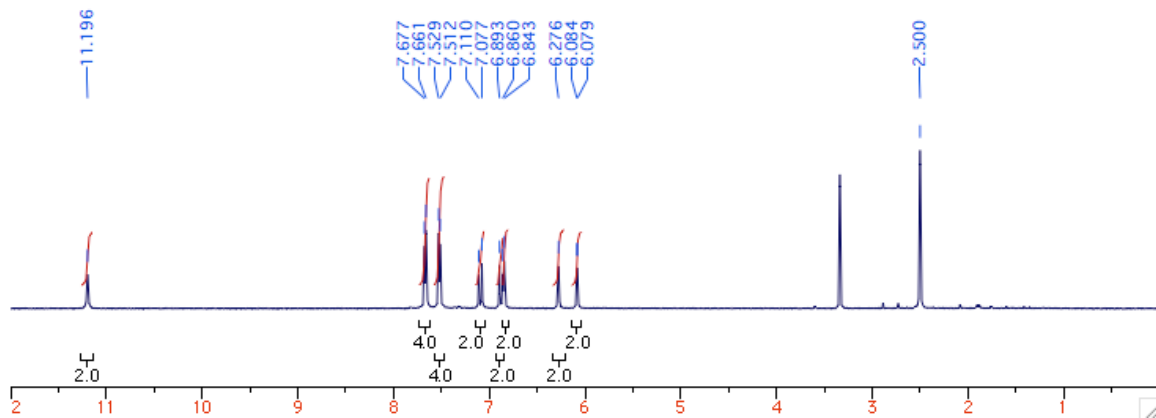
¹³C udefr NMR (THF-d₈, 125 MHz):



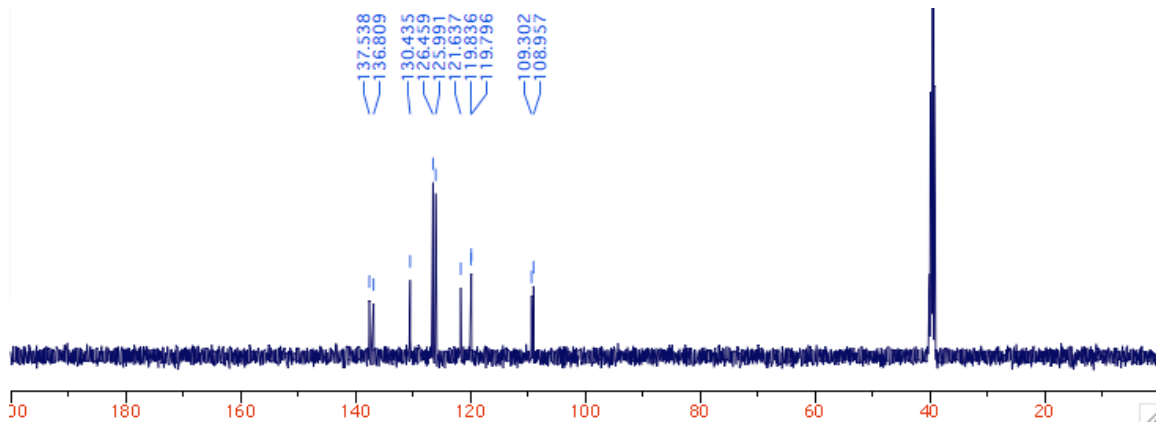
4,4'-Bis((E)-2-(1H-pyrrol-2-yl)vinyl)-1,1'-biphenyl (2c)



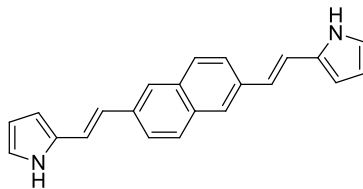
¹H NMR (DMSO-d₆, 500 MHz):



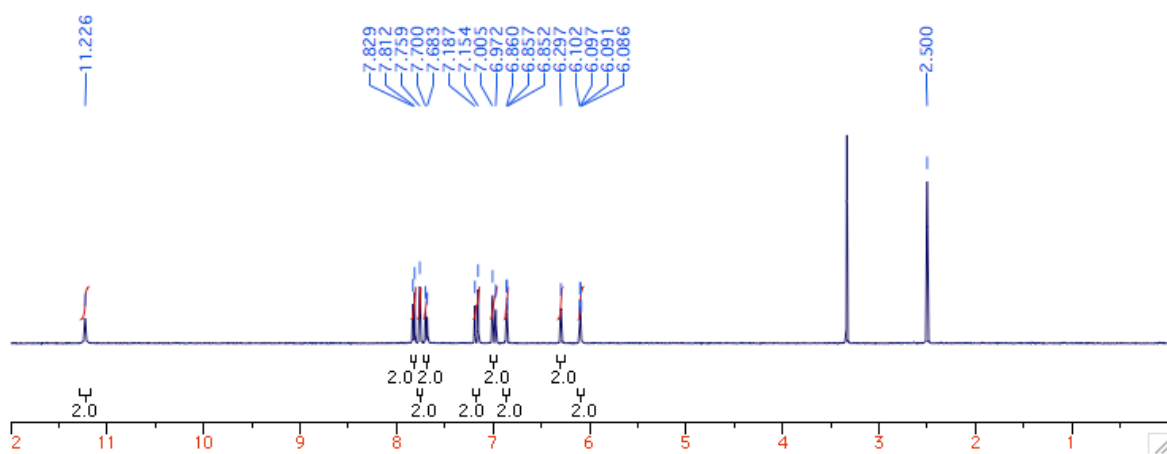
¹³C udefr NMR (DMSO-d₆, 125 MHz):



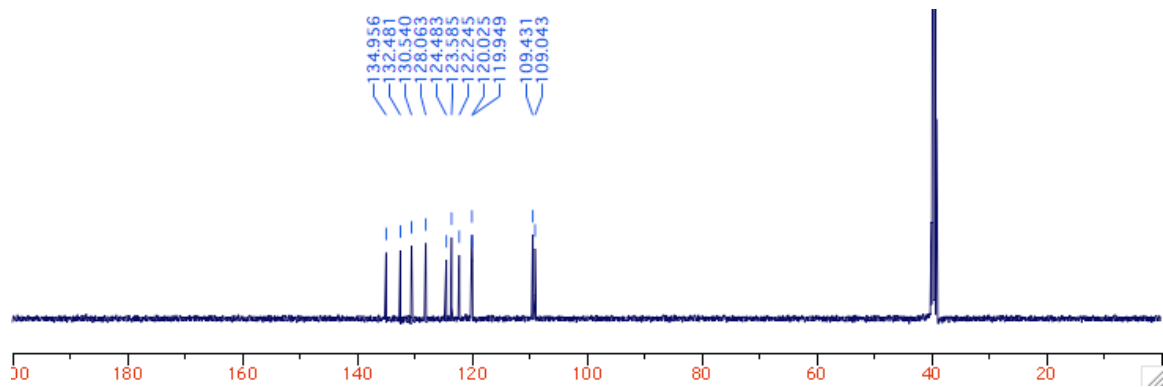
2,6-Bis((E)-2-(1H-pyrrol-2-yl)vinyl)naphthalene (2d)



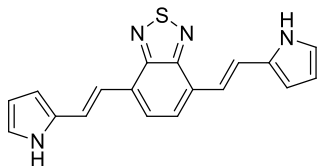
^1H NMR (DMSO- d_6 , 500 MHz):



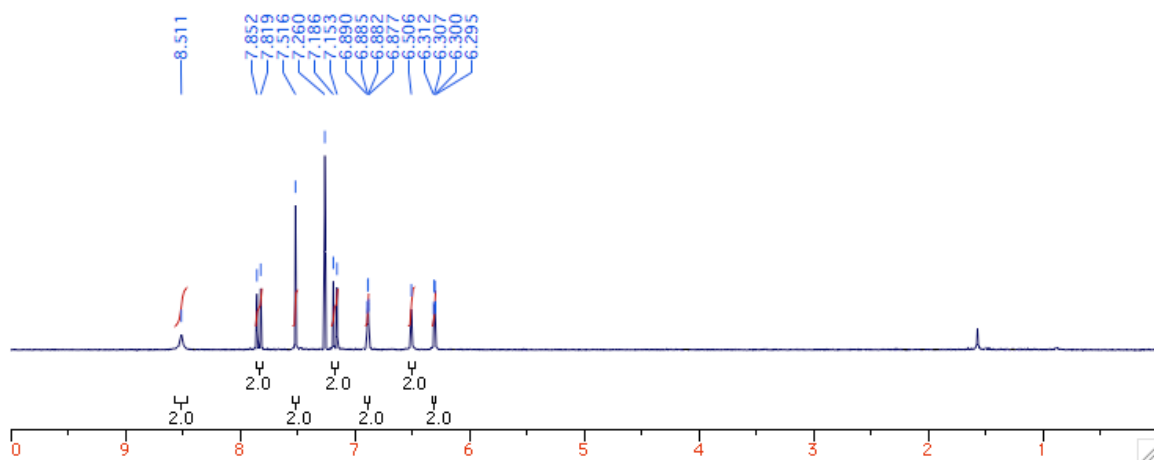
^{13}C NMR (DMSO- d_6 , 125 MHz):



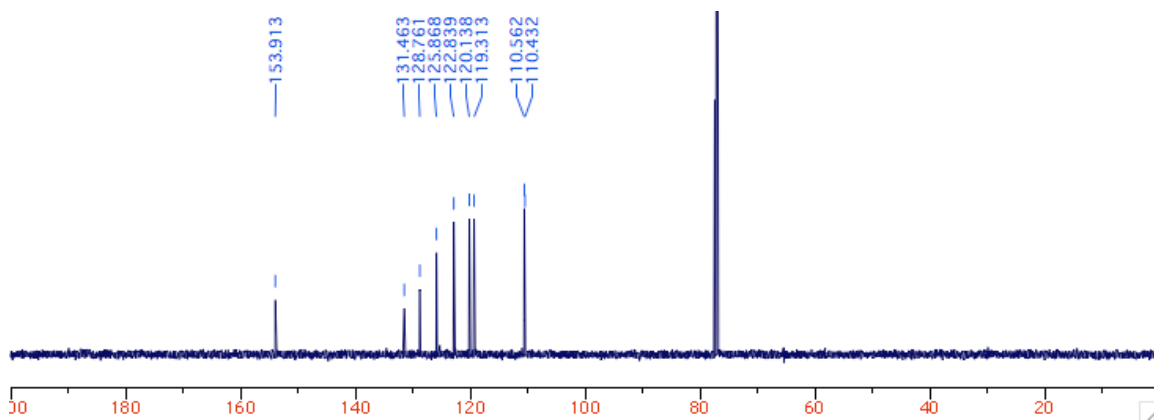
4,7-Bis((E)-2-(1H-pyrrol-2-yl)vinyl)benzo[*c*][1,2,5]thiadiazole (2e)



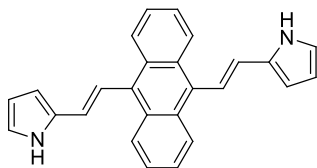
¹H NMR (CDCl₃, 500 MHz):



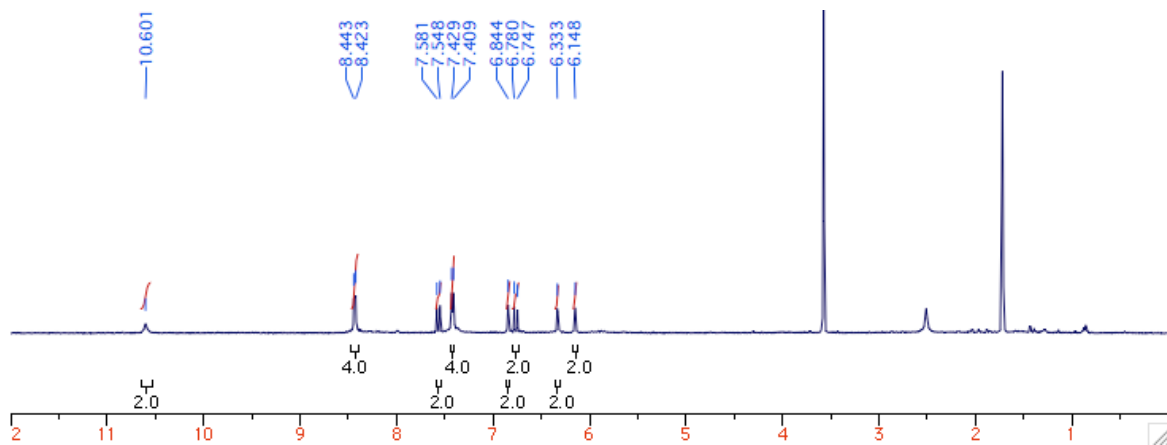
¹³C NMR (CDCl₃, 125 MHz):



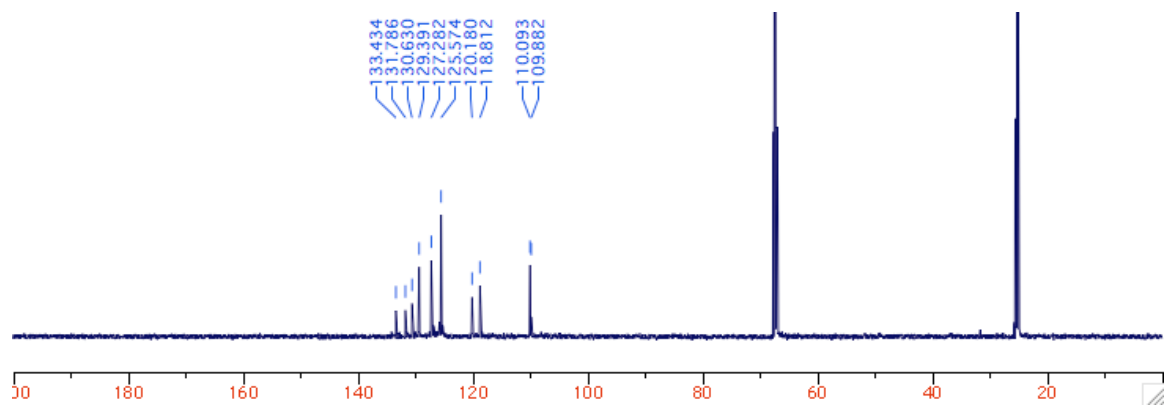
9,10-Bis((E)-2-(1H-pyrrol-2-yl)vinyl)anthracene (2f)



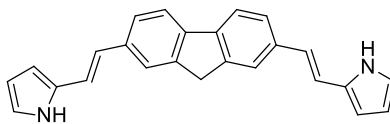
¹H NMR (THF-d₈, 500 MHz):



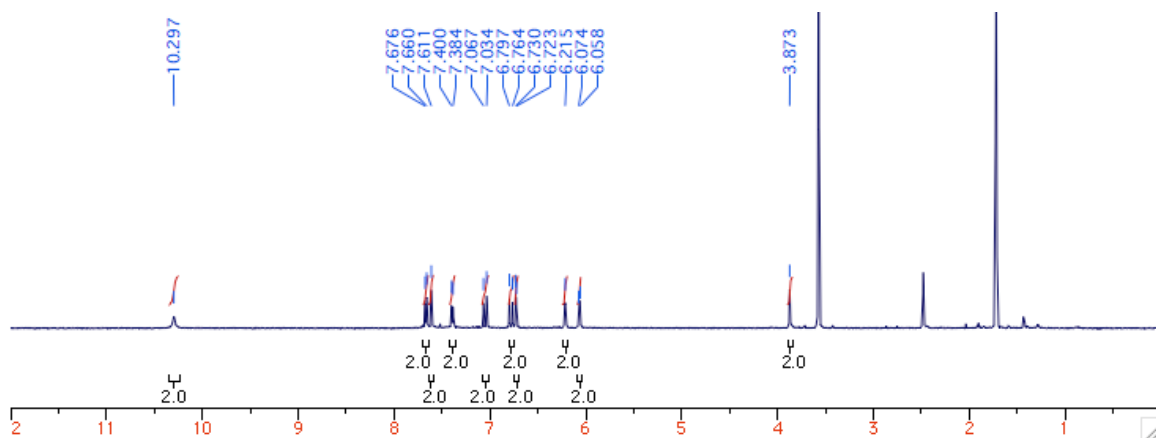
¹³C NMR (THF-d₈, 125 MHz):



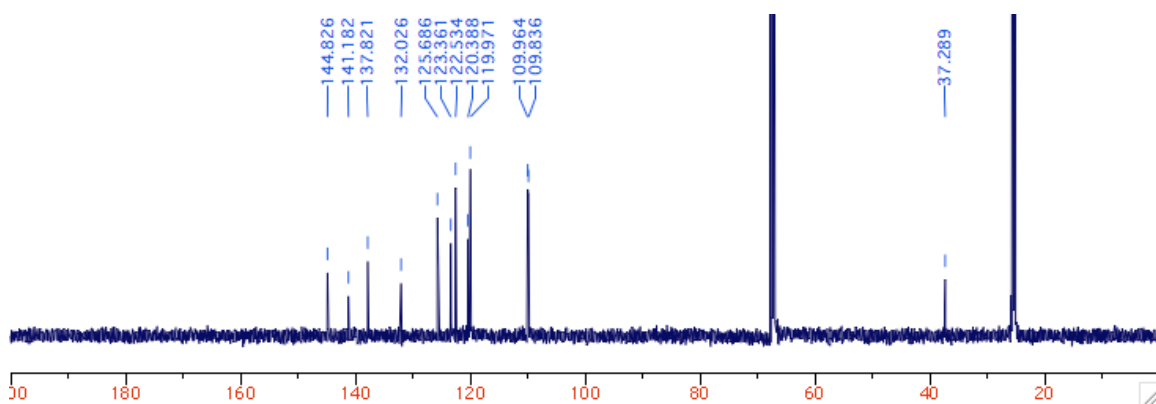
2,7-Bis((E)-2-(1H-pyrrol-2-yl)vinyl)-9H-fluorene (2g)



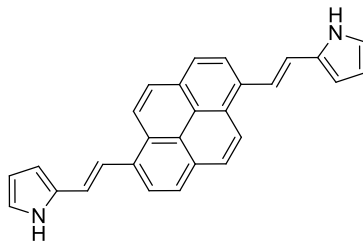
^1H NMR (THF- d_8 , 500 MHz):



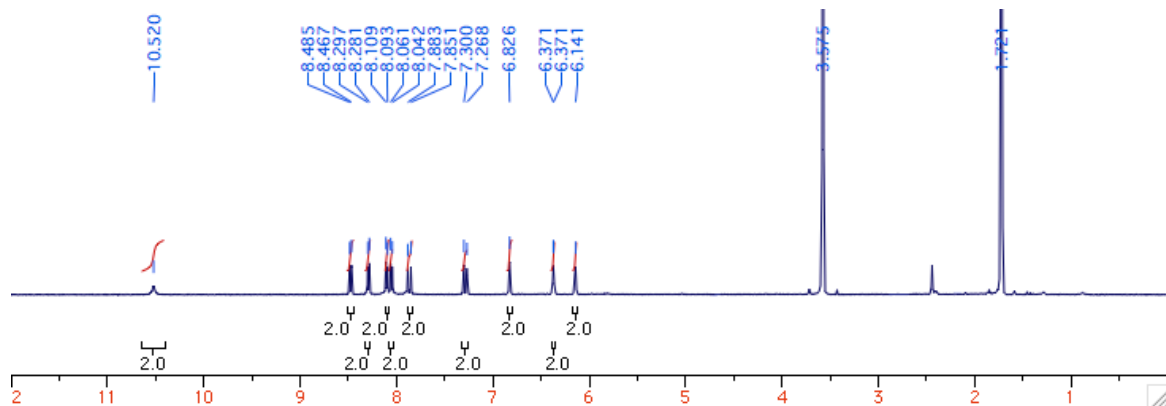
^{13}C udefr NMR (THF- d_8 , 125 MHz):



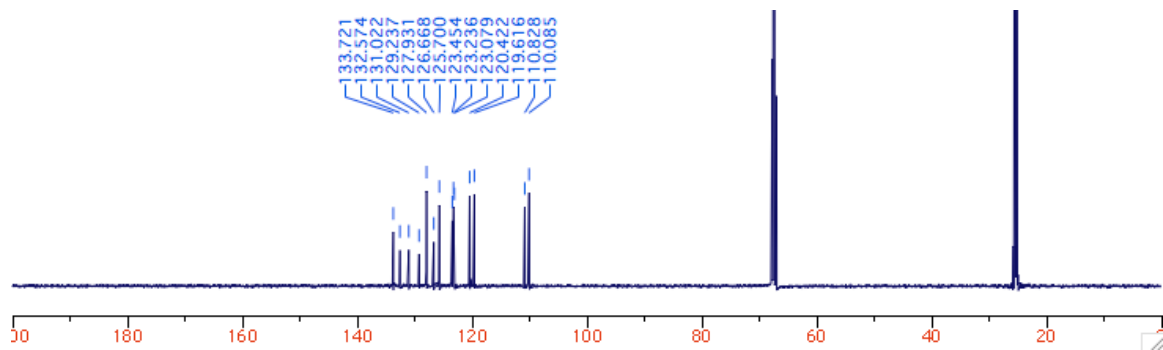
1,6-Bis((E)-2-(1H-pyrrol-2-yl)vinyl)pyrene (2h)



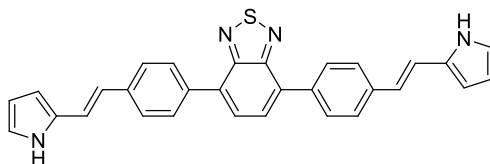
¹H NMR (THF-d₈, 500 MHz):



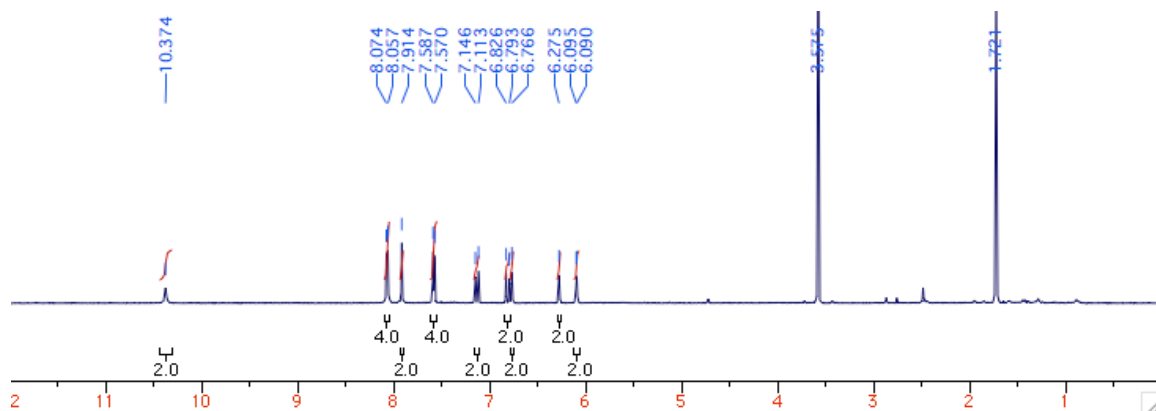
¹³C NMR (THF-d₈, 125 MHz):



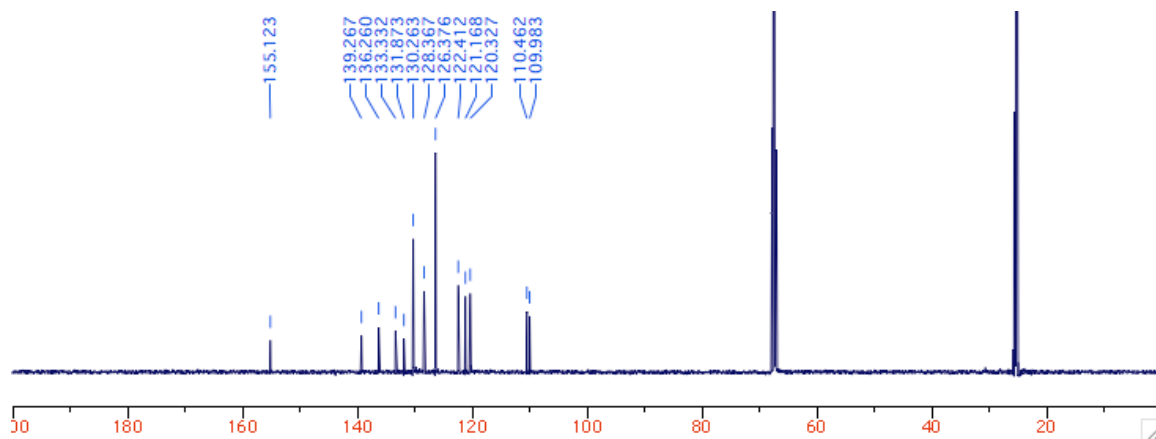
4,7-Bis(4-((E)-2-(1H-pyrrol-2-yl)vinyl)phenyl)benzo[c][1,2,5]thiadiazole (2i)



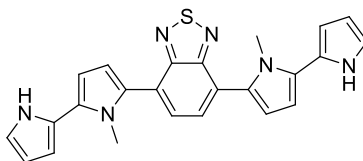
¹H NMR (THF-d₈, 500 MHz):



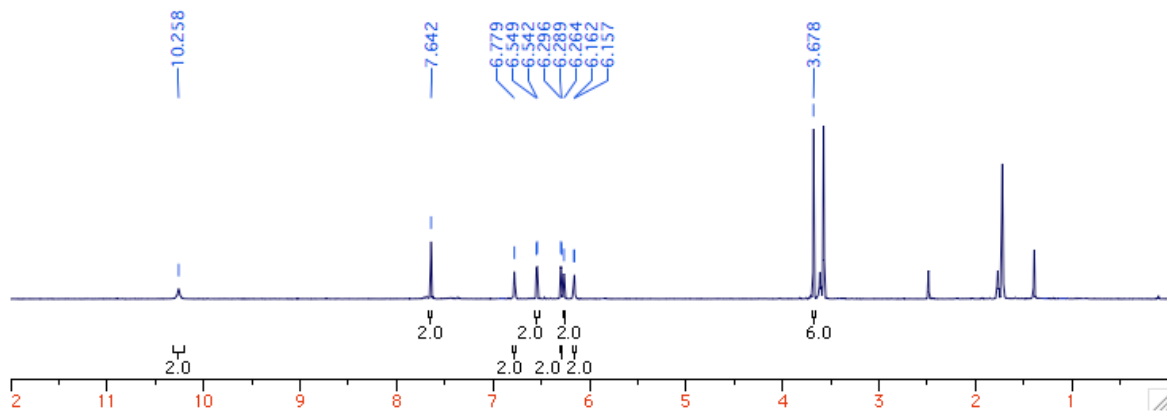
¹³C udefr NMR (THF-d₈, 125 MHz):



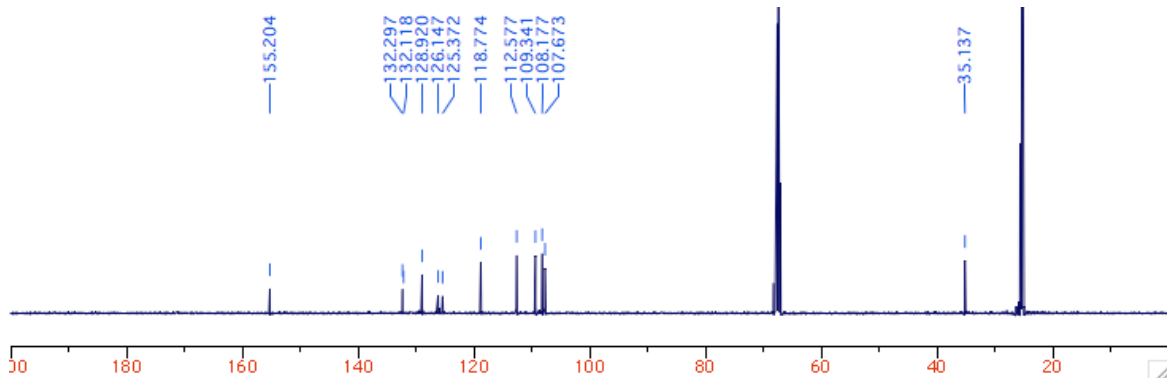
4,7-Bis(1-methyl-1H-[2,2'-bipyrrrol]-5-yl)benzo[c][1,2,5]thiadiazole (2j)



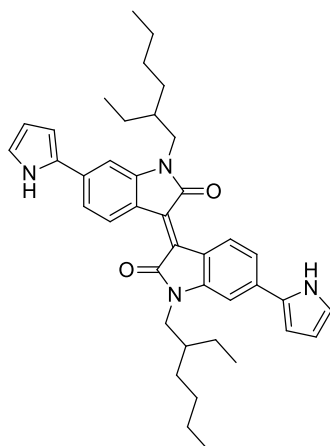
¹H NMR (THF-d₈, 500 MHz):



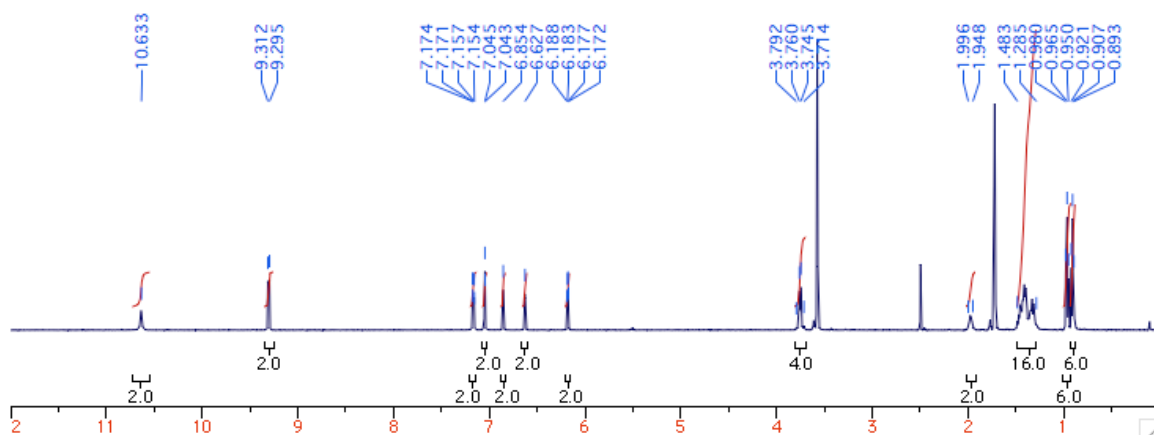
¹³C NMR (THF-d₈, 125 MHz):



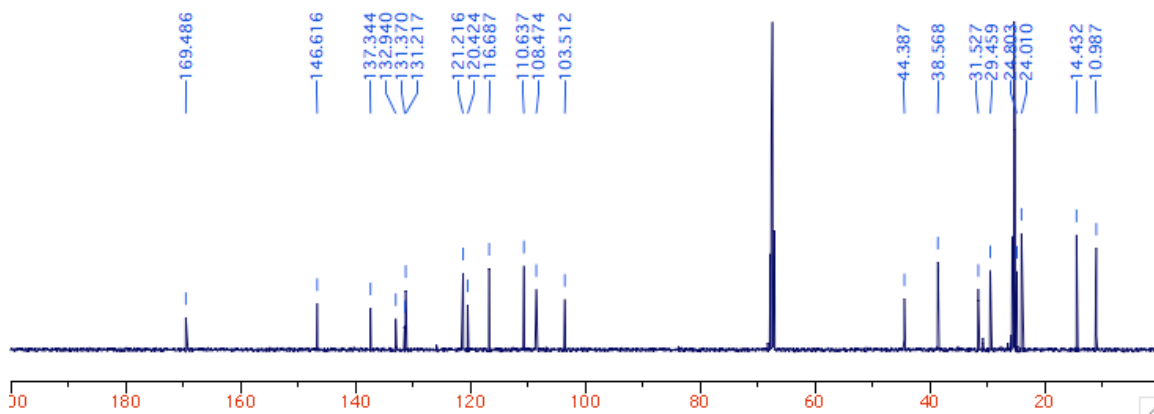
***N,N'*-Bis(2-ethylhexyl)-6,6'-Bis(1H-pyrrol-2-yl)isoindigo (2k)**



¹H NMR (THF-d₈, 500 MHz):

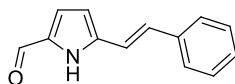


¹³C NMR (THF-d₈, 125 MHz):

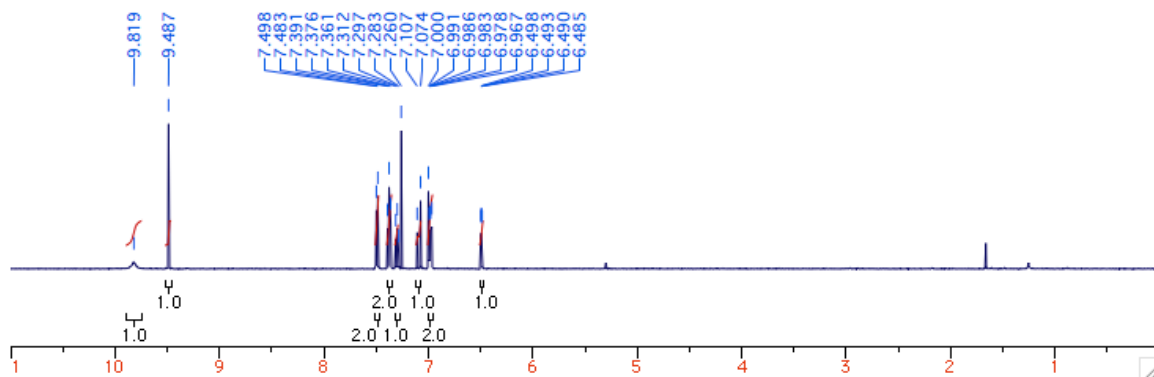


Bis(formylpyrroles) (3)

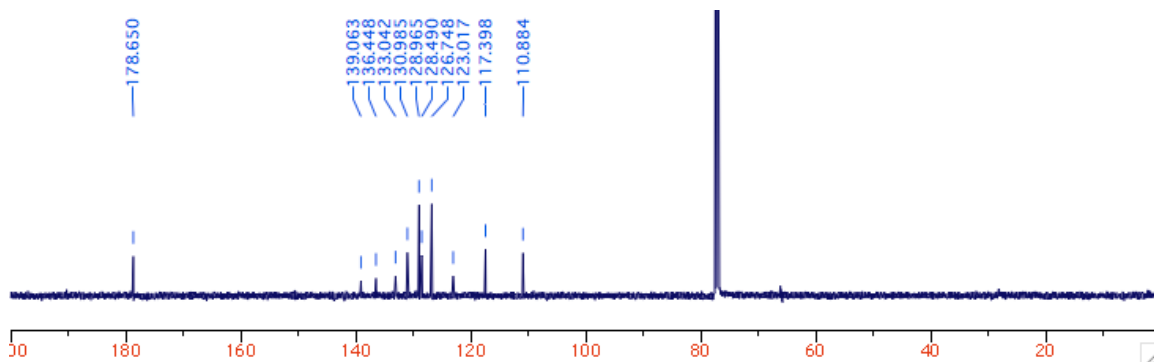
(E)-5-Styryl-1H-pyrrole-2-carbaldehyde (3a)



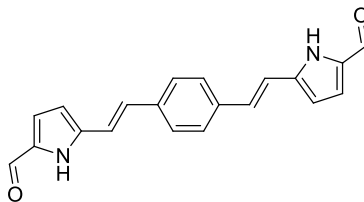
¹H NMR (CDCl₃, 500 MHz):



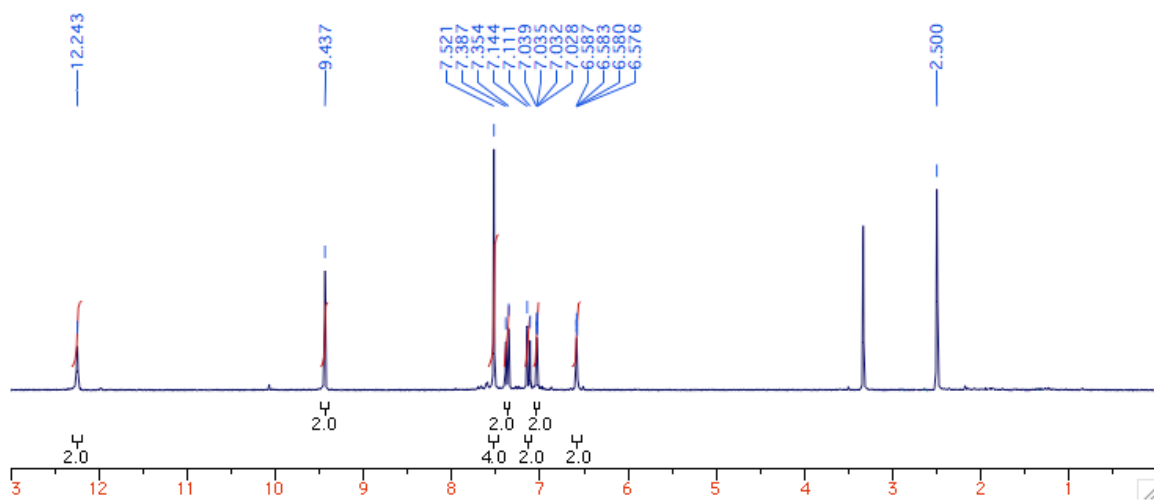
¹³C NMR (CDCl₃, 125 MHz):



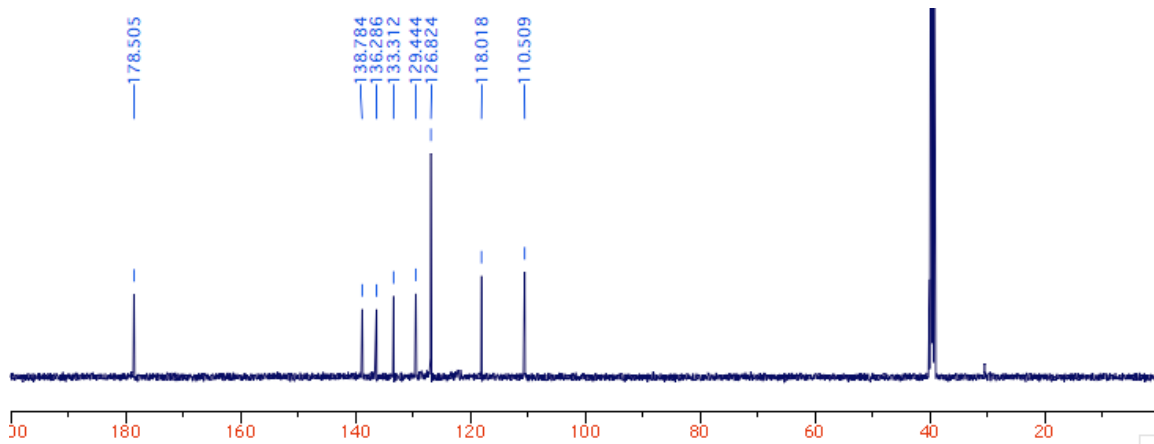
5,5'-((1E,1'E)-1,4-Phenylenebis(ethene-2,1-diyl))bis(1H-pyrrole-2-carbaldehyde) (3b)



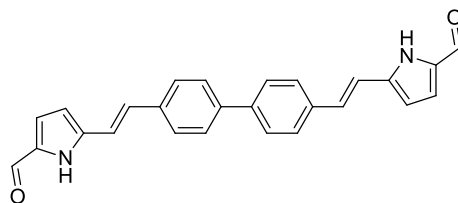
^1H NMR (DMSO- d_6 , 500 MHz):



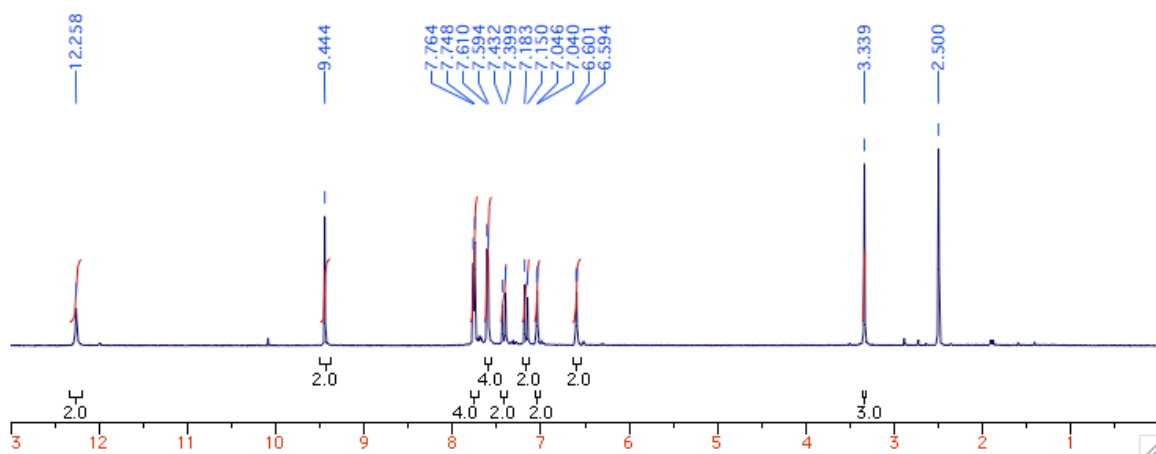
^{13}C NMR (DMSO- d_6 , 125 MHz):



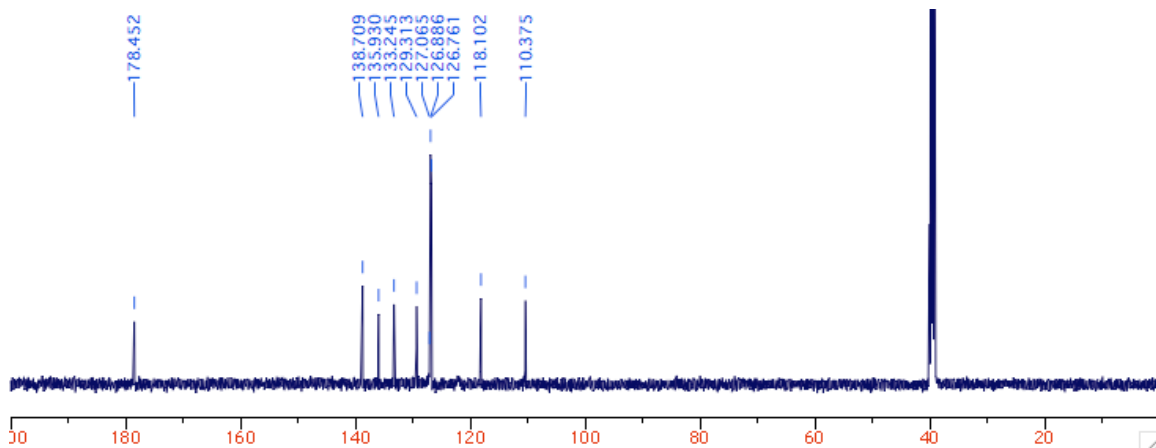
**5,5'-((1E,1'E)-[1,1'-biphenyl]-4,4'-diylbis(ethene-2,1-diyl))bis(1H-pyrrole-2-carbaldehyde)
(3c)**



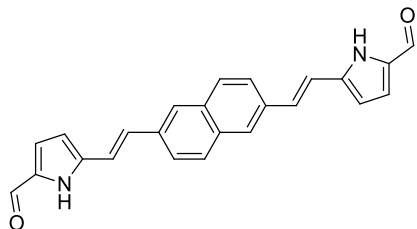
¹H NMR (DMSO-d₆, 500 MHz):



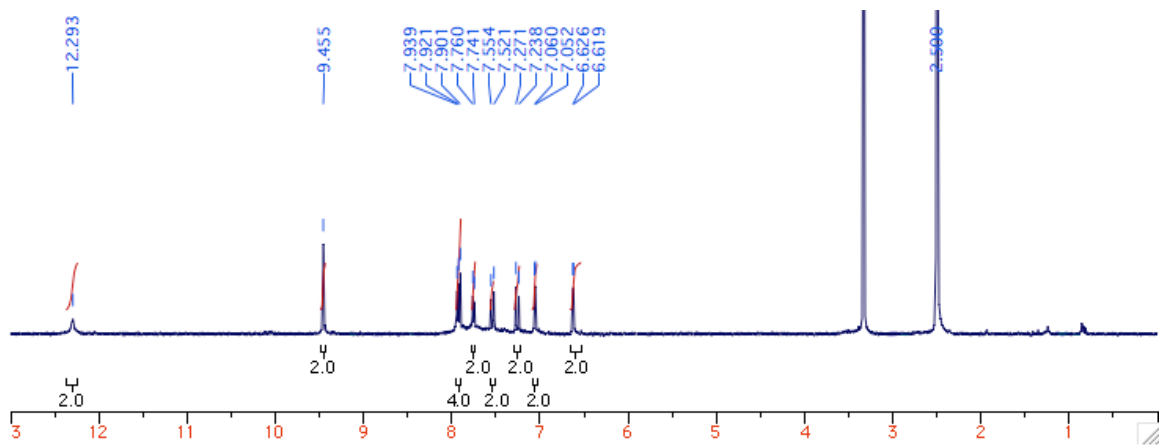
¹³C udefr NMR (DMSO-d₆, 125 MHz):



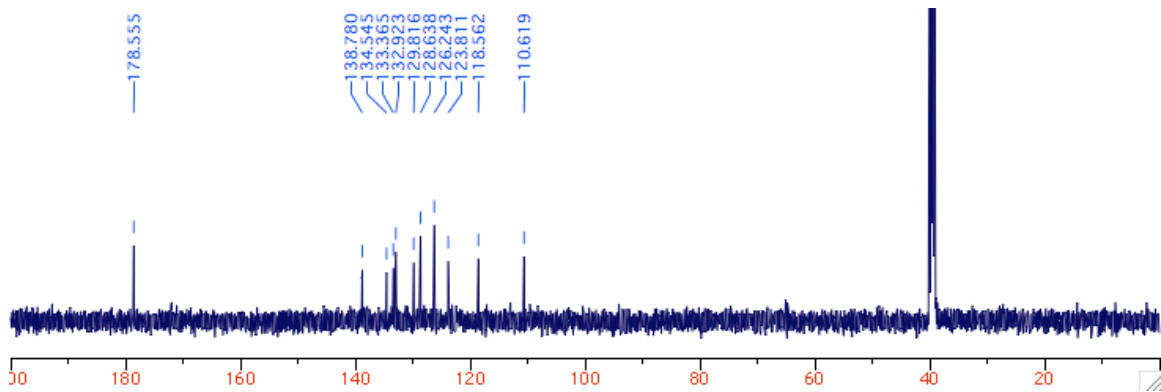
5,5'-((1E,1'E)-naphthalene-2,6-diylbis(ethene-2,1-diyl))bis(1H-pyrrole-2-carbaldehyde) (3d)



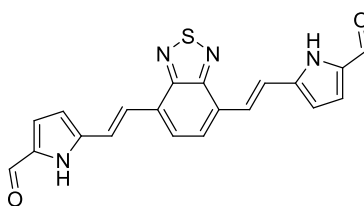
¹H NMR (DMSO-d₆, 500 MHz):



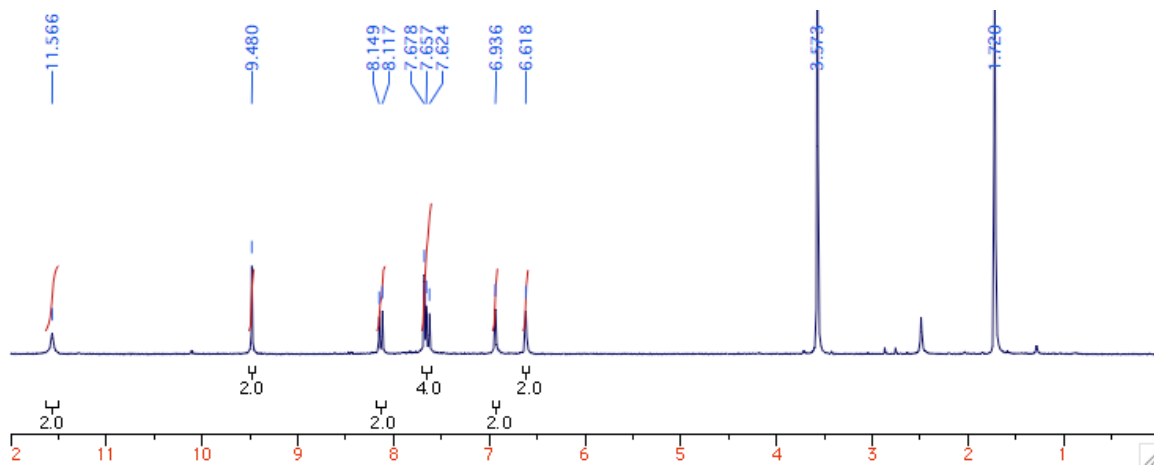
¹³C NMR (DMSO-d₆, 125 MHz):



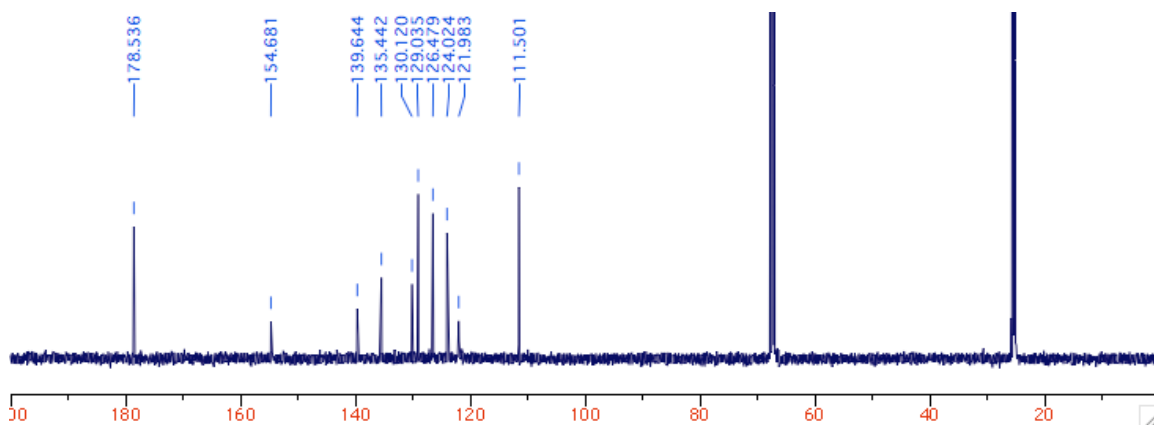
5,5'-((1E,1'E)-benzo[c][1,2,5]thiadiazole-4,7-diylbis(ethene-2,1-diyl))bis(1H-pyrrole-2-carbaldehyde) (3e)



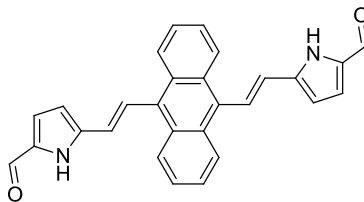
¹H NMR (THF-d₈, 500 MHz):



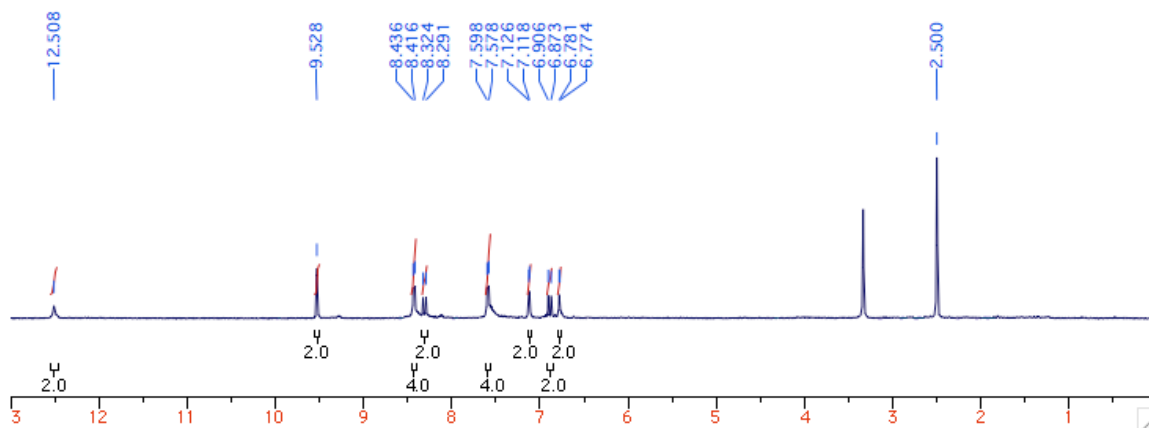
¹³C udefr NMR (THF-d₈, 125 MHz):



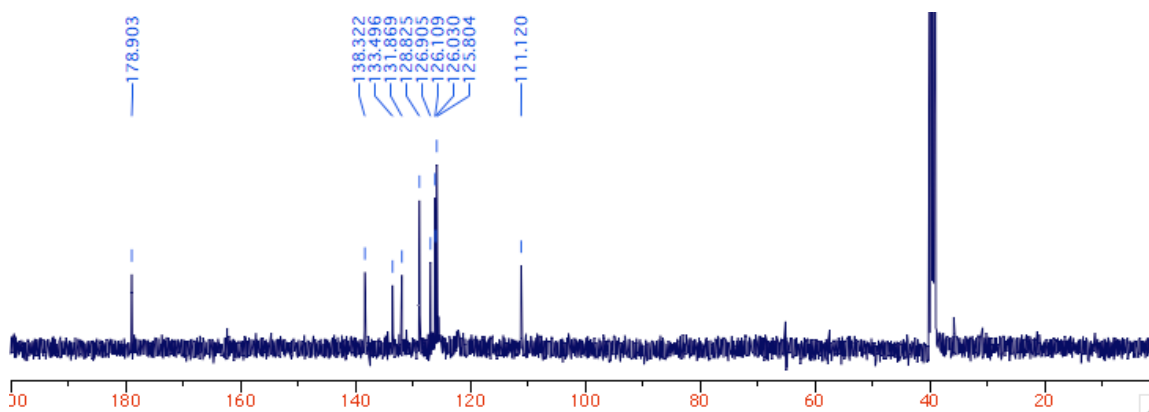
5,5'-((1E,1'E)-Anthracene-9,10-diylbis(ethene-2,1-diyl))bis(1H-pyrrole-2-carbaldehyde) (3f)



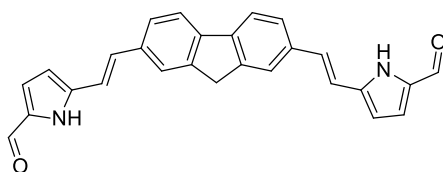
¹H NMR (DMSO-d₆, 500 MHz):



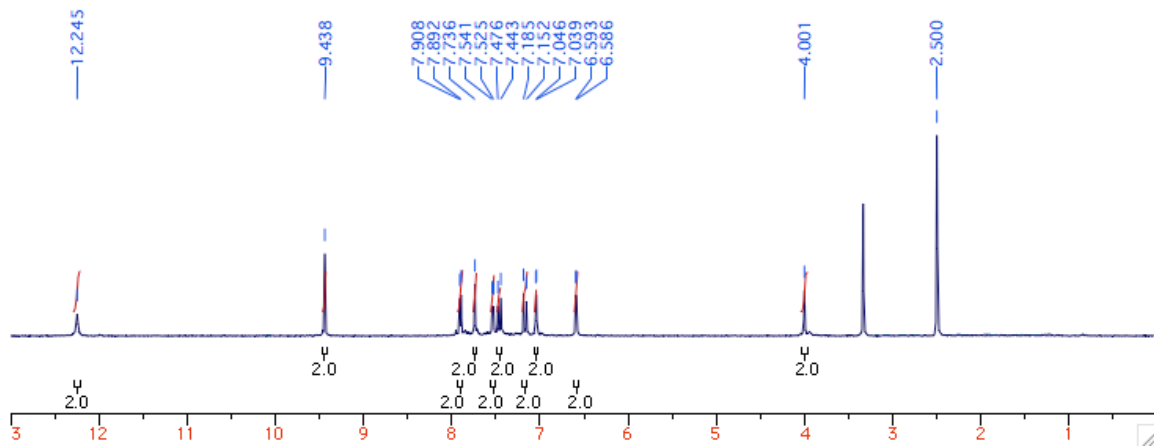
¹³C udefr NMR (DMSO-d₆, 125 MHz):



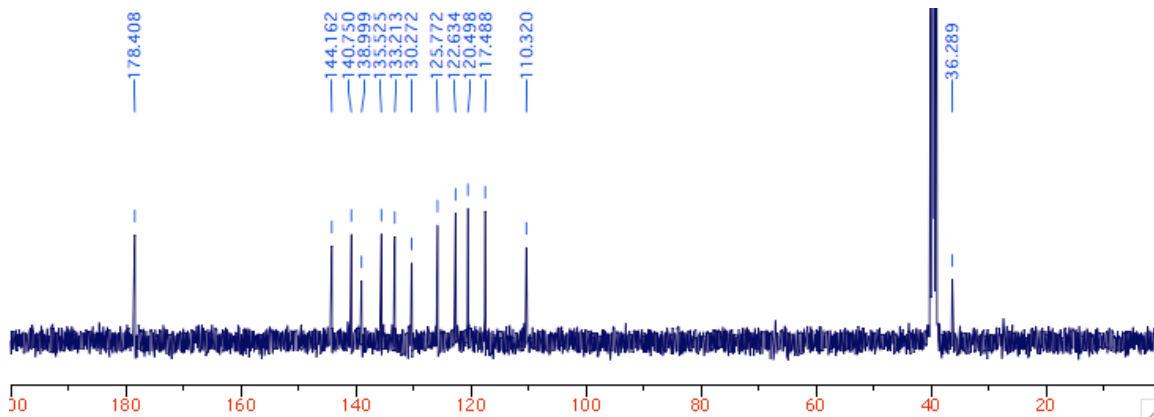
5,5'-((1E,1'E)-(9H-Fluorene-2,7-diyl)bis(ethene-2,1-diyl))bis(1H-pyrrole-2-carbaldehyde)
(3g)



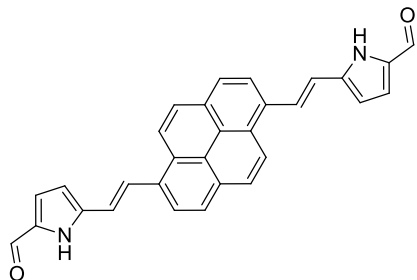
¹H NMR (DMSO-d₆, 500 MHz):



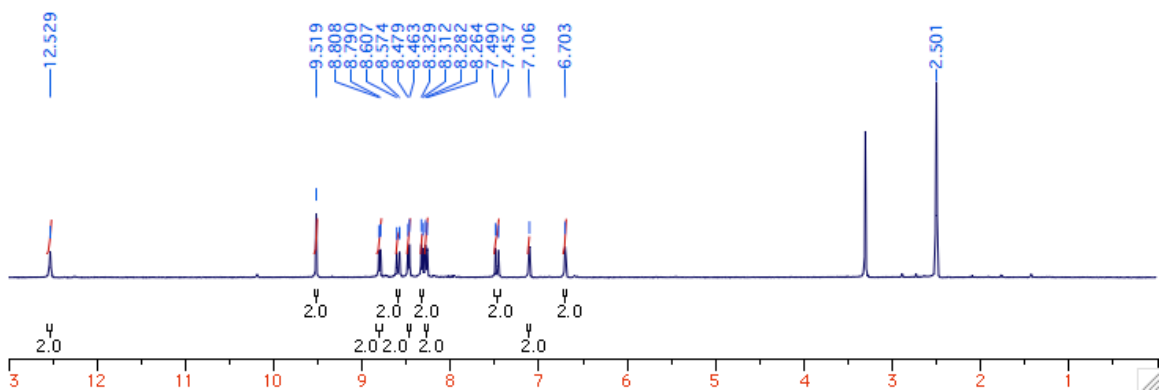
¹³C NMR (DMSO-d₆, 125 MHz):



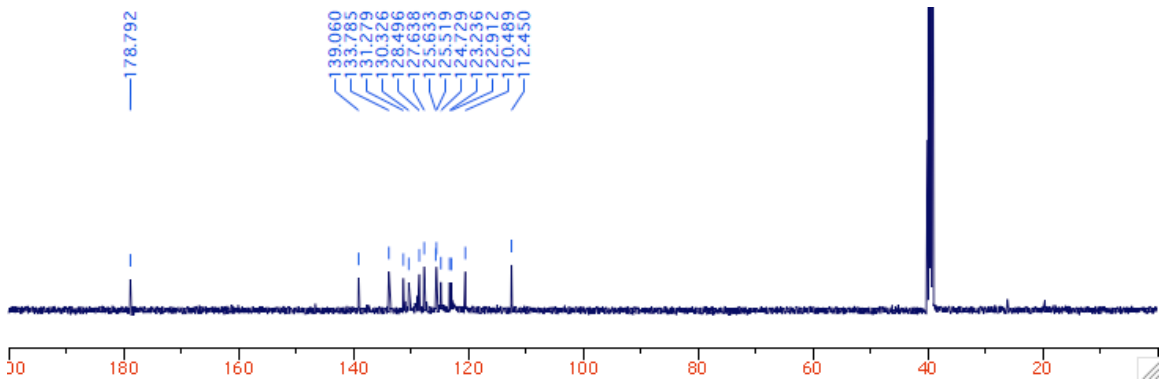
5,5'-((1E,1'E)-Pyrene-1,6-diylbis(ethene-2,1-diyl))bis(1H-pyrrole-2-carbaldehyde) (3h)



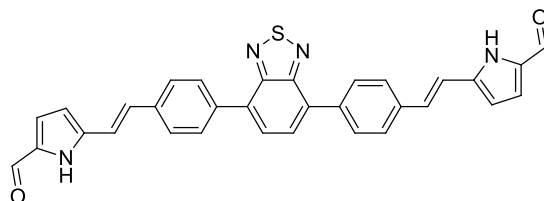
¹H NMR (DMSO-d₆, 500 MHz):



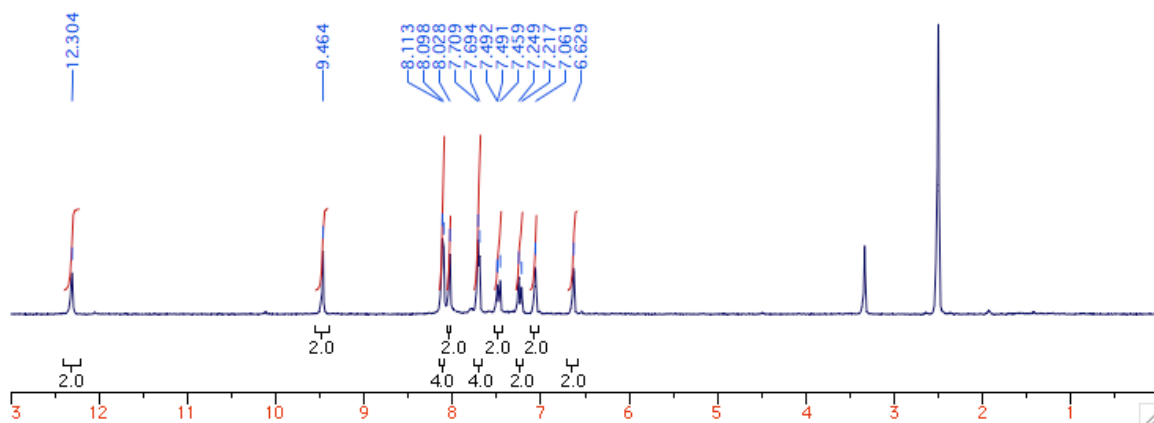
¹³C NMR (DMSO-d₆, 125 MHz):



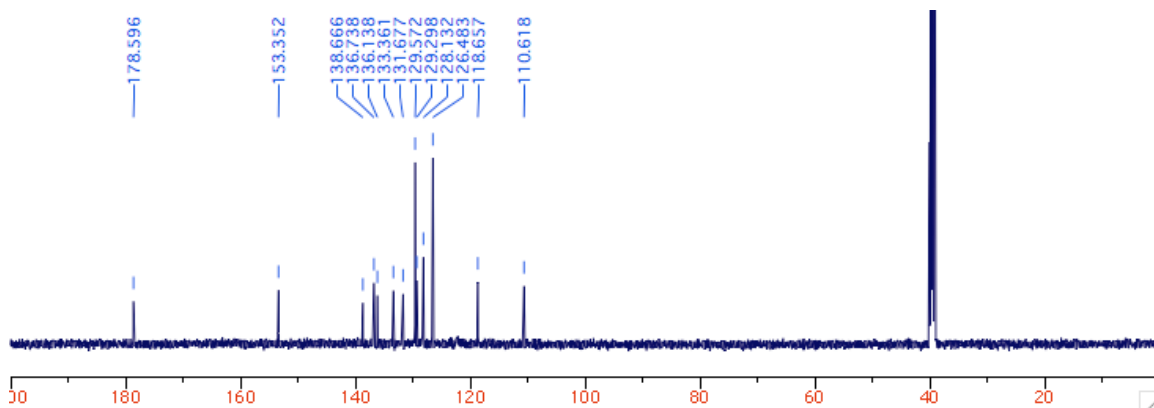
5,5'-((1E,1'E)-(Benzo[c][1,2,5]thiadiazole-4,7-diylbis(4,1-phenylene))bis(ethene-2,1-diyl))bis(1H-pyrrole-2-carbaldehyde) (3i)



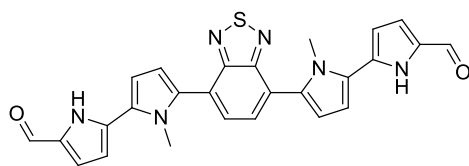
¹H NMR (DMSO-d₆, 500 MHz):



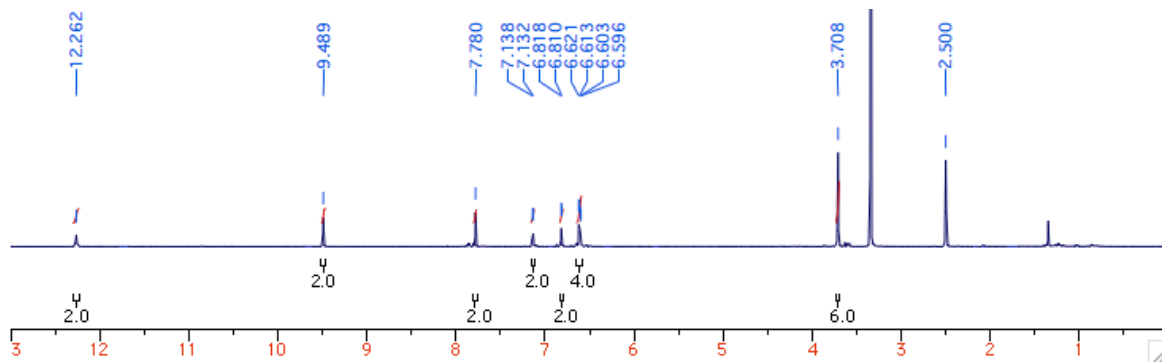
¹³C udefr NMR (DMSO-d₆, 125 MHz):



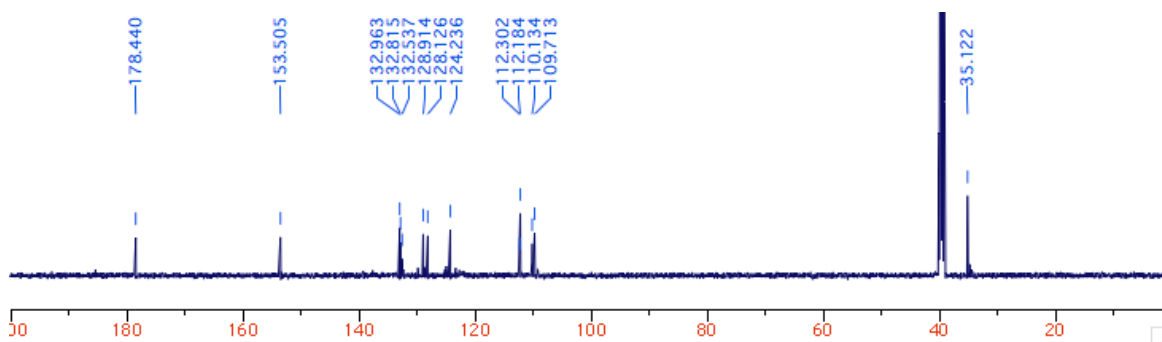
5',5'''-(Benzo[c][1,2,5]thiadiazole-4,7-diyl)bis(1'-methyl-1H,1'H-[2,2'-bipyrrole]-5-carbaldehyde) (3j)



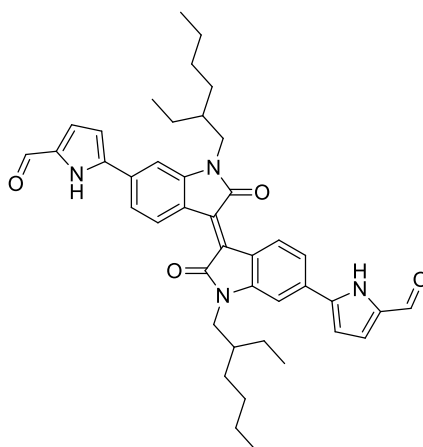
¹H NMR (DMSO-d₆, 500 MHz):



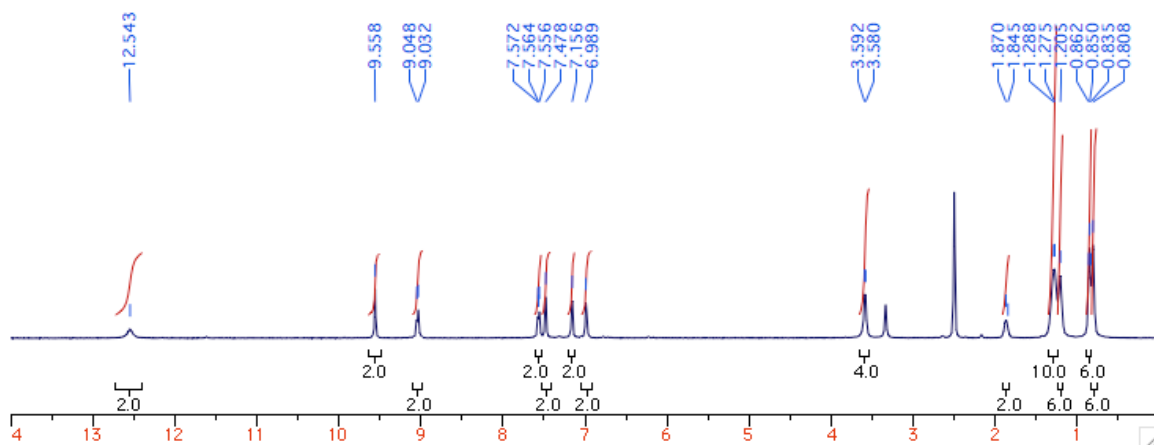
¹³C NMR (DMSO-d₆, 125 MHz):



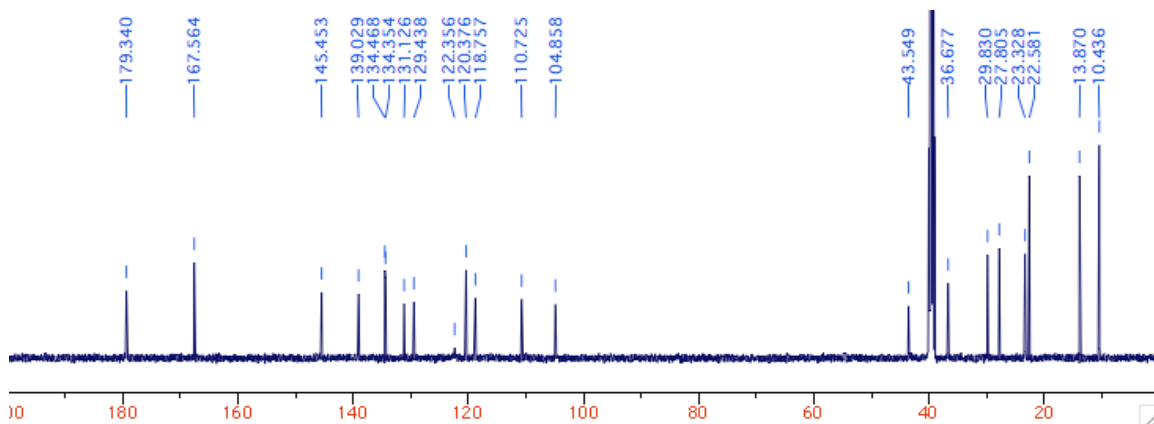
(E)-5,5'-(1,1'-Bis(2-ethylhexyl)-2,2'-dioxo-[3,3'-biindolinylidene]-6,6'-diyl)bis(1H-pyrrole-2-carbaldehyde) (3k)



¹H NMR (DMSO-d₆, 500 MHz):

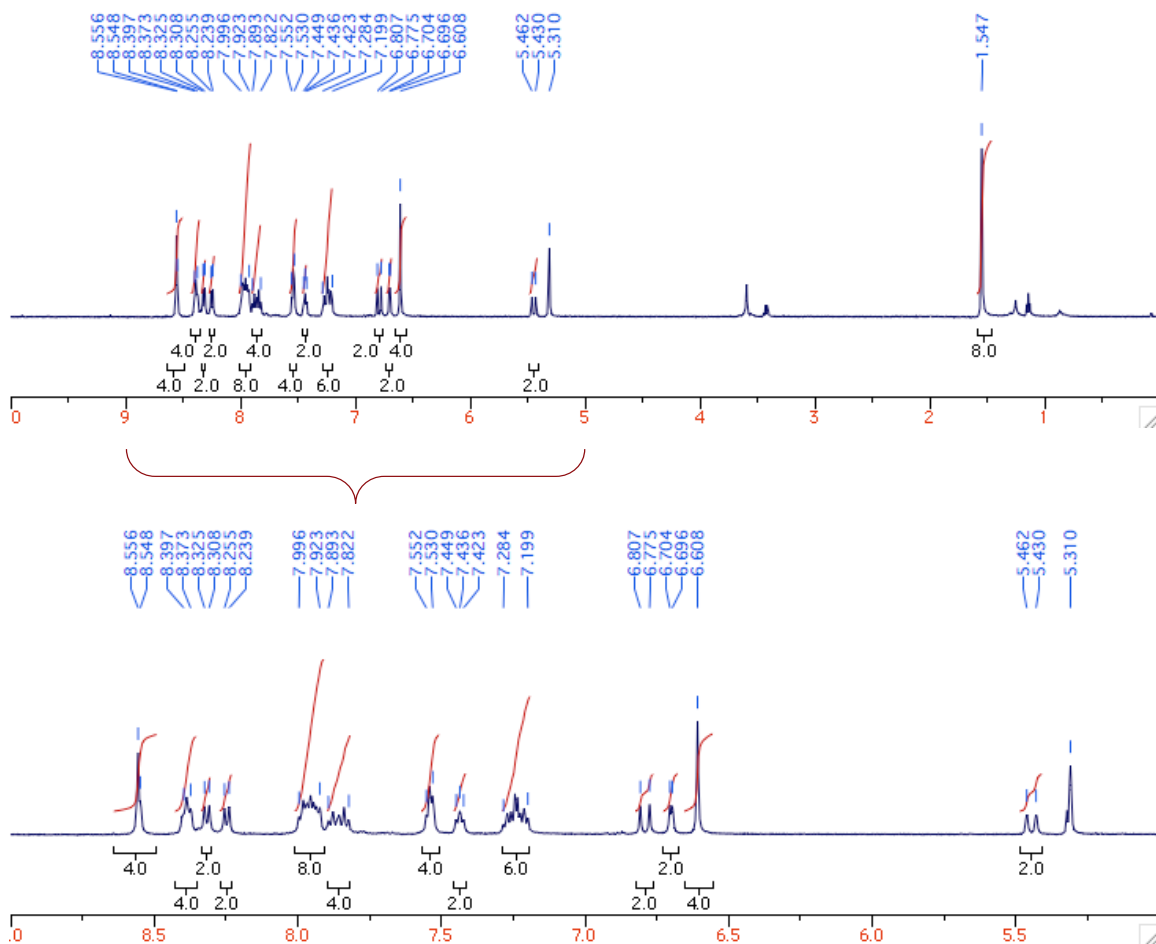


¹³C udefr NMR (DMSO-d₆, 125 MHz):

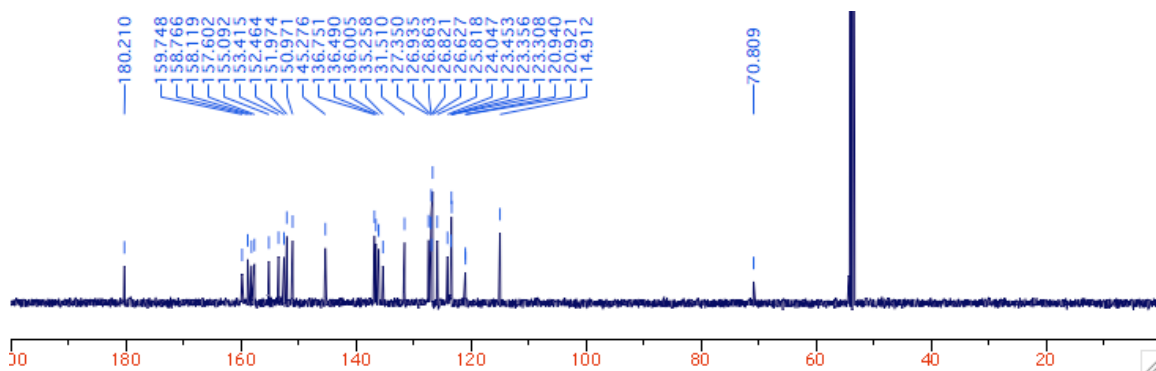


[Ru₂(3b)(bpy)₄](PF₆)₂ complex salt (4b)

¹H NMR (CD₂Cl₂, 500 MHz):

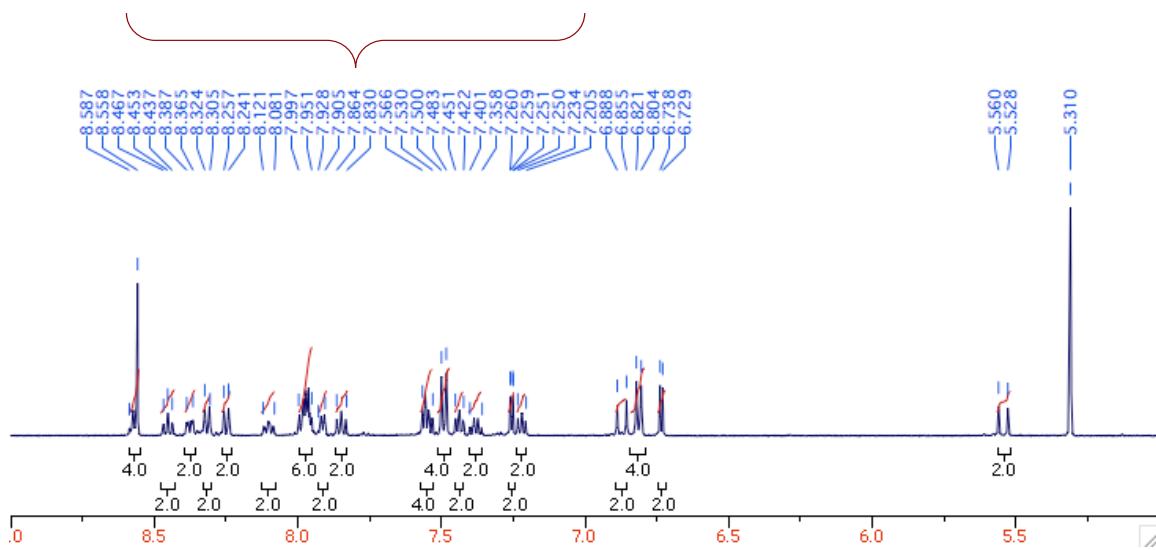
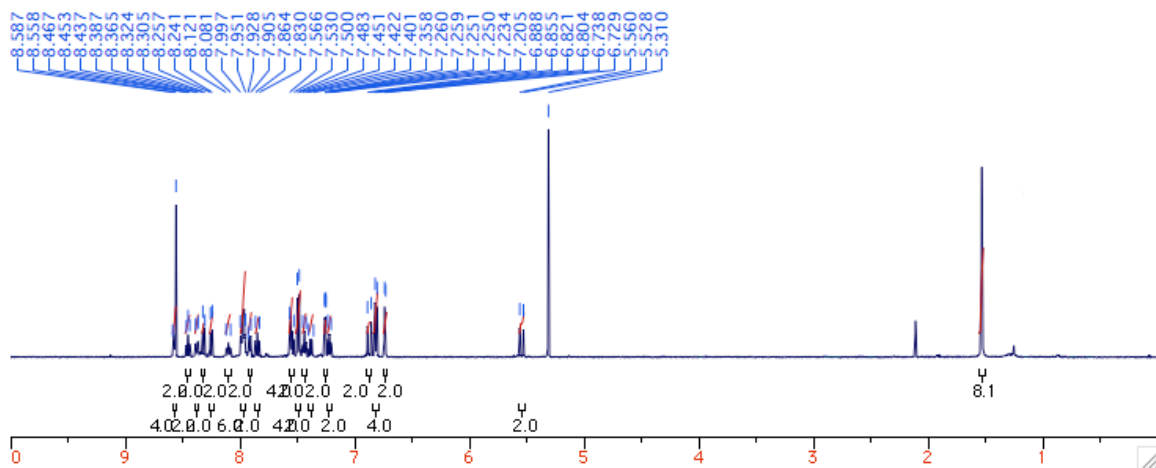


¹³C udeflt NMR (CD₂Cl₂, 125 MHz):

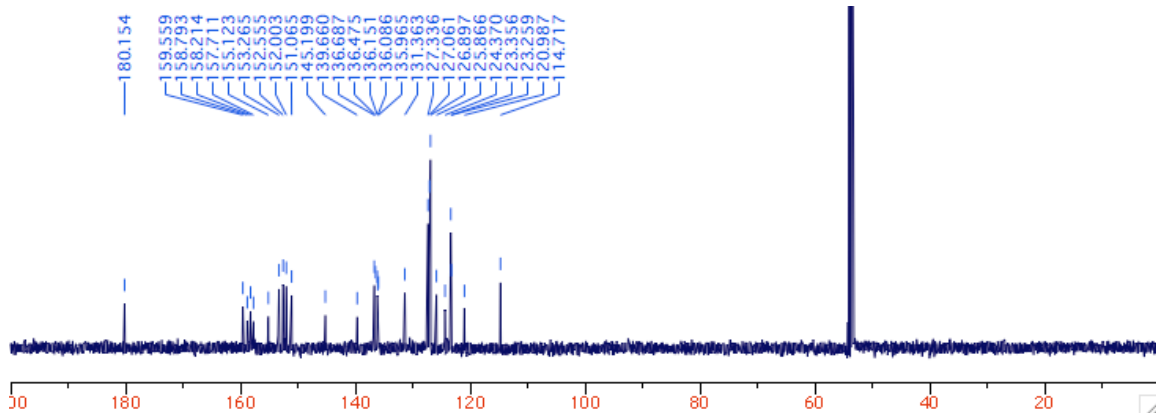


[Ru₂(3c)(bpy)₄](PF₆)₂ complex salt (4c)

¹H NMR (CD₂Cl₂, 500 MHz):

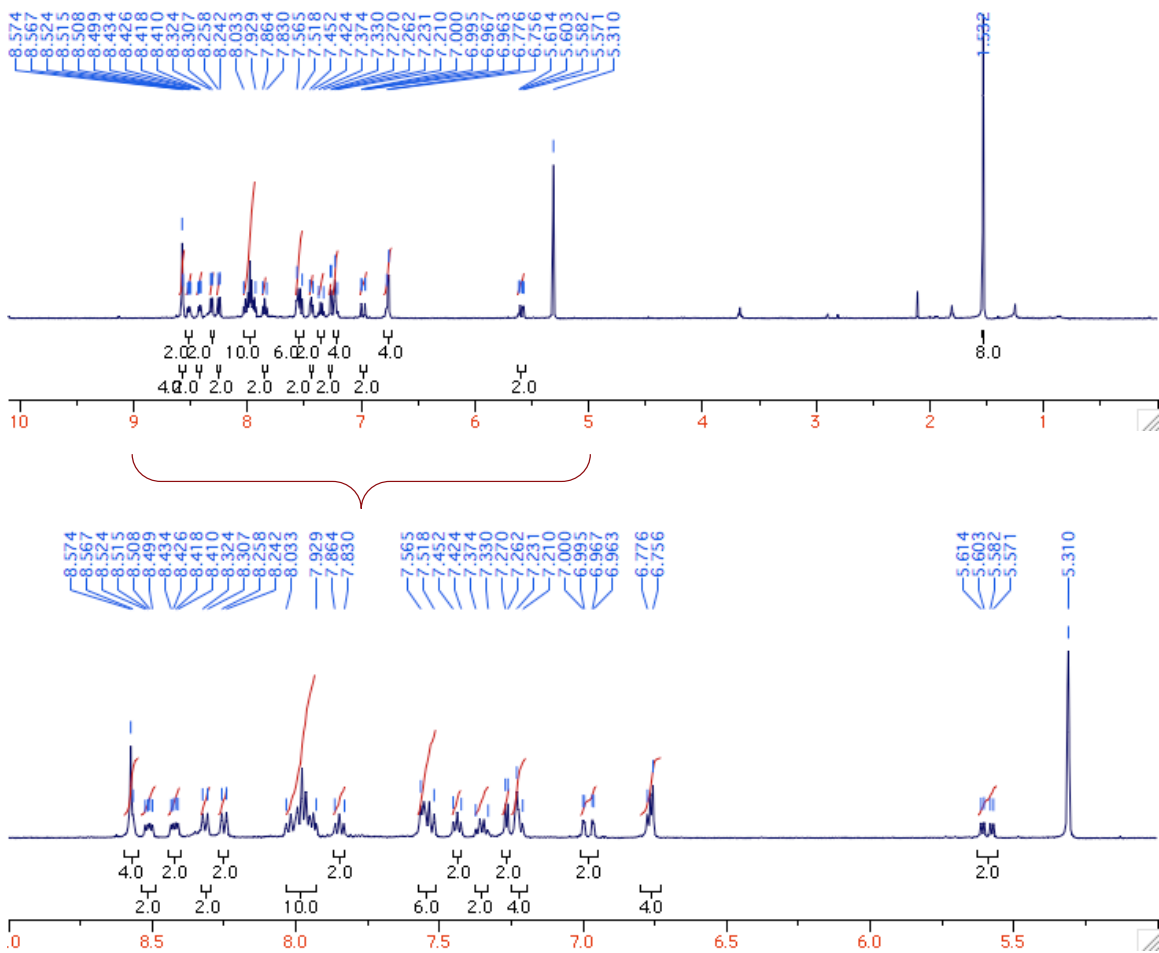


¹³C NMR (CD₂Cl₂, 125 MHz):

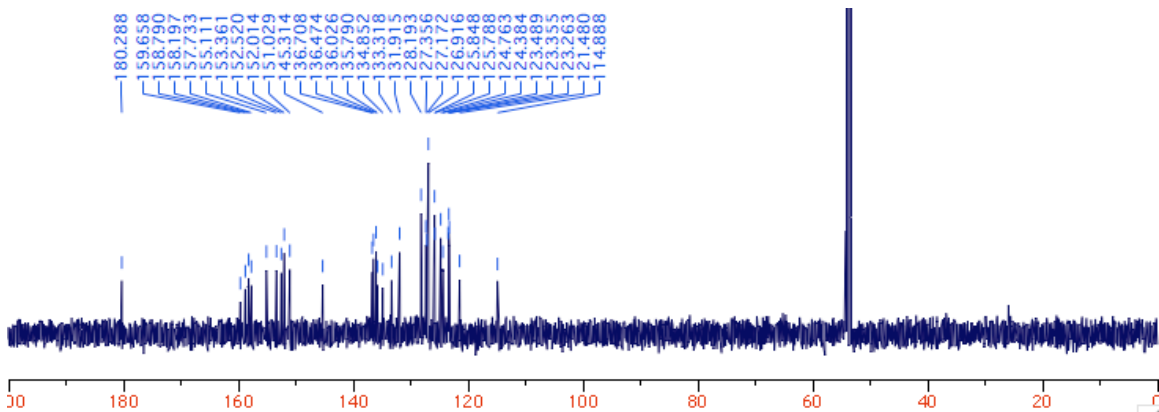


[Ru₂(3d)(bpy)₄](PF₆)₂ complex salt (4d)

¹H NMR (CD₂Cl₂, 500 MHz):

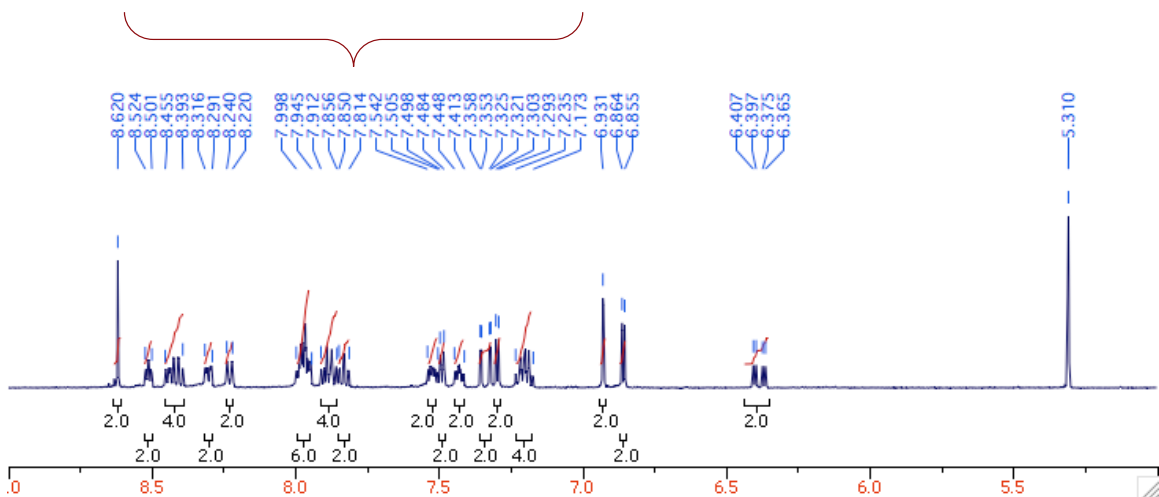
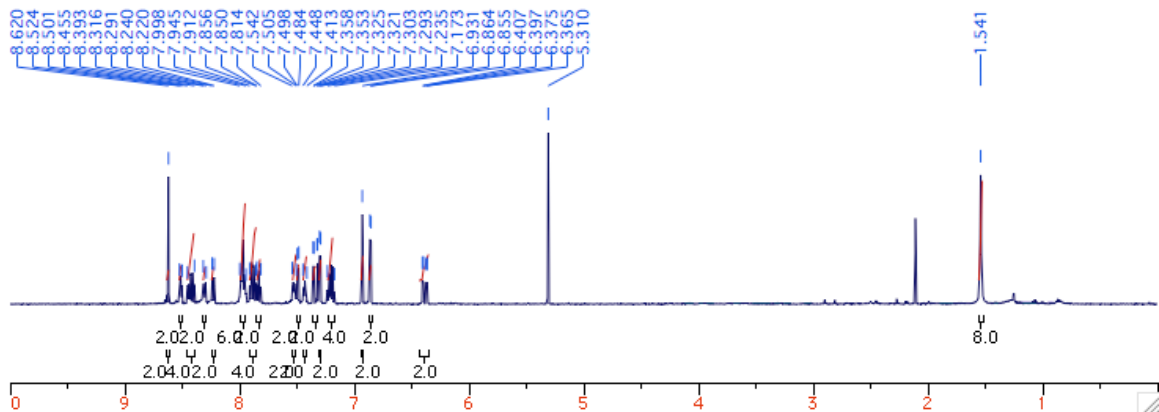


¹³C NMR (CD₂Cl₂, 125 MHz):

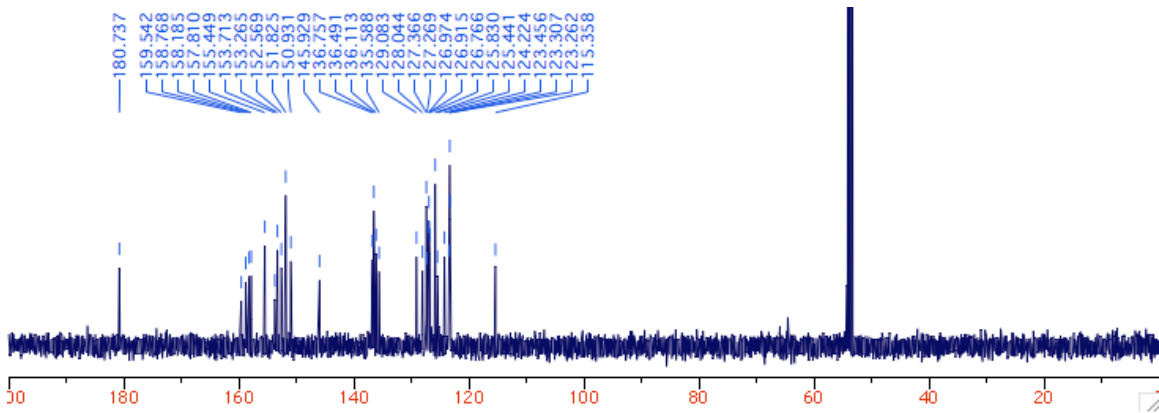


[Ru₂(3e)(bpy)₄](PF₆)₂ complex salt (4e)

¹H NMR (CD₂Cl₂, 500 MHz):

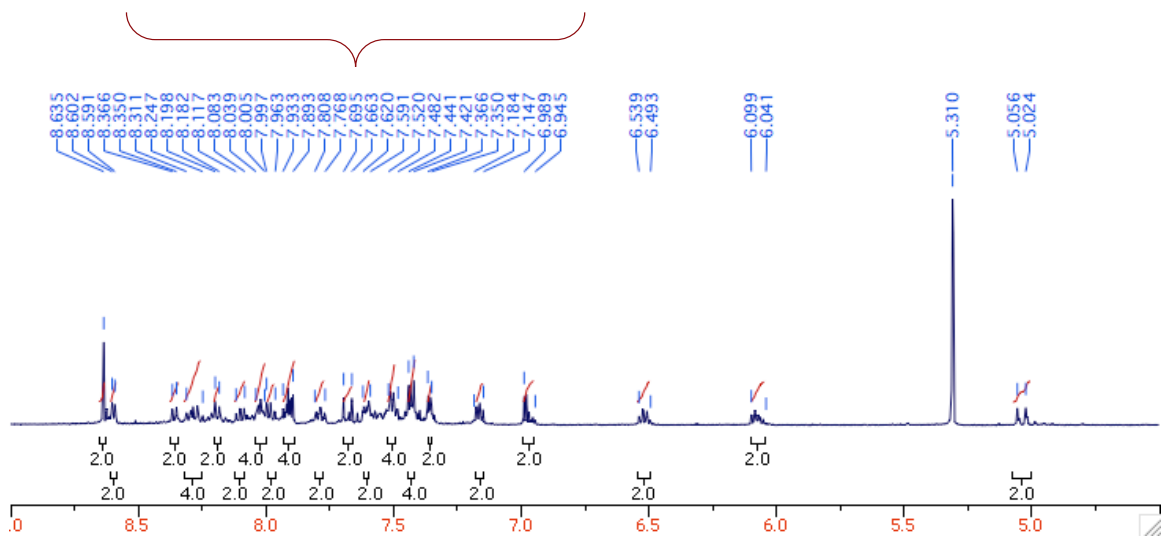
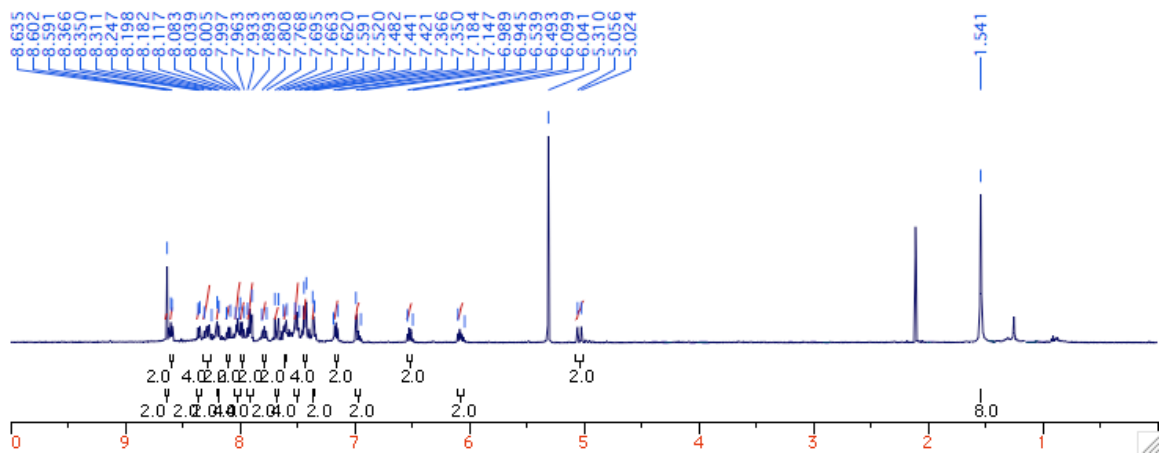


¹³C udefr NMR (CD₂Cl₂, 125 MHz):

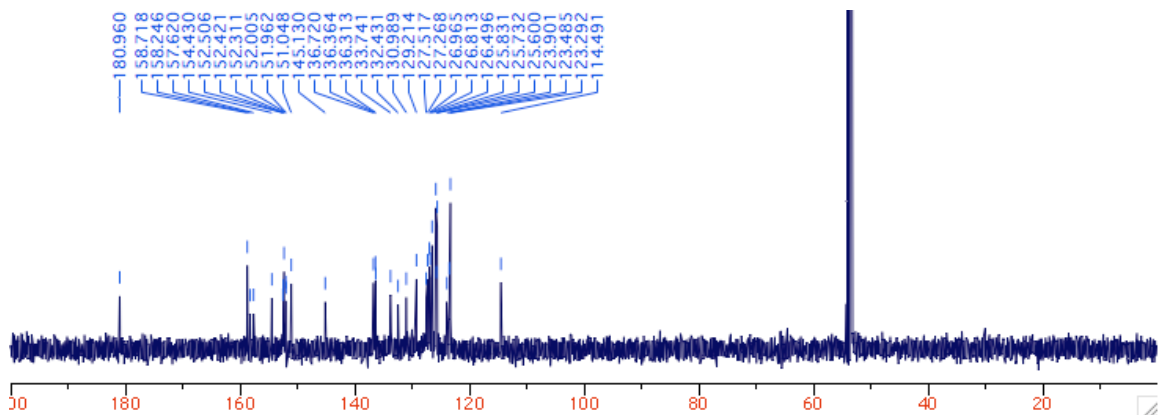


[Ru₂(3f)(bpy)₄](PF₆)₂ complex salt (4f)

¹H NMR (CD₂Cl₂, 500 MHz):

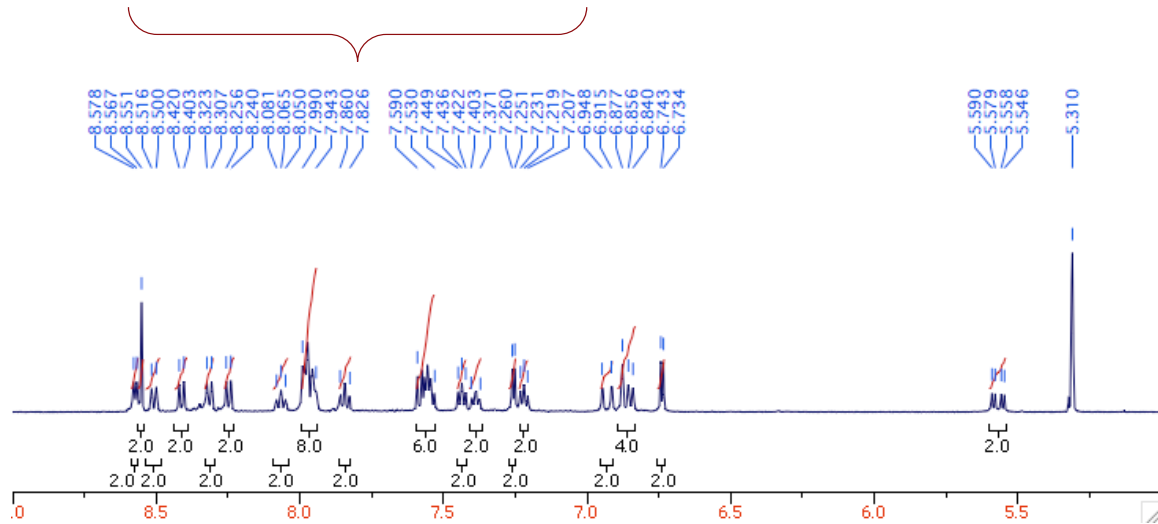
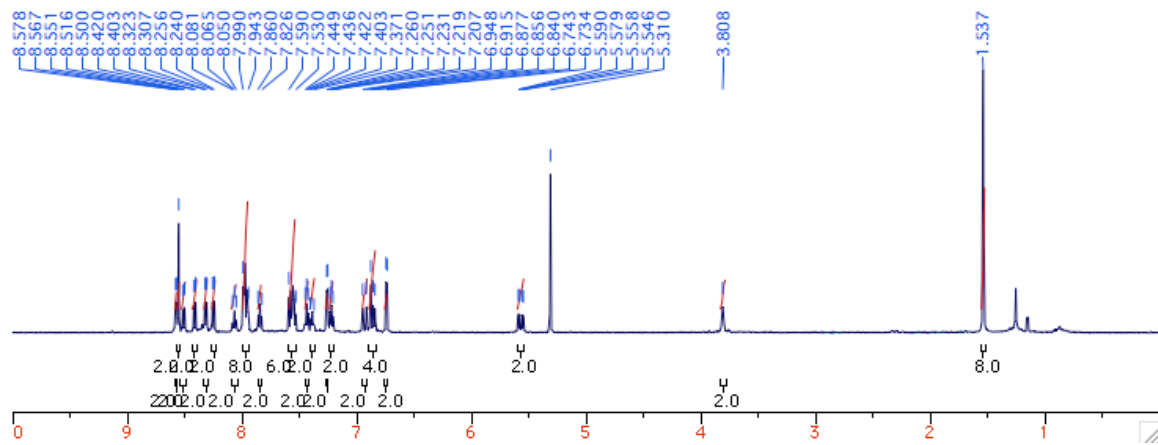


¹³C NMR (CD₂Cl₂, 125 MHz):

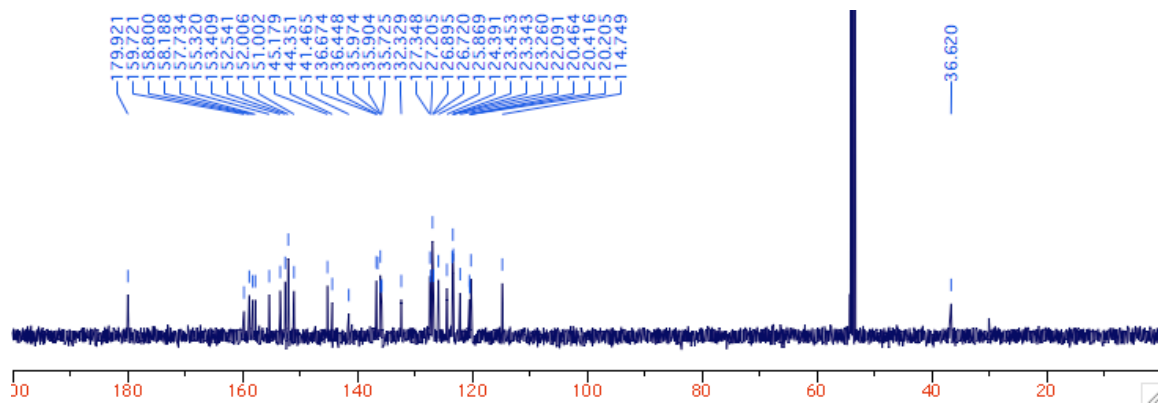


[Ru₂(3g)(bpy)₄](PF₆)₂ complex salt (4g)

¹H NMR (CD₂Cl₂, 500 MHz):

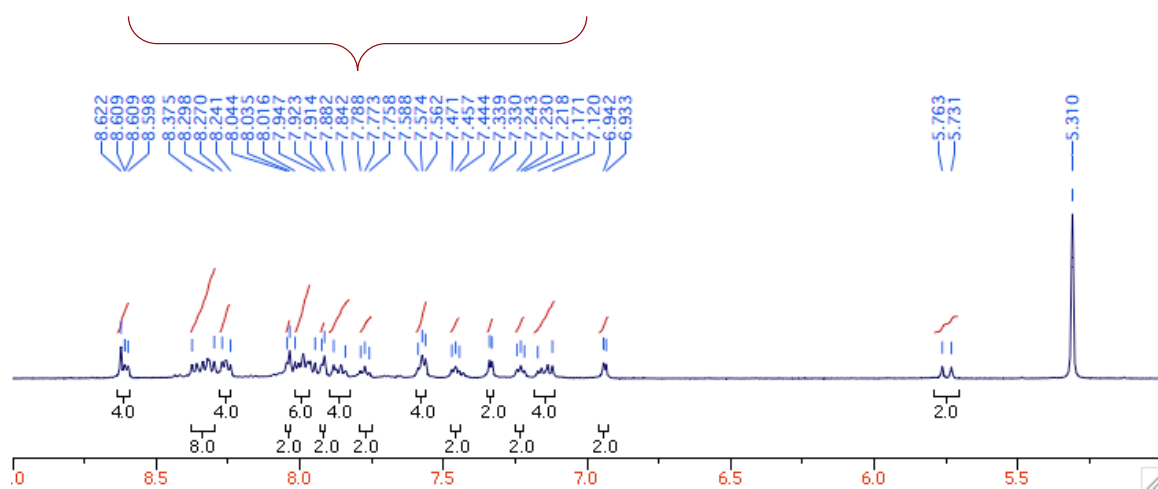
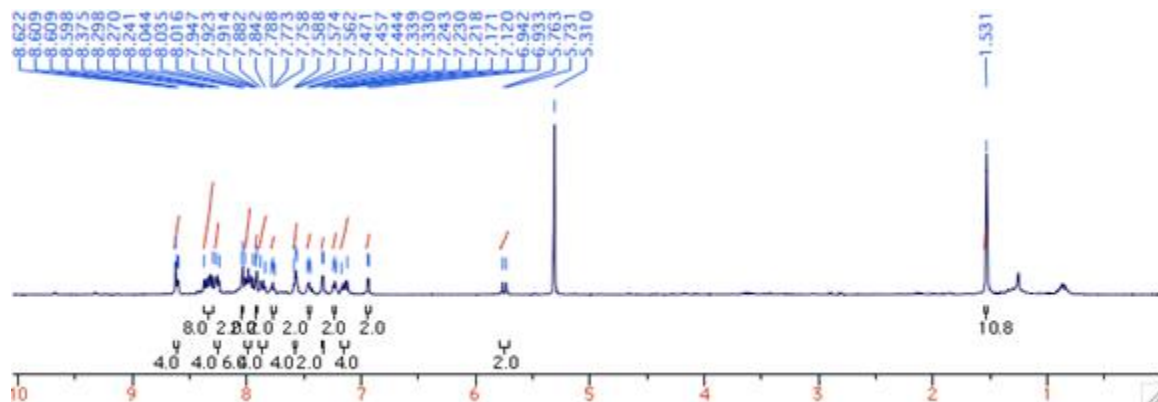


¹³C udeft NMR (CD₂Cl₂, 125 MHz):

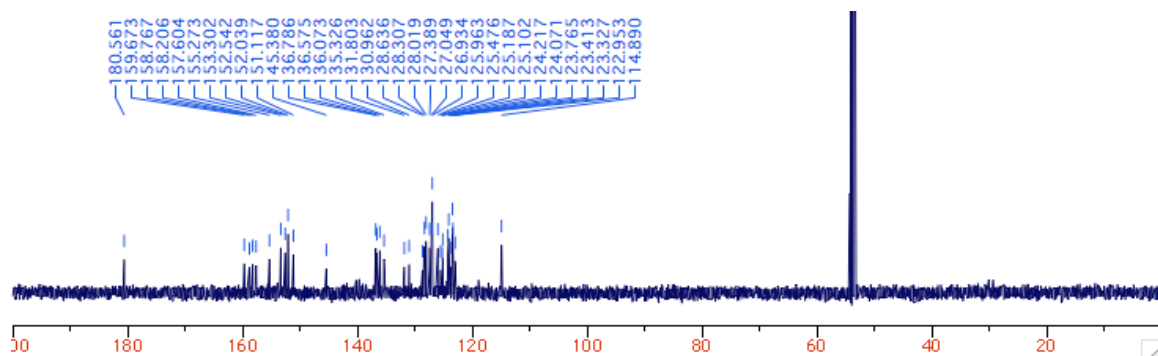


[Ru₂(3h)(bpy)₄](PF₆)₂ complex salt (4h)

¹H NMR (CD₂Cl₂, 500 MHz):

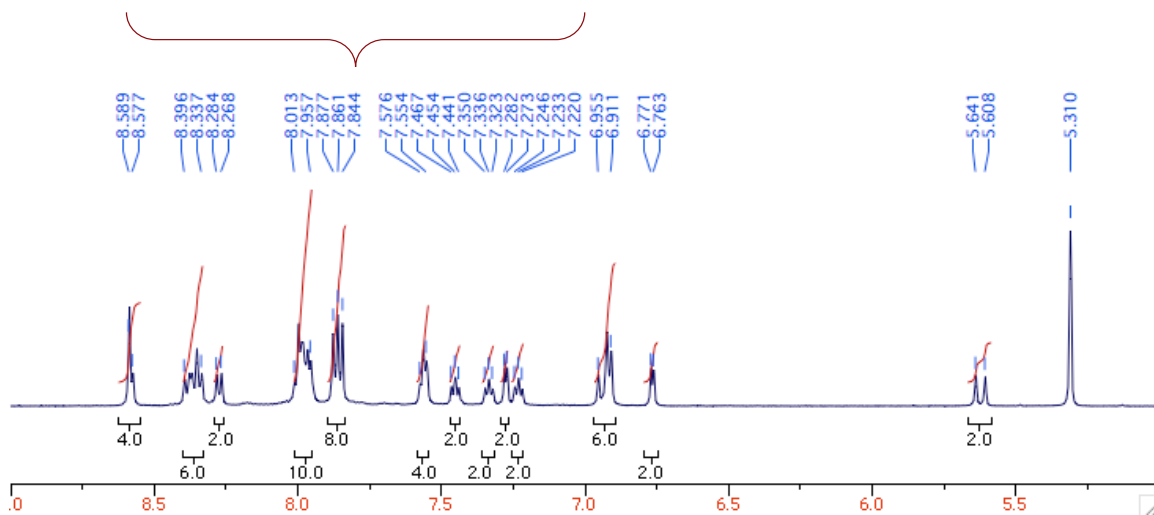
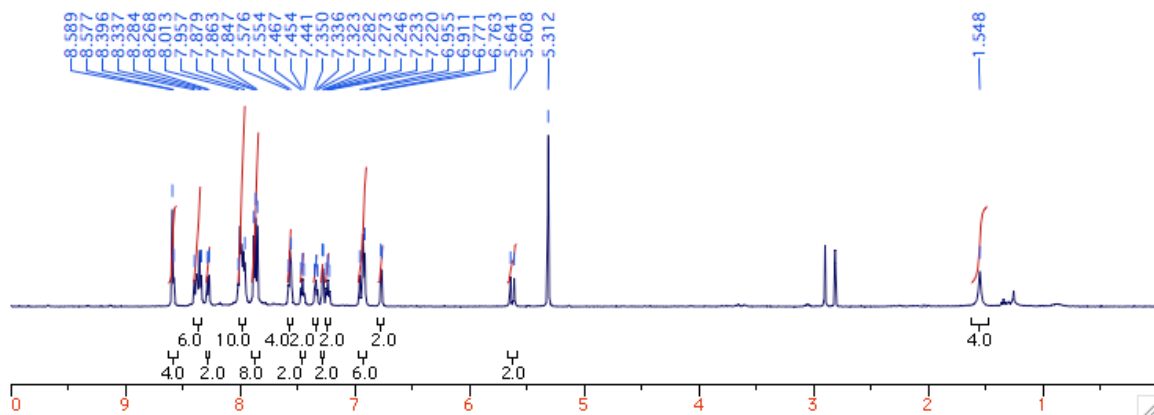


¹³C NMR (CD₂Cl₂, 125 MHz):

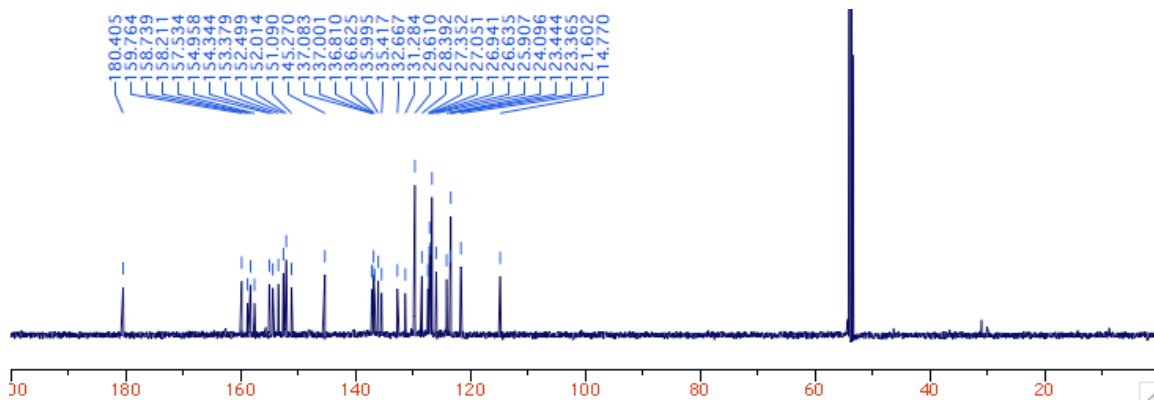


$[Ru_2(3i)(bpy)_4](PF_6)_2$ complex salt (4i)

1H NMR (CD_2Cl_2 , 500 MHz):

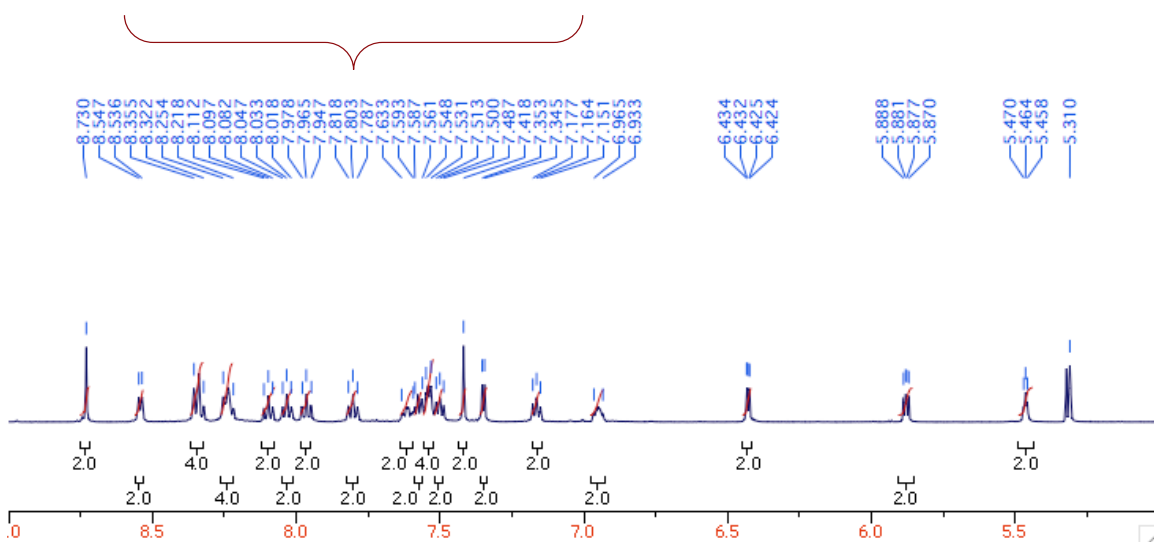
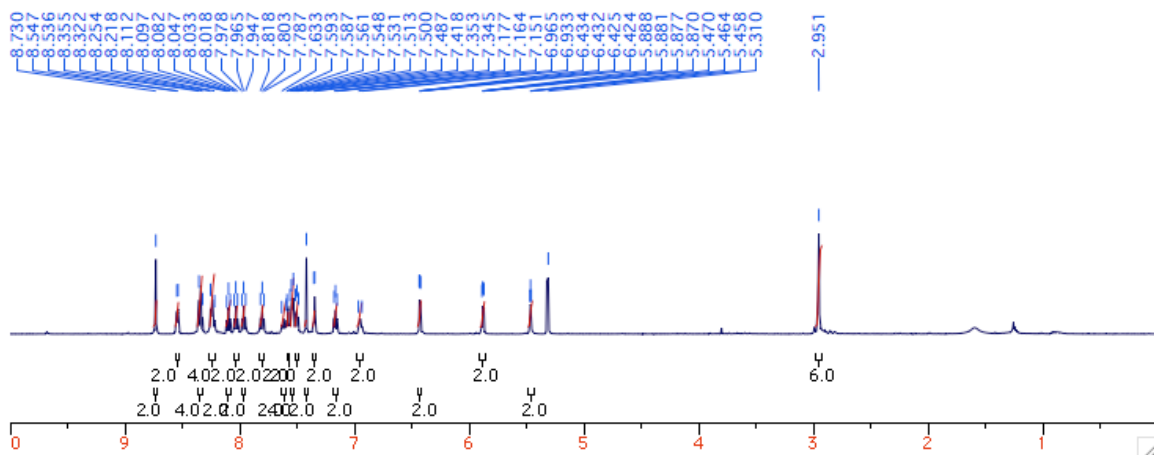


^{13}C udefr NMR (CD_2Cl_2 , 125 MHz):

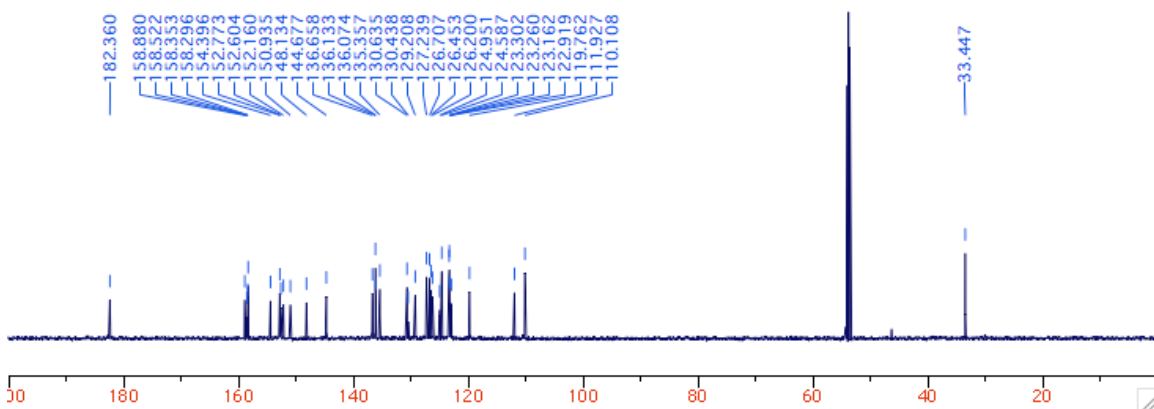


[Ru₂(3j)(bpy)₄](PF₆)₂ complex salt (4j)

¹H NMR (CD₂Cl₂, 500 MHz):

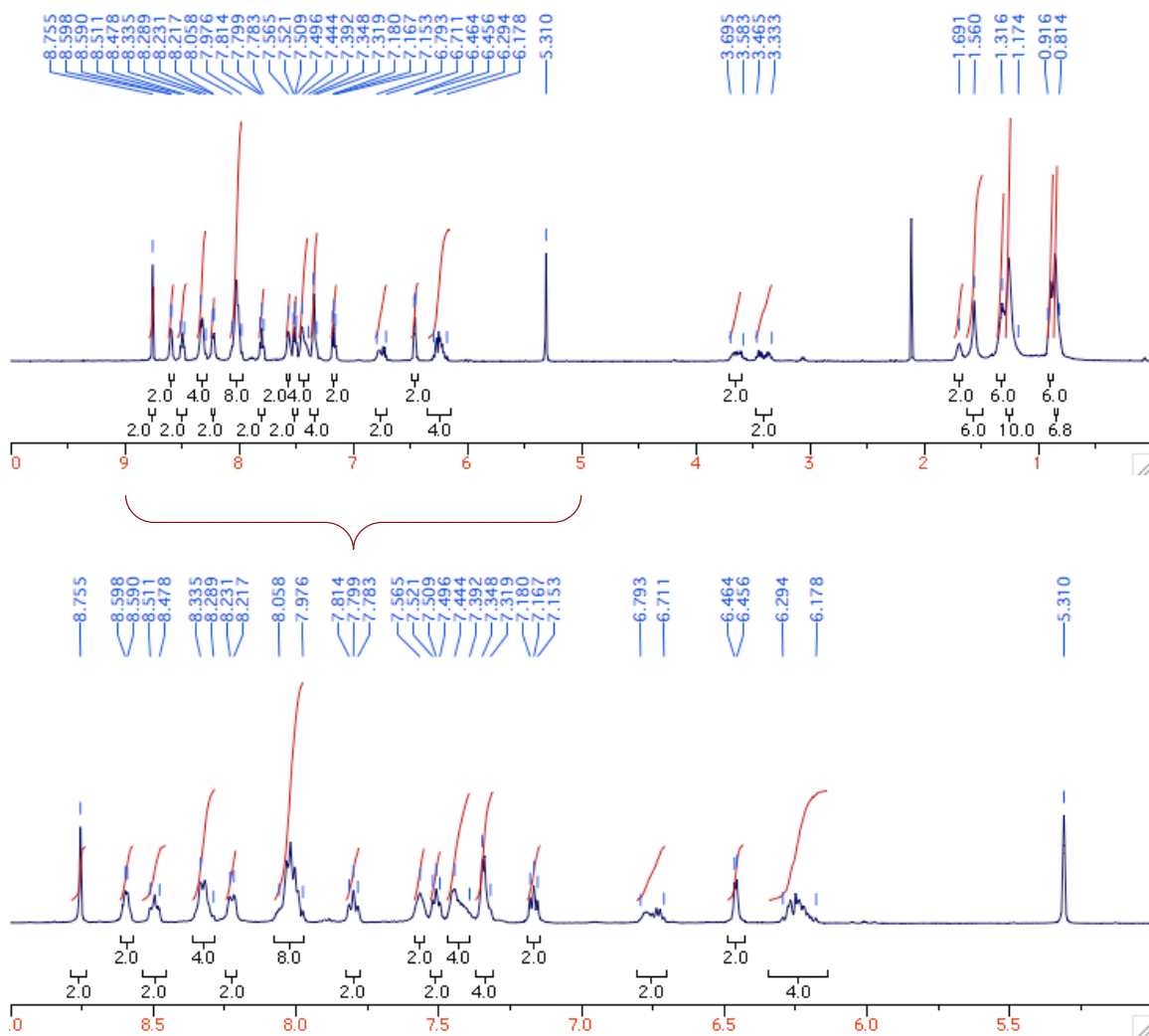


¹³C NMR (CD₂Cl₂, 125 MHz):

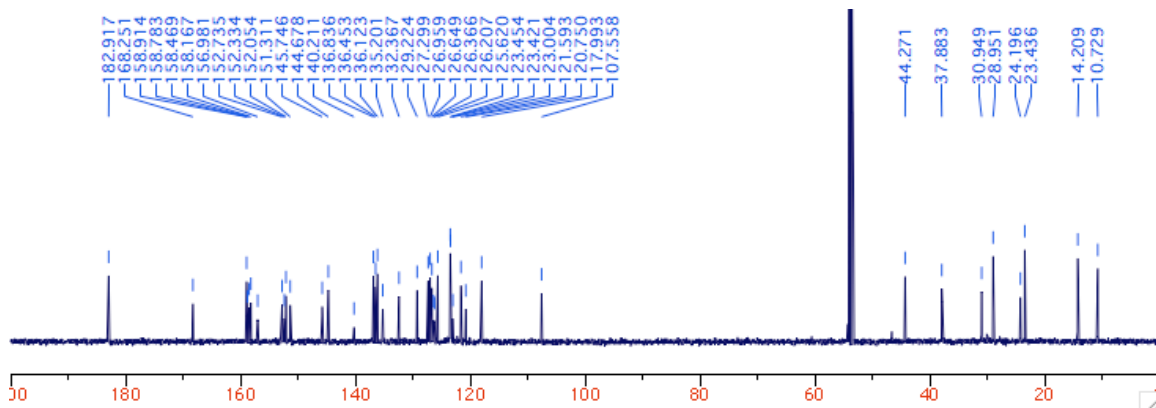


[Ru₂(3k)(bpy)₄](PF₆)₂ complex salt (4k)

¹H NMR (CD₂Cl₂, 500 MHz):

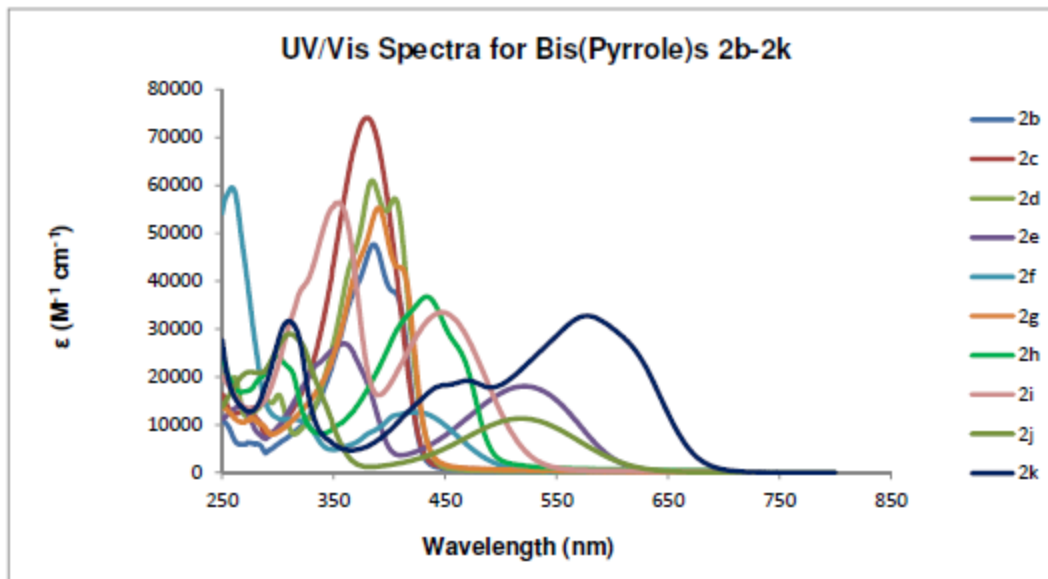


¹³C NMR (CD₂Cl₂, 125 MHz):



UV Spectra

Bis(pyrroles)



UV/Vis spectra recorded for bis(pyrroles) 2

Key:

Phenyl Linker = **2b**

Biphenyl Linker = **2c**

Naphthyl Linker = **2d**

Benzothiadiazole Linker = **2e**

Anthracene Linker = **2f**

Fluorene Linker = **2g**

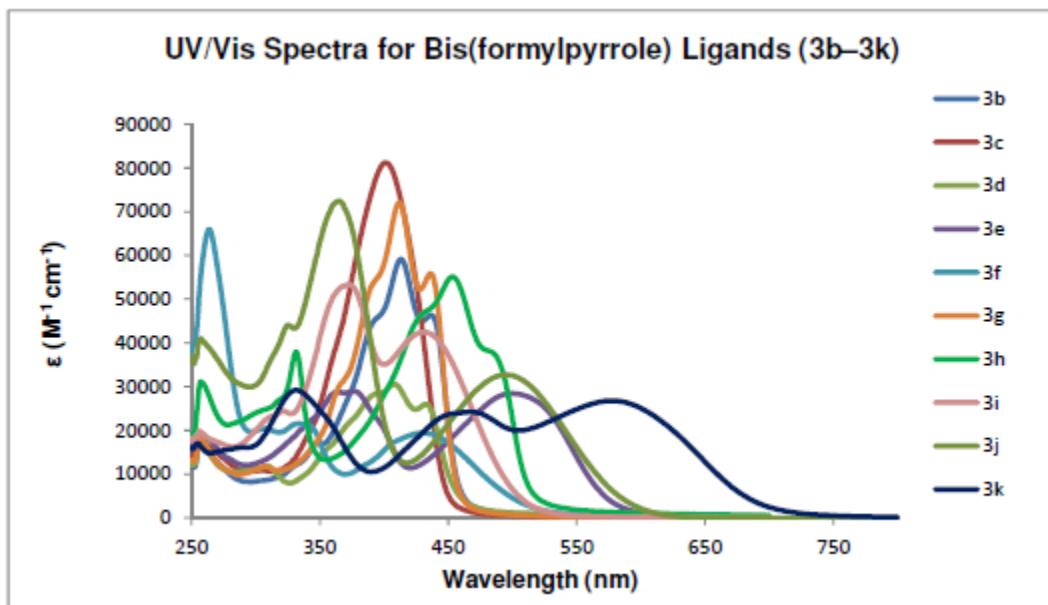
Pyrene Linker = **2h**

4,7-Diphenylbenzothiadiazole Linker = **2i**

4,7-Bis(1-methyl-1H-pyrrol-2-yl)benzothiadiazole Linker = **2j**

Isoindigo Linker = **2k**

Bis(formylpyrroles)



UV/Vis spectra recorded for ligands **3**

Key:

Phenyl Linker = **3b**

Biphenyl Linker = **3c**

Naphthyl Linker = **3d**

Benzothiadiazole Linker = **3e**

Anthracene Linker = **3f**

Fluorene Linker = **3g**

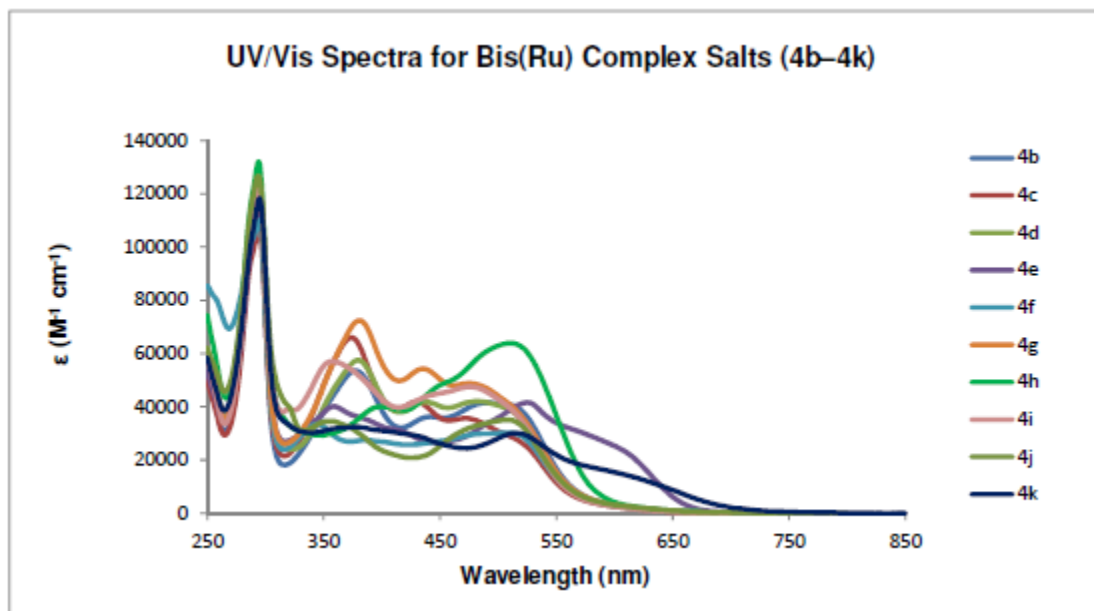
Pyrene Linker = **3h**

4,7-Diphenylbenzothiadiazole Linker = **3i**

4,7-Bis(1-methyl-1H-pyrrol-2-yl)benzothiadiazole Linker = **3j**

Isoindigo Linker = **3k**

Bis(ruthenium) Complex Salts



UV/Vis spectra recorded for bis(ruthenium) complexes **4**

Key:

4a

Phenyl Linker = **4b**

Biphenyl Linker = **4c**

Naphthyl Linker = **4d**

Benzothiadiazole Linker = **4e**

Anthracene Linker = **4f**

Fluorene Linker = **4g**

Pyrene Linker = **4h**

4,7-Diphenylbenzothiadiazole Linker = **4i**

4,7-Bis(1-methyl-1H-pyrrol-2-yl)benzothiadiazole Linker = **4j**

Isoindigo Linker = **4k**

References

- (1) Waser, J.; Gaspar, B.; Nambu, H.; Carreira, E. M. *J. Am. Chem. Soc.* **2006**, *128*, 11693.
- (2) Liu, J.; Bu, L.; Dong, J.; Zhou, Q.; Geng, Y.; Ma, D.; Wang, L.; Jing, X.; Wang, F. *J. Mater. Chem.* **2007**, *17*, 2832.
- (3) Sun, M.; Lan, L.; Wang, L.; Peng, J.; Cao, Y. *Macromol. Chem. Phys.* **2008**, *209*, 2504.
- (4) Mei, J.; Graham, K. R.; Stalder, R.; Reynolds, J. R. *Org. Lett.* **2010**, *12*, 660.

SI_Ru-pyrrolide-triads_200724.pdf (2.30 MiB)

[view on ChemRxiv](#) • [download file](#)
